NASA/TM–20240001178

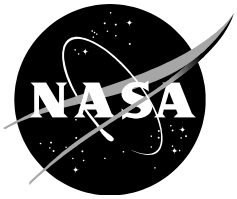

Characterizing Face Sheet/Core Disbonding Using the Single Cantilever Beam Test: Results from an International Round Robin

Ronald Krueger
National Institute of Aerospace, Hampton, VA, USA

James G. Ratcliffe
NASA Langley Research Center, Hampton, VA, USA

Daniel O. Adams
University of Utah, Salt Lake City, UT, USA

Zhi-Ming Chen
Federal Aviation Administration, William J. Hughes Technical Center, Atlantic City, NJ, USA

Waruna Seneviratne, Chris Oline
NIAR, Wichita State University, Wichita, KS, USA

Christian Berggreen, Francesco Attanasio, Vishnu Saseendran
Technical University of Denmark, Kgs. Lyngby, Denmark

Sönke-Class Fimmen
Airbus Operations GmbH, Bremen, Germany

Ralf Schäuble
Fraunhofer Institute for Microstructure of Materials and Systems IMWS, Halle, Germany

Yannick Albertone
DuPont, Geneva, Switzerland

February 2024

NASA STI Program Report Series

The NASA STI Program collects, organizes, provides for archiving, and disseminates NASA's STI. The NASA STI program provides access to the NTRS Registered and its public interface, the NASA Technical Reports Server, thus providing one of the largest collections of aeronautical and space science STI in the world. Results are published in both non-NASA channels and by NASA in the NASA STI Report Series, which includes the following report types:

- TECHNICAL PUBLICATION. Reports of completed research or a major significant phase of research that present the results of NASA Programs and include extensive data or theoretical analysis. Includes compilations of significant scientific and technical data and information deemed to be of continuing reference value. NASA counterpart of peer-reviewed formal professional papers but has less stringent limitations on manuscript length and extent of graphic presentations.

- TECHNICAL MEMORANDUM. Scientific and technical findings that are preliminary or of specialized interest, e.g., quick release reports, working papers, and bibliographies that contain minimal annotation. Does not contain extensive analysis.

- CONTRACTOR REPORT. Scientific and technical findings by NASA-sponsored contractors and grantees.

- CONFERENCE PUBLICATION. Collected papers from scientific and technical conferences, symposia, seminars, or other meetings sponsored or co-sponsored by NASA.

- SPECIAL PUBLICATION. Scientific, technical, or historical information from NASA programs, projects, and missions, often concerned with subjects having substantial public interest.

- TECHNICAL TRANSLATION. English-language translations of foreign scientific and technical material pertinent to NASA's mission.

Specialized services also include organizing and publishing research results, distributing specialized research announcements and feeds, providing information desk and personal search support, and enabling data exchange services.

For more information about the NASA STI program, see the following:

- Access the NASA STI program home page at http://www.sti.nasa.gov

- Help desk contact information:

https://www.sti.nasa.gov/sti-contact-form/ and select the "General" help request type.

NASA/TM–20240001178

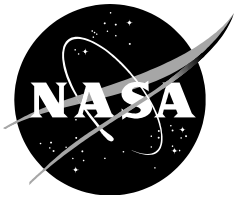

Characterizing Face Sheet/Core Disbonding Using the Single Cantilever Beam Test: Results from an International Round Robin

Ronald Krueger
National Institute of Aerospace, Hampton, VA, USA

James G. Ratcliffe
NASA Langley Research Center, Hampton, VA, USA

Daniel O. Adams
University of Utah, Salt Lake City, UT, USA

Zhi-Ming Chen
Federal Aviation Administration, William J. Hughes Technical Center, Atlantic City, NJ, USA

Waruna Seneviratne, Chris Oline
NIAR, Wichita State University, Wichita, KS, USA

Christian Berggreen, Francesco Attanasio, Vishnu Saseendran
Technical University of Denmark, Kgs. Lyngby, Denmark

Sönke-Class Fimmen
Airbus Operations GmbH, Bremen, Germany

Ralf Schäuble
Fraunhofer Institute for Microstructure of Materials and Systems IMWS, Halle, Germany

Yannick Albertone
DuPont, Geneva, Switzerland

National Aeronautics and
Space Administration

Langley Research Center
Hampton, VA 23681

February 2024

The use of trademarks or names of manufacturers in this report is for accurate reporting and does not constitute an official endorsement, either expressed or implied, of such products or manufacturers by the National Aeronautics and Space Administration.

Available from:

NASA STI Program / Mail Stop 050
NASA Langley Research Center
Hampton, VA 23681-2199

Characterizing Face Sheet/Core Disbonding Using the Single Cantilever Beam Test: Results from an International Round Robin

Ronald Krueger
National Institute of Aerospace, Hampton, VA, USA

James G. Ratcliffe
NASA Langley Research Center, Hampton, VA, USA

Daniel O. Adams
University of Utah, Salt Lake City, UT, USA

Zhi-Ming Chen
Federal Aviation Administration, William J. Hughes Technical Center, Atlantic City, NJ, USA

Waruna Seneviratne, Chris Oline
NIAR, Wichita State University, Wichita, KS, USA

Christian Berggreen, Francesco Attanasio, Vishnu Saseendran
Technical University of Denmark, Kgs. Lyngby, Denmark

Sönke-Class Fimmen
Airbus Operations GmbH, Bremen, Germany

Ralf Schäuble
Fraunhofer Institute for Microstructure of Materials and Systems IMWS, Halle, Germany

Yannick Albertone
DuPont, Geneva, Switzerland

ABSTRACT

Test results from an international round robin are presented. The single cantilever beam (SCB) test was used to characterize face sheet/core disbonding in sandwich components in an effort to help standardization. Each of the seven participating laboratories performed a set of five baseline tests using the same protocol, however, using their own specific equipment. In addition, each laboratory performed two sets of tests with altered tests conditions which included using a test fixture with a translating carriage and performing the tests with different loading and unloading speeds. The orientation of the disbond front with respect to the honeycomb core cells was varied and the effect on the fracture toughness was also studied. Additional factors that could influence test results were investigated, such as the use of a saw cut starter disbond as an alternative to Teflon® release film, and the effects of using a face sheet doubler to increase the bending stiffness. For each set of tests, summary results such as load/displacements plots, observed disbond growth location and calculated energy release rates are reported and a comparison of results between labs is presented. Critical strain energy release rate measurements from SCB tests are also compared with measurements made from an alternative test, namely the double cantilever beam with uneven bending moments (DCB-UBM) test, which has been studied extensively at the Technical University of Denmark and proposed as a mixed-mode test standard. A set of recommendations are made with respect to improving the SCB test and a path to standardization is presented.

NOMENCLATURE

a	=	disbond length, mm,
$a_{bending}$	=	minimum disbond length for bending dominated deformation, mm,
a_{cs}	=	minimum disbond length to meet compliance solution requirements, mm,
a_0	=	initial disbond length, mm,
a_{max}	=	maximum disbond length, mm,
a_{prop}	=	maximum amount of disbond propagation during a test, mm,
b	=	width of SCB specimen, mm,
C	=	compliance, δ/P, mm/N,
C_{SCB}	=	compliance of SCB specimen modeled as a cantilever beam on an elastic foundation, mm/N,
CSDE	=	crack surface displacement extrapolation,
DCB-UBM	=	double cantilever beam with uneven bending moments,
D_f	=	compliance coefficient related to the bending rigidity of the disbonded face sheet, 1/Nmm^2,
DTU	=	Technical University of Denmark,
CV	=	coefficient of variation, %,
E_c	=	compressive modulus of core material, MPa,
E_f	=	flexural modulus of disbonded face sheet, MPa,
F_i	=	hyperbolic functions of λ,
G	=	strain energy release rate, kJ/m^2,
G_c^{est}	=	estimated value of interfacial fracture toughness, kJ/m^2,
G_c	=	peel-load-associated interfacial fracture toughness, kJ/m^2,
$G_{xz,f}$	=	shear modulus of disbonded face sheet, MPa,
h_f	=	thickness of face sheet, mm,
h_p	=	loading rod length, mm,
$h_{p,min}$	=	minimum loading rod length, mm,
h_s	=	thickness of steel doubler, mm,
k	=	elastic foundation stiffness, N/mm,
L	=	length of SCB specimen, mm,
LaRC	=	Langley Research Center,
L_b	=	length of intact specimen to remain after maximum disbond length is reached or length of clamped region for DCB-UBM fixture, mm,
L_{hinge}	=	length of specimen under the piano hinge end or end block, mm,
m	=	slope of the load-displacement curve, N/mm,
MBT	=	modified beam theory,
NIAR	=	National Institute for Aviation Research,
P	=	applied load, N,
P_c	=	applied load at the onset of disbond growth, N,
$P_{5\%/\max}$	=	critical load at 5%/max point of loading curve, N,
P_{tab}	=	expected load on the loading tab, N,
P_{vis}	=	critical load when disbond growth is observed to initiate, N,
t_c	=	thickness of core, mm,
t_f	=	thickness of disbonded face sheet, mm,
t_i	=	initial approximation of $t_{f,strength}$, MPa,

$t_{f,smalldisp}$ = minimum disbonded face sheet thickness to avoid geometric non-linearities, mm,
$t_{f,strength}$ = minimum disbonded face sheet thickness to avoid bending failure, mm,
SCB = single cantilever beam,
SD = standard deviation,
U = strain energy, kJ,
V_f = fiber volume fraction, %,
δ = load-point deflection, mm,
Δ = effective disbond extension, mm,
λ = effective ratio of elastic foundation modulus to the cantilever beam stiffness, 1/mm,
σ_c = estimated compressive strength of disbonded face sheet, MPa, and
ψ = phase angle.

1. INTRODUCTION

Typical damage modes in light honeycomb sandwich structures include face sheet/core disbonding[1] and core crushing, both of which pose a threat to the structural integrity of a component. These damage modes are of particular interest to certification authorities since several in-service occurrences, such as rudder structural failure [1] and other control surface malfunctions, have been attributed to disbonding [2]. Extensive studies have shown that face sheet/core disbonding can lead to damage propagation caused by internal pressure changes in the core due to ground-air-ground (GAG) cycles [3, 4]. Future composite structure applications, including, for instance, composite sandwich construction of the fuselage of high-altitude business jets, are also driving a need to understand the phenomenon of disbond growth under generalized load conditions, including maneuvers and gust conditions.

In order to identify, describe and address the phenomenon associated with face sheet/core disbonding, a reliable means of characterizing face sheet/core disbonding must be developed. In monolithic laminates, disbond or delamination is typically characterized by measuring the critical strain energy release rate, G_c, in a unidirectional laminate. A similar approach is utilized here, whereby G_c for face sheet/core disbonding of a sandwich composite, of the type typically applied in aircraft, is measured. However, unlike a delamination in unidirectional monolithic laminates, face sheet/core disbonding in a sandwich will not necessarily be confined to a particular interface. Studies have shown that disbond growth location can be significantly affected by parameters such as core thickness, face sheet thickness, mode-mix and disbond driving force [5, 6]. Characterization tests must therefore be developed that ensure that disbond growth occurs at the same interface as observed in service. Furthermore, face sheet/core disbonding generally takes place under mixed-mode loading conditions, owing to effects from geometry and the typically disparate properties of the constituent materials of a sandwich structure. With these considerations in mind, test methods have been developed for measuring fracture toughness associated with mixed-mode loading [7, 8]. As is the case with delaminations in monolithic laminates, a critical disbonding process in sandwich structure is likely to be mode-I dominated, corresponding to loading scenarios where the face sheet is peeled from the core. The literature contains several examples of test methods designed to measure the critical strain energy release rate associated with face sheet/core peel [9-12]. A review of these test methods [13] indicated that a method based on a single cantilever beam (SCB) geometry, introduced in [9], was most suitable for standardization due to the relative simplicity of the associated test procedure. A procedure for sizing the SCB specimen was later developed [14], utilizing an existing Winkler-type model of a tilted sandwich disbond test geometry [15] that is closely related to the SCB specimen geometry.

In this report, results from an international round robin are presented. This round robin was conducted to assess the suitability of the SCB test as a standardized test method for measuring G_c associated with mode-I dominant loading conditions. First, a general description of the SCB test is given and the test procedure used by the participating round robin laboratories is outlined. Second, a description is given of the double cantilever beam with uneven bending moments (DCB-UBM) test that was used to provide G_c measurements for validating those measurements from the SCB tests. The DCB-UBM test has been studied extensively at the Technical University of Denmark and proposed as a candidate for single-mode and mixed-mode testing [16]. Third, the

[1] *Disbonding* is used as an overarching term similar to face sheet-to-core separation, describing an actual disbond of the face sheet-to-core interface but also a fracture of the core near the face sheet to core interface region.

test setup and equipment used by the seven labs is briefly discussed. Fourth, the results from all participating labs are presented together with observations made during the tests. Fifth, a set of recommendations are made with respect to improving the suggested test method. Finally, unresolved questions are summarized and a path to standardization is presented. Comprehensive details of the specimen manufacturing and test procedure as well as all individual test results from all participating laboratories are provided in appendices.

2. DEVELOPMENT OF STANDARD TEST METHOD FOR FACE SHEET/CORE PEEL

In a recent study, the suitability of five test methods for measuring disbond toughness associated with face sheet/core disbonding was evaluated [13]. An SCB-type configuration, as shown in Figure 1, was identified as the most appropriate test. This determination was based on the following findings:

- the test involves a simple loading fixture;
- disbond front loading conditions were found to be independent of disbond length;
- disbonding was found to take place along or near to the face sheet/core interface, rather than kinking into the core; and
- the data reduction method used for computing disbond toughness involves a straightforward compliance calibration procedure.

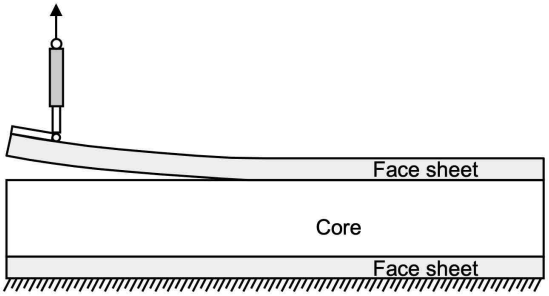

Figure 1. SCB specimen.

A procedure was developed for determining dimensions of the SCB specimen comprised of a given sandwich system [14]. Based on a Winkler foundation model of the SCB specimen [15, 17], this procedure determines specimen dimensions that promote bending-dominated face sheet deformation and discourage damage modes other than disbonding. The procedure also yields specimen dimensions that promote a specific compliance solution exhibited by the SCB specimen, which is of importance for the test data reduction procedure as will be discussed later. While this procedure generally yields SCB specimens that are practical for use as laboratory test coupons, it does not account for the fracture loading conditions in the SCB specimen, only assuming the resulting SCB specimen exhibits mode-I-dominant conditions. A mixed-mode fracture study of SCB specimens with dimensions based on the above procedure was recently performed [18]. This study evaluated the disbond driving force mode-I/II mix of the SCB specimen in terms of the phase angle, ψ, a parameter introduced by Hutchinson [19] that is proportional to the ratio of shear and opening crack-tip displacements. Findings from this mixed-mode fracture study indicated in general that the sizing procedure [14] yields SCB specimens that exhibit mode-I-dominant fracture loading conditions (including SCB specimens that are the subject of this round robin exercise).

However, the study also identified certain sandwich configurations that exhibit significant mixed-mode-I/II fracture loading conditions. Specifically, SCB specimens comprised of low-density core materials (such as *Divinycell H80*[2] foam) reinforced with factsheets above 5.08 mm (0.2 in) in thickness were found to exhibit significant mixed-mode loading conditions.

Based on the studies discussed above [13, 14, 18], a first draft *ASTM International* test standard was written which was utilized in this round robin. The participating laboratories are listed in Table I.

Table I. List of laboratories participating in round robin.

Lab 1	University of Utah, Salt Lake City, UT, USA
Lab 2	National Institute for Aviation Research (NIAR), Wichita State University, Wichita, KS, USA
Lab 3	DuPont International Operations, Geneva, Switzerland
Lab 4	NASA Langley Research Center (LaRC), Hampton, VA, USA
Lab 5	Fraunhofer Institute for Microstructure of Materials and Systems IMWS, Halle, Germany
Lab 6	Airbus Operations GmbH, Bremen, Germany
Lab 7	Technical University of Denmark (DTU), Kgs. Lyngby, Denmark

2.1 SCB Specimen Configuration

The SCB specimen, illustrated in Figure 2, consists of a sandwich construction containing a non-adhesive insert that serves as a disbond initiator on one face sheet/core interface across the entire width, b, and spanning a distance, a_0, along the specimen length.

[2] Divinycell foam core material is a product of DIAB. The use of trade names is not an endorsement by the National Aeronautics and Space Administration

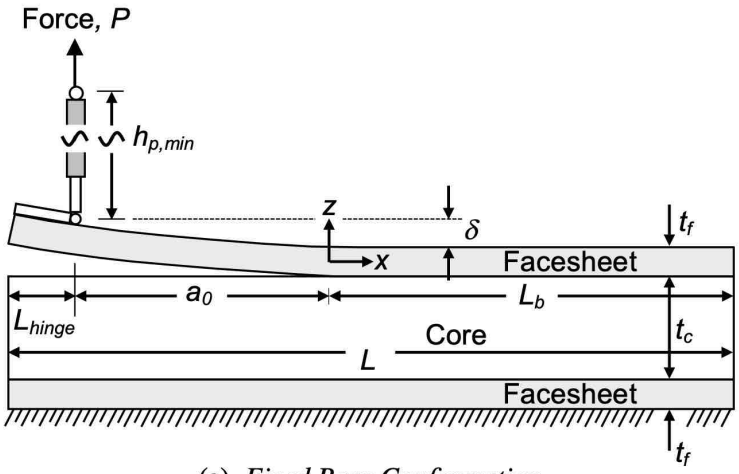

(a). *Fixed Base Configuration*.

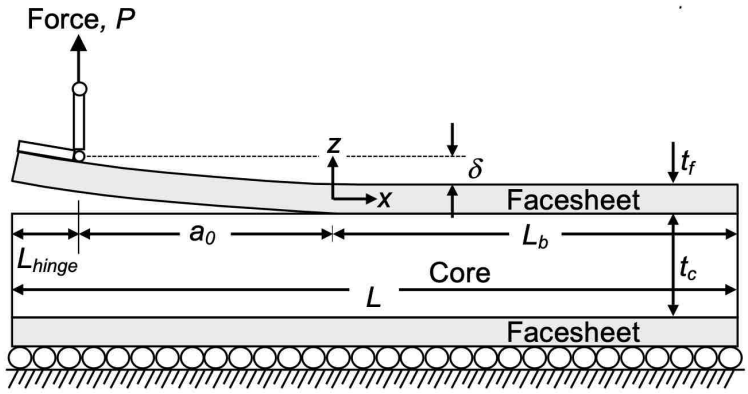

(b). *Translatable Carriage Base Configuration*.

Figure 2. SCB Configurations and dimensions (specimen width, b, into the page).

Opening forces are applied to the SCB specimen by means of a hinge or loading block (hinge depicted in Figure 2) bonded to the end of the disbonded face sheet. The opposing face sheet of the specimen is fixed to a base plate (see Figure 2a) or attached to a sliding carriage (see Figure 2b). The SCB test is performed by controlling either the opening displacement (e.g., gap between face sheet and core interface surfaces in the plane of load application) or the crosshead movement, while the load and disbond length are recorded. Nominal dimensions and constituent materials of the SCB specimen used in this round robin are given in
Table II.

Table II. SCB specimen dimensions and materials[3].

a_0	12.7 mm (0.5 in)
b	50.8 mm (2.0 in)
$h_{p,min}$	500 mm (20 in)
L	305 mm (12 in)
L_{hinge}	25.4 mm (1.0 in)
t_c	25.4 mm (1.0 in)
t_f	0.772 mm (0.0304 in)
Face sheet	T650/5320 PW Layup (4 plies): $[45/0]_s$ 0-dir along specimen length
Core	*Hexcel HexWeb® HRH-10®:* Cell size = 3.2 mm (0.125 in) Density = 48kg/m^3 (3lb/ft^3)

2.2 SCB Specimen Manufacturing[3]

The specimens were manufactured at NIAR. The face sheets were made of four plies [45/0/0/45] of *Cytec T650/5320EO* graphite/epoxy plain weave fabric [20] with a nominal total cured thickness of 0.79 mm (0.0304 in). The core consisted of 25.4-mm-thick (1.0 in) *Hexcel HexWeb® HRH-10® Nomex®* honeycomb with a cell size of 3.2 mm (0.125 in) and a density of 48 kg/m^3 (3lb/ft^3) [21]. Material properties are listed in Table III.

Table III. Face sheet and core properties[3].

Ply properties# : E_{11} = 67.4 GPa (9.8 Msi) , G_{12} ≈ 4 GPa (5.8 Msi), ν_{12} = 0.06			
E_f = 24.73 GPa * (3.56 Msi)	E_c = 138 MPa ¶ (20.02 ksi)	Min G_c^{est} = 0.69 kJ/m^2 † (3.94 in-lb/in^2)	Max G_c^{est} = 0.90 kJ/m^2 † (5.13 in-lb/in^2)

Sources: # NIAR, * Laminated plate theory using NIAR data, ¶ Hexcel, † Ref. 6.

Sandwich plates measuring 609.6 mm x 771.2 mm (24 in x 28 in) were manufactured with a 38.1-mm (1.5-in) -wide *Teflon®* insert, which was placed on the bag side of the sandwich assembly. The insert was located between the core and face sheet in a region of the sandwich structure assembly without any film adhesive. The vacuum-bagged assembly was co-bonded using FM300-2 film adhesive in an oven (out-of-autoclave) at 221.1°C (250°F) for 75 minutes and then at 143.3°C (290°F) for 150 minutes, with a ramp rate of 2.8°C (5°F) per minute. The plate was cut into 50.8 mm x 304.8 mm (2 in x 12 in) long SCB specimens as shown in Figure *3*a. The majority of the specimens were manufactured such that the disbond would advance along the ribbon direction (L) as shown in Figure 3b. Ten specimens were manufactured such that the disbond advance along the expansion direction (W). In addition, 10 disbond specimens were manufactured

[3] Sandwich panels were fabricated and specimens were cut using processes, specifications and dimensions in US customary units.

without *Teflon*® inserts and the starter disbond was cut into the specimens as shown in Figure 3c. A complete list of all specimens manufactured is provided in appendix A.

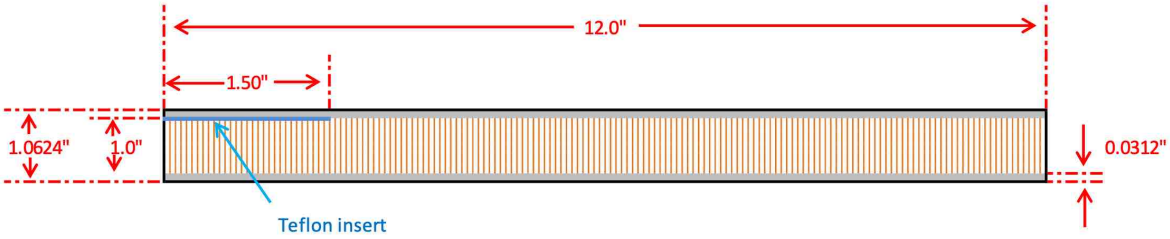

(a). *SCB specimen dimensions*.

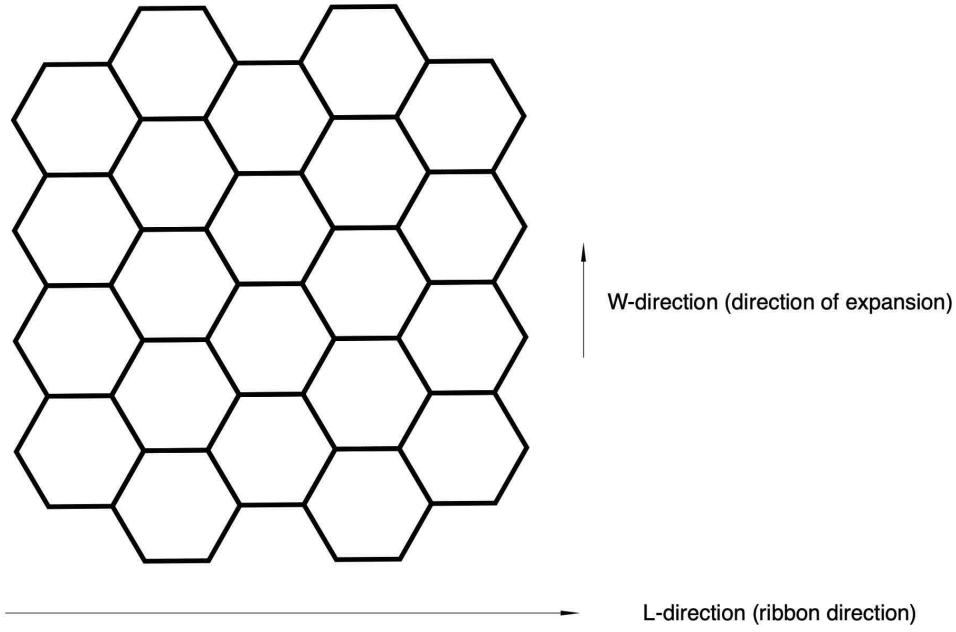

(b). *Honeycomb orientation*.

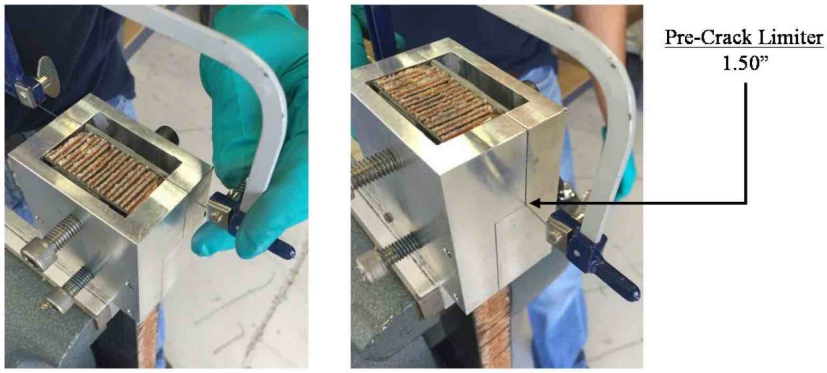

(c). *Introduction of saw cut starter crack*.

Figure 3. *SCB round robin rest specimen configuration and manufacturing*[3].

2.3 Round Robin Test Procedure

The SCB test procedure written into the first draft ASTM standard was followed during testing in the round robin exercise. A brief description of the test procedure used in the round robin exercise is presented in what follows. Appendix B contains the actual SCB test protocol used by all participating round robin laboratories.

SCB tests were performed using the fixed-base configuration illustrated in Figure 2a. A picture of an actual SCB loading fixture (with an SCB specimen in position) at one of the round robin laboratories is contained in Figure 4. Cameras were mounted to view disbond growth along both edges of a specimen (edges painted white to enhance view of disbond front location). Specimens were loaded in displacement control at a rate of 5 mm/min and unloaded at the same rate after approximately 10 mm of disbond growth had taken place. Load-displacement response and disbond growth path were recorded during the entire loading cycle. This procedure was repeated five times.

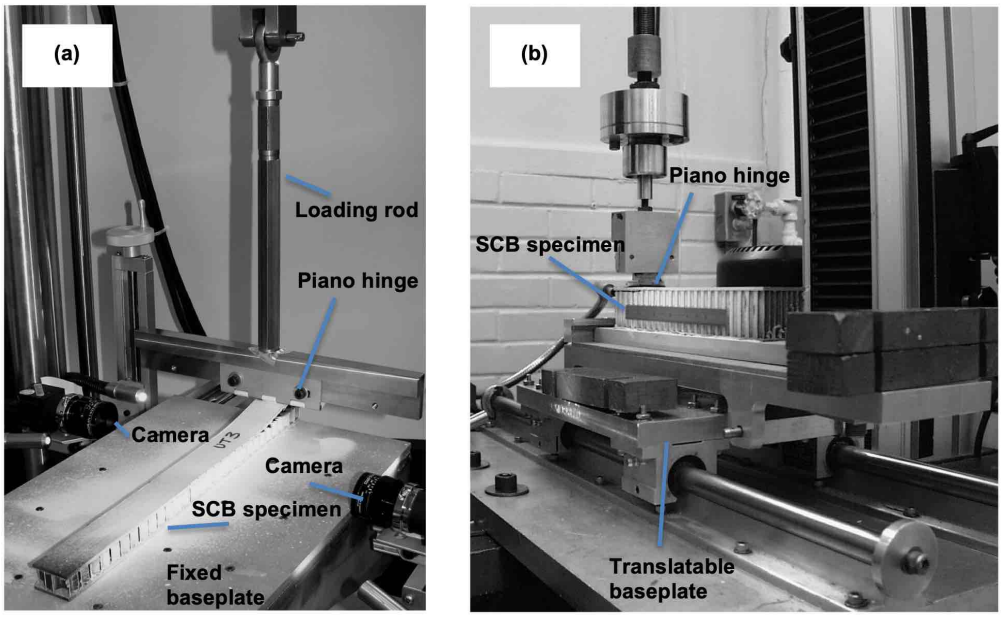

(a). *Fixed Base Plate* (b). *Translatable Carriage Base Plate*

Figure 4. Test fixtures.

Two data reduction methods were used to calculate the mode-I critical energy release rate or peel-load-associated interfacial fracture toughness, G_{Ic}, referred to here as the modified beam theory (MBT) method and the area method. The MBT method assumes the SCB specimen compliance solution takes the following form:

$$C_{SCB} = D_f[a + \Delta]^3 \tag{1}$$

where D_f is a coefficient related to the bending rigidity of the disbonded face sheet of the SCB specimen and Δ is a disbond length extension factor that serves to adjust the compliance solutions to account for the non-zero slope boundary condition of the disbonded face sheet. This factor is

evaluated from the SCB test data as described in appendix B. The specimen sizing method mentioned previously acts to encourage SCB specimens adopting the compliance solution of Equation 1 [14].

Starting with the change of compliance given by Equation 1 with respect to disbond length, the Irwin-Kies relation [22] is obtained and used to calculated G_c:

$$G_{Ic} = \frac{3P\delta}{2b(a+|\Delta|)} \tag{2}$$

where P and δ are load and load-point displacement at a given increment of disbond growth, respectively.

The second data reduction method, the area method, yields a single calculation of G_{Ic} corresponding to each loading cycle using the following expression:

$$G_{Ic} = \frac{dU}{dA} \tag{3}$$

where dU is the energy dissipated during a disbond growth increment corresponding to an increase in disbond area, dA. Details of this data reduction method are given in appendix B.

2.4 Test Matrix

All seven labs ran one set of five specimens under the same condition (referred to as baseline tests) as part of the round robin exercise. These baseline tests were used to study lab-to-lab variation. Details of the baseline tests are included in what follows and the complete test matrix from the round robin exercise is presented in Table IV.

- Specimens contained a *Teflon®* insert acting as a starter disbond, spanning 38.1 mm (1.5 in) along the specimen length, as shown in Figure 3a. To prevent bonding, this *Teflon®* insert was placed directly between the core and the face sheet without any film adhesive.
- Disbond growth occurred along the ribbon (L) direction as shown in Figure 3b.
- Tests involved the fixed SCB test fixture illustrated in Figure 2a.
- Specimens were loaded in displacement control at a rate of 5 mm/min and were unloaded at a rate of 30 mm/min after approximately 10 mm of disbond growth had taken place.
- The end of each loading cycle was defined as the instant applied load reached 0 N.

Further, each lab ran two additional sets of tests with five specimens each. These tests deviated from the baseline and were designed to study the effects of different specimen and test configurations on specimen response and G_c measurements. The deviations were as follows:

- Pre-inserted disbond type: A 38.1-mm (1.5-in) -long saw cut starter disbond as an alternative to the *Teflon®* insert.
- Disbond growth direction: Specimens were cut from the parent plate in an orientation that resulted in disbonding occurring along the transverse (W) direction. (Figure 3b)
- SCB fixture type: Tests were performed using the sliding carriage system (Figure 2b).

- Loading rate: Tests were conducted at loading rates of 10 mm/min, 20 mm/min, and 30 mm/min. Unloading rate was kept at 30 mm/min except for labs 1 and 4 which used 5 mm/min.
- Specimen unloading condition: Specimens were unloaded to the original load-point displacement position to evaluate any residual loading
- Specimen reinforcement: Specimens were tested with reinforcement layers (doublers) of various thickness.

Table IV. Test matrix.

	Baseline Test	Additional Tests	
	Conditions	**Conditions**	**Participating Labs**
Disbond directions	L	W	3, 5
Starter Disbond	Teflon® (T)	Saw Cut	2, 6
Doubler Thickness (mm)	0	3.18 2.38 1.59	4 6 7
Fixture Type: Fixed (F), Translating (T)	F	T	2, 7
Unloading	0 N	0 mm	1, 3, 4, 5, 6
Loading Speed (mm/min)	5	10 20 30	1 3 5
Unloading Speed (mm/min)	30*	=	1 3 5
Δa per loop (mm)	10	=	-
Number of loops	> 5	=	-

= same as baseline

*5 mm/min unloading used by labs 1 and 4

3. ALTERNATE METHOD BASED ON THE DCB-UBM TEST

3.1 DCB-UBM Specimen Configuration

The DCB-UBM, shown in Figure 5, was first introduced by Sørensen et al. [16] for fracture testing in laminated composites. The test configuration comprises a double cantilever beam (DCB) specimen loaded with bending moments as shown in Figure 5a, where the moments M_1 and M_2 are applied in opposite directions. The aim of the test is to propagate the disbond between two arms by controlling the ratio of bending moments between two beams, defined as moment ratio, $MR = M_1/M_2$. For specific elastic properties of the beams, local mode-mixity at the disbond tip depends on MR. The local mode-mixity is expressed using the phase angle (ψ), which can be roughly described as the ratio of shear and normal loading at the crack tip. Therefore, by maintaining a constant MR during fracture testing, the disbond propagates under a constant ψ. It should also be noted that since the DCB-UBM fracture specimen enables testing under a constant mode-mixity it is not necessary to continuously monitor the disbond position. The failure criterion for mixed-mode disbond propagation along an interface is of the form [19]:

$$G = \Gamma(\psi) \tag{4}$$

where Γ is the interface fracture toughness and G is the energy release rate. The traditional DCB-UBM test rig comprises a system with long wires, which is not suitable for rapid load changes usually encountered when disbond jumps are non-uniform as well as during cyclic loading conditions [23]. A compact fatigue-rated, stand-alone test rig was constructed and assembled in-house at the DTU Structural Lab. Fracture testing was performed using this setup and the results of round robin testing are presented below. A schematic illustration of this novel test rig is shown in Figure 5b with moments M_1 and M_2 applied in the same direction [24].

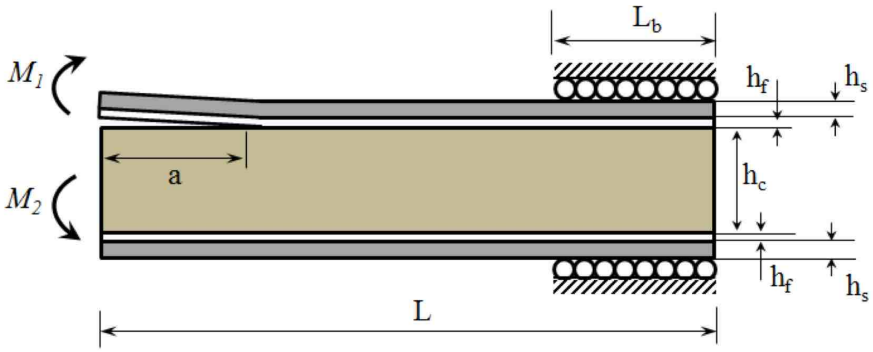

(a). *DCB-UBM specimen reinforced with steel doubler layers, loaded with end moments.*

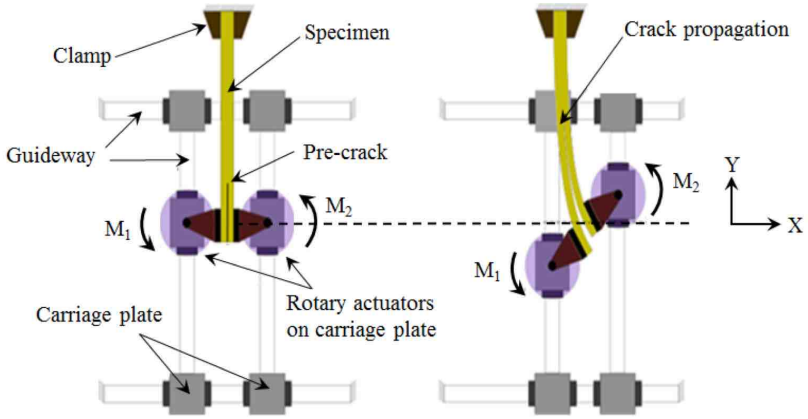

(b). *Schematic illustration of test principle of DCB-UBM.*

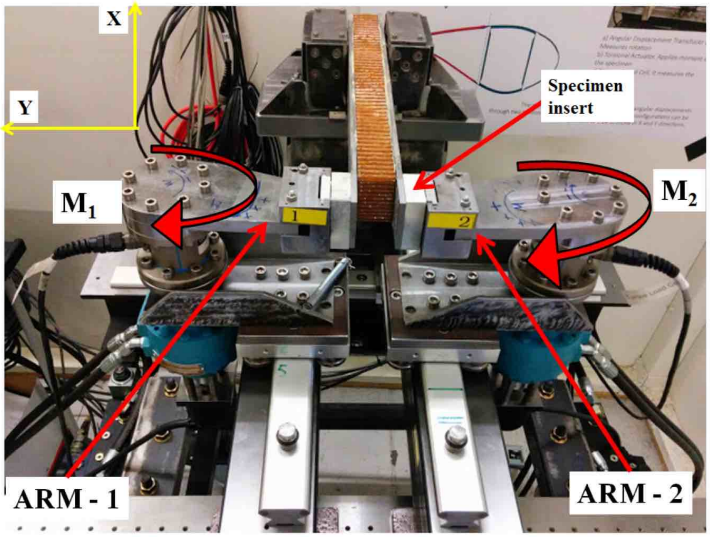

(c). *Test Machine and DCB-UBM Test Fixture.*

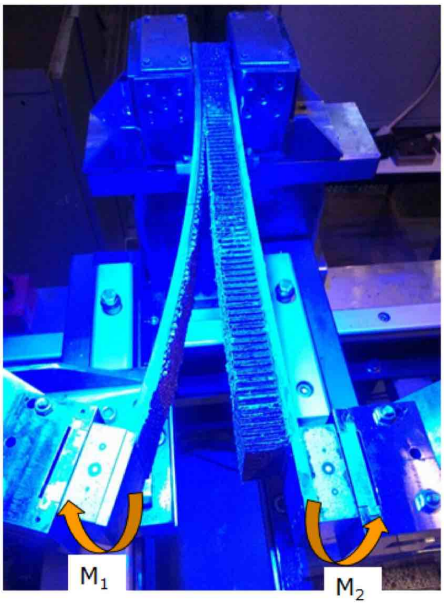

(d). *Specimen under loading.*

Figure 5. DCB-UBM specimen.

In the current test rig, bending moments are applied on specimen edges with the aid of two independent torsional actuators. The disbonded flanks of the fracture specimen are held between

the two actuators and are supported by rollers on the opposite end. The rollers provide support without any vertical loading at the specimen end. The actuator assembly is supported on carriage plates mounted on rollers, enabling the specimen to slide in the *x*-*y* plane as the disbond propagates. The basic principle of the modified DCB-UBM specimen with independent torsional actuators, mounted on carriage plate-roller system, is illustrated in Figure 5b.

The DCB-UBM fracture testing in laminates was extended to perform fracture testing of sandwich composites by Lundsgaard-Larsen et al. [7] by attaching reinforcement layers (referred to as "doublers") on both sides of face sheets. The attachment of reinforcement layers onto specimen faces provides several advantages:

- increases the extent of the fracture process zone (for generating cohesive laws);
- enables testing of sandwich specimens with thin face sheets, as it makes it easy to clamp specimen edges onto actuators arms; and
- enables fracture testing of specimens with soft cores.

The reinforcement layers are chosen to prevent plastic deformation and to keep the fracture analysis in the geometrically linear regime. A 6-mm-thick steel plate material with a yield strength $\sigma_y > 800$ MPa was chosen as reinforcement layers.

3.2 DCB-UBM Specimen Manufacturing

The DCB-UBM sandwich specimens were manufactured at NIAR using the process described in section 2.2. The steel chosen as reinforcement layers was *IMPAX*, manufactured by *Uddeholm*, Sweden, with a thickness of 6 mm. The reinforcement layers were bonded to the specimen faces using two-component epoxy-based adhesive, *Araldite® 2015*. Prior to bonding, the specimen faces were mechanically abraded with sandpaper and were then cleaned with acetone. The reinforcement layers were sandblasted and thoroughly cleaned with acetone prior to bonding. The bonded specimens were cured at room temperature for 24 hours.

3.3 DCB-UBM Test Procedure

3.3.1 Test Setup

The DCB-UBM fracture testing is inherently *G*-controlled in nature, as the mode-mixity is held constant throughout the test. A two-channel *MTS FlexTest™ SE* controller is used to control the two independent torsion actuators. Two 565-Nm torsion load cells attached atop the actuators measure the applied moment. Fracture tests were carried out in rotation control and a control algorithm was implemented such that the test is carried out under a constant *MR*. Rotation of specimen edges were measured using angular displacement transducers attached beneath the actuators. Rotation command and *MR* were manually input to begin the test. The controller applied rotation command to Arm 1 and applies a moment on Arm 2 such that the ratio between the two arms ($MR = M_1/M_2$) is held constant as provided before the start of the test. Both rotation and moment from both actuators were measured continuously at 10 Hz using *MTS TestSuite™*. The specimen is mounted such that side containing the pre-disbond is treated as Arm 1 in Figure 5c with moments M_1 and M_2 applied in the same direction. Each specimen was loaded in rotation control at a rate of 5 deg/min. The test was stopped by manually pressing stop button in the program when the disbond propagated > 20 mm. A deformed specimen is shown in Figure 5d, where the moments M_1 and M_2 are applied in opposite directions to create the desired mode-I opening. Markings on the reinforcement layer were used as an aid to check if the disbond

propagated more than 20 mm. The specimens were unloaded manually after the program was stopped and data was not collected.

Prior to start of the test, the *MR* corresponding to the ψ at which fracture characterization was intended to be performed was selected. A numerical mode-mixity method, the crack surface displacement extrapolation (CSDE) method [23], was utilized to map various *MR* vs. ψ values to pick the *MR* values. Two *MR* values corresponding to predominant mode-I conditions were picked (*MR* = −5, ψ = 17° and *MR* = −2, ψ = 15°). Specimens: 8-7-1-L-T-U-N-F-05-1 and 8-7-1-L-T-U-N-F-05-2 were tested with *MR* = −5, and Specimens 8-7-1-L-T-U-N-F-05-3, 8-7-1-L-T-U-N-F-05-4 and 8-7-1-L-T-U-N-F-05-5 were tested with *MR* = −2. The test matrix of the DCB-UBM test campaign is presented in Table V.

Table V. Test Matrix for DCB-UBM tests.

	Baseline Test Conditions
Disbond direction	L
Starter Disbond	Teflon® (T)
Doubler thickness (mm)	6
Unloading	0 deg
Loading speed (deg/min)	5
Unloading speed (mm/min)	--
Moment ratios	−5 and −2

3.3.2 Interfacial Fracture Toughness Calculations

The fracture energy obtained from DCB-UBM experiments is calculated using strain energy release rate expressions that relate to the moments applied on each arm. The moment on each arm can be expressed as:

$$M = \frac{EI\theta}{a} \tag{5}$$

where *EI* is the flexural rigidity and θ is the rotation of the disbonded flank.

The critical energy release rate, expressed in terms of the applied moments is then given by [23]:

$$G_c = \frac{1}{2A}\left[\frac{M_{1c}^2}{(EI)_1} + \frac{M_{2c}^2}{(EI)_2}\right] \tag{6}$$

where M_c is the critical moment which initiates disbond propagation.

The *EI* of the beams can also be obtained using laminate beam theory using *A*, *B* and *D* stiffness matrices of each beam as: $D - B^2/A$. The critical moment can be identified as the sudden departure in the slope of *M vs.* θ plot. For an equal loading case with symmetric beams, $M_1 = M_2$ and equal compliance of the arms $C_1 = C_2 = C$, which leads to dC/dA = 2/EI.

A typical plot of moment vs. rotation of the disbonded arm is provided in Figure 6a. The disbonded arm is referred to as the arm which contains the initial disbond and is subjected to moment, M_1

(see Figure 5c). A typical plot of G vs. rotation is shown in Figure 6b. The G_{Ic} value is associated with the deviation from a linear slope in the G vs. rotation plot. Alternatively, critical moments can be identified from the moment vs. rotation plots. The fracture toughness values obtained using DCB-UBM test are shown in Figure 6c.

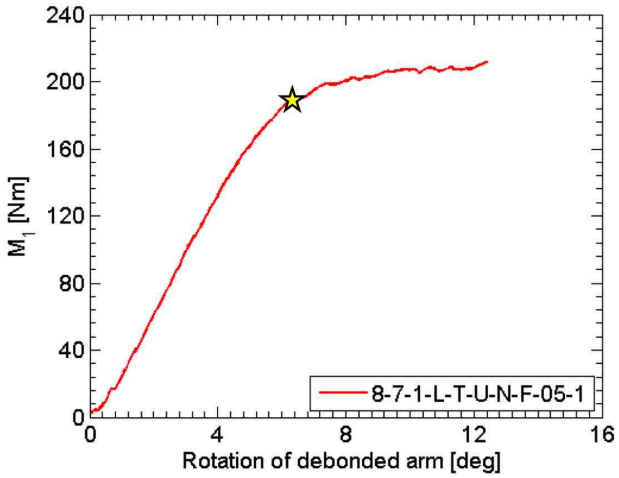

(a). *Moment vs. rotation plot for DCB-UBM specimen.*

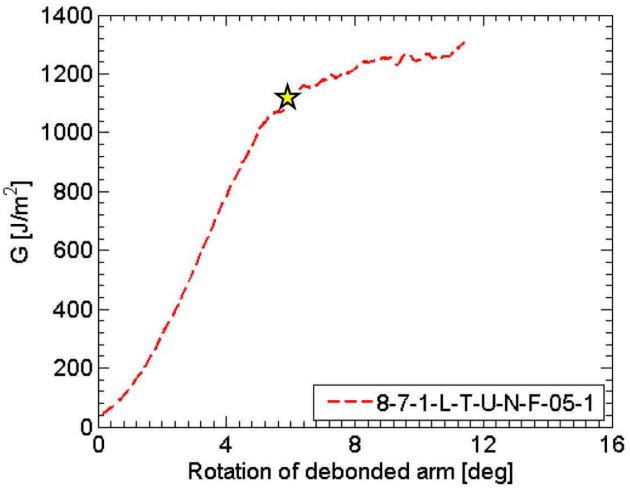

(b). *Energy-release rate vs. rotation of debonded arm for DCB-UBM specimen. Critical energy release rate (G_{Ic}) is highlighted*

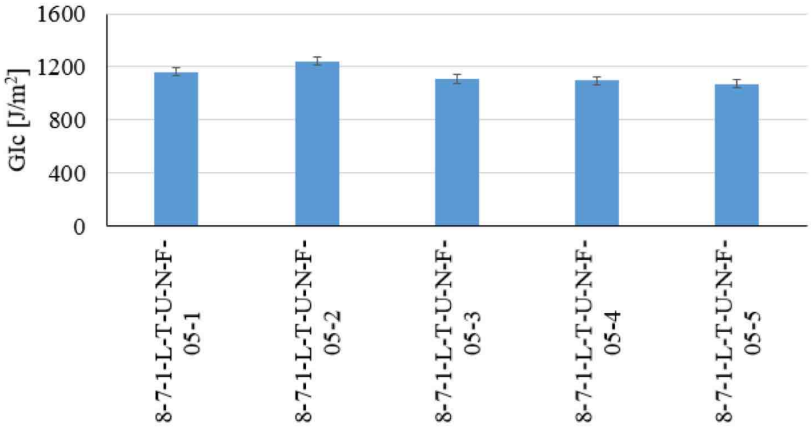

(c). *Fracture toughness (G_{Ic}) values obtained for DCB-UBM specimens.*

Figure 6. Typical results obtained for DCB-UBM specimens tested at DTU.

For all specimens, the disbond was found to propagate just beneath the meniscus layer. For specimen 8-7-1-L-T-U-N-F-05-3 (MR = −5), the disbond kinked into the core for a small distance and dived back to the earlier path. The reason of disbond diving into the core may be due to resin rich cells which were present in the disbond path.

4. FRACTURE TEST EQUIPMENT

Each of the participating laboratories used equipment that was available at the facility and that local operators were familiar with. A summary of the key SCB test parameters of each laboratory is presented in Table VI. The general test procedure was very similar between laboratories, as mandated by the round robin test protocol in appendix B. Deviations in test parameters between laboratories included data sample rate, pre-test conditioning, load cell capacity, load frame type, and disbond tracking method. Specific details of the SCB test equipment of each laboratory are given in appendix C.

Table VI. Inter-laboratory baseline SCB test parameters.

	Laboratory						
Test Parameter	1	2	3	4	5	6	7
Load frame	Electro-mechanical	Hydraulic	Electro-mechanical	Hydraulic	Electro-mechanical	Electro-mechanical	Hydraulic
Specimen-fixture base attachment	Clamp	Clamp	RT cure adhesive	RT-cure adhesive	Clamp	Clamp	RT-cure adhesive
Load rod attachment	Hinge	Hinge	Block	Hinge	Hinge	Block	Hinge
Load rod length	610 mm	610 mm	500 mm	500 mm	520 mm	326 mm	620 mm
Load cell capacity	250 kN	2.2 kN (500 lbf)	1 kN	25 kN	1 kN	2.5 kN	5 kN
Load-point displacement indicator	Crosshead	Crosshead	Crosshead	Crosshead	Crosshead	Crosshead	Piston LVDT
Test control mode	Displacement	Displacement	Displacement	Displacement	Displacement	Displacement	Displacement
Loading rate	Load: 5mm/min Unload: 5 mm/min	Load: 5mm/min Unload: 30mm/min	Load: 5mm/min Unload: 30mm/min	Load: 5mm/min Unload: 5mm/min	Load: 5mm/min Unload: 30mm/min	Load: 5mm/min Unload: 30mm/min	Load: 5mm/min Unload: 30mm/min
Load-displacement data sample rate	5 Hz	1 Hz	5 Hz	20 Hz	2 Hz	1 Hz	10 Hz
Disbond monitoring method	10x-50x digital cameras on both specimen edges	Digital microscopes on both specimen edges	Digital camera on one specimen edge	Digital cameras on both specimen edges	Digital cameras on both specimen edges	25X digital camera: one edge during test	Digital cameras on both specimen edges
Disbond-test data synching	Manual	Manual	Software automated	Software automated	Manual	Manual	Manual
Special specimen preparation	Trim core along specimen edges	None	1-day conditioning at 20C and 60% RH	None	None	None	None
Test conditions	RT, ambient	RT, ambient	20C, 60% RH	RT, ambient	RT, ambient	RT, ambient	RT, ambient

5. TEST RESULTS AND OBSERVATIONS

Each participating laboratory performed a set of five SCB baseline tests using the same protocol discussed previously, however, using their own specific equipment listed in Table VI. Additionally, they performed two sets with altered test conditions introduced in Table VI and listed in the test matrix (see Table IV). For each set of tests, summary results such as load vs. displacement plots, observed disbond growth location and calculated energy release rates are presented by each lab in the following section. A comparison of results between labs is also discussed. Individual test results can be found in the appendices.

5.1 Lab 1: University of Utah, Salt Lake City, UT, USA

5.1.1 Baseline Testing

The baseline test specimens followed the majority of the parameters outlined in Table IV with two differences. Each specimen was unloaded at a rate of 5 mm/min as opposed to 30 mm/min, and the starter disbond was machined into the core just below the face sheet-adhesive interface. The average length of the starter disbond in the five specimens was 13.7 mm. During each loading loop, the disbond grew by an average length of 10.2 mm (i.e., the average disbond growth produced in the five specimens). The approximate total times to complete six loading and unloading cycles are listed in Table VII.

Table VII. Approximate total time to complete six load/unload cycles.

Test Rate (mm/min)	Time (min)
5	69
10	38
20	18
30	13
40	10

Typical results from the baseline tests are shown in Figure 7a for the first coupon, 1-1-1-L-S-X-N-F-30-06. The highest load value of 158 N was achieved during the initial load cycle, and the average load during the sixth cycle approximately equaled 57.4 N. Disbonding took place in a stable manner until a honeycomb cell wall, or node, was reached. The load then increased until enough energy was available to grow the disbond beyond this position. The through-thickness location of the disbond stabilized immediately within the core and below the meniscus of the cured film adhesive as shown in Figure 7b.

The average values (from all five baseline tests) of the critical strain energy release rate for each loading cycle are show in Figure 7c. The values of G_c for the first, second, and third cycles were 991±104 J/m^2, 991±34.8 J/m^2, and 1000±53.2 J/m^2 respectively. Note that although the disbond in initial load cycle grew from a machined starter disbond, the value of G_c is comparable to those measured in the subsequent two cycles. The lowest value of G_c was measured during the fifth load cycle and is equal to 931±117 J/m^2. The total average value of G_c for all baseline specimens was 971±27.8 J/m^2.

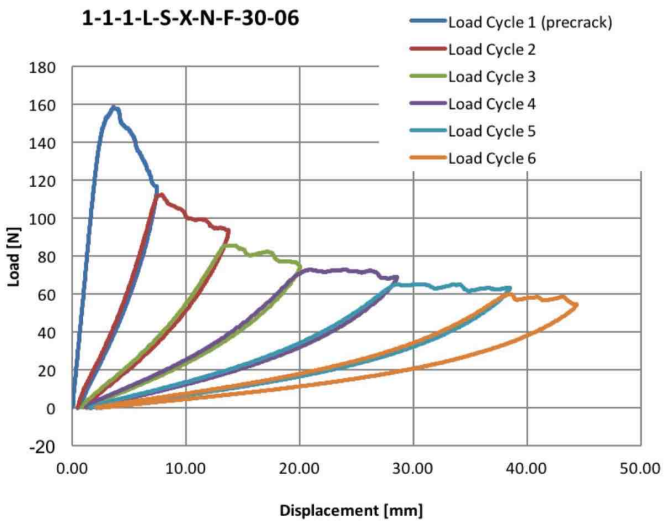

(a). *Typical load/displacement plot with six loading and unloading cycles.*

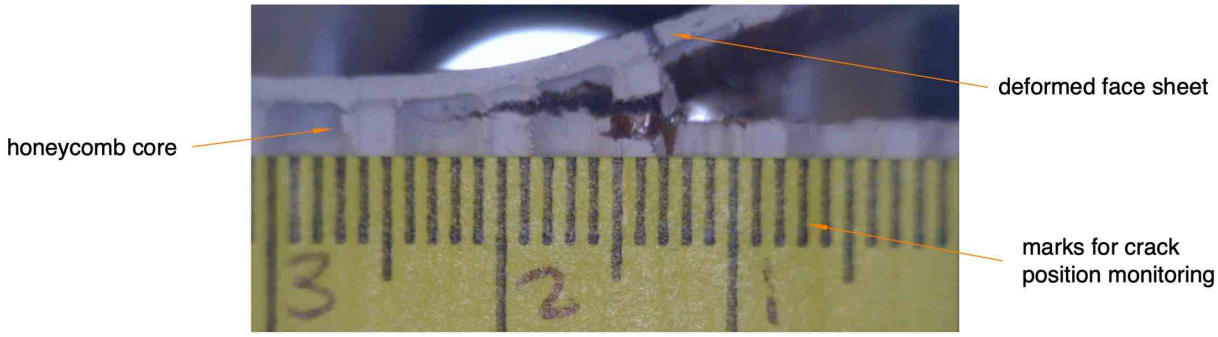

(b). *Stabilized disbond location grown from machined starter crack for the baseline tests.*

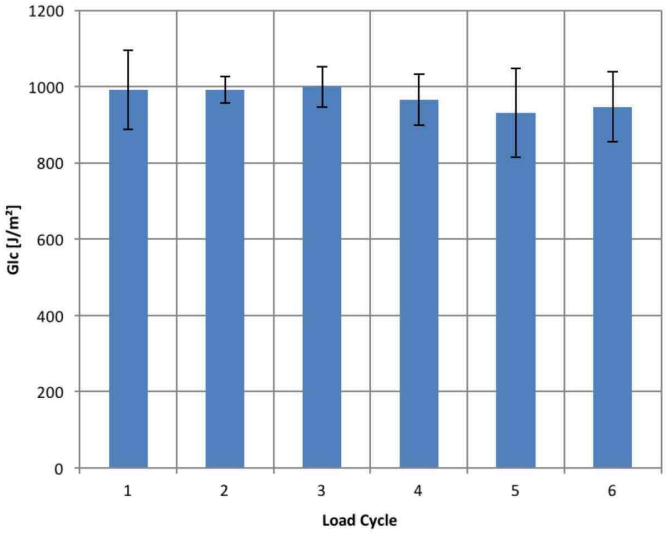

(c). *Average values of the critical strain energy release rate for the baseline specimens.*

Figure 7. Typical results obtained from baseline testing at The University of Utah.

5.1.2 Additional Tests

Zero-Displacement Effects

The first set of additional tests involved unloading a specimen until the load-point returned to its original position (referred to here as the zero-displacement condition). Two specimens included a Teflon® insert-based starter disbond, and the remaining three included machined starter disbonds. Unloading the specimens to zero displacement caused a compressive force to develop in each specimen, as shown in Figure 8.

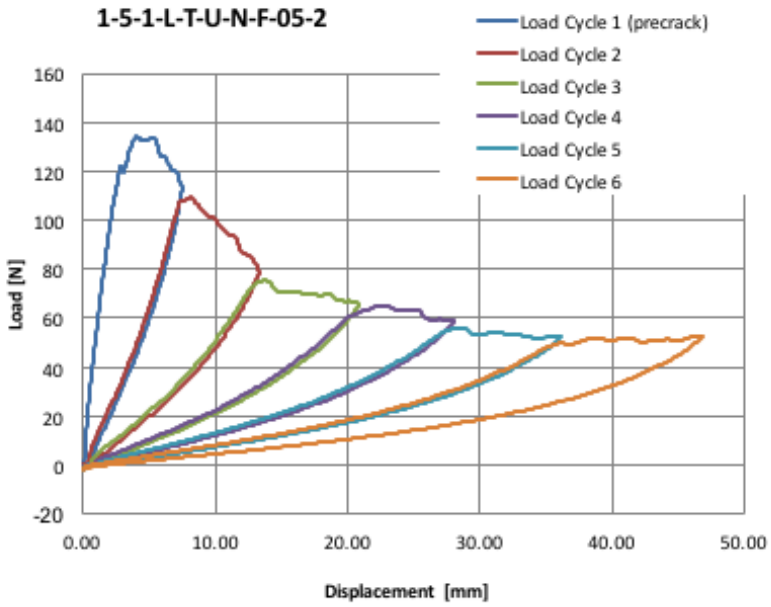

(a). *Typical load vs. displacement diagram*.

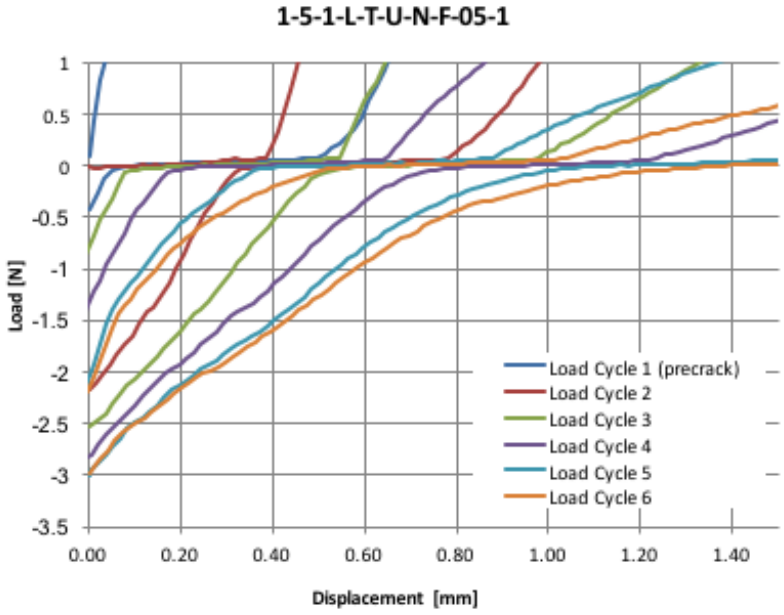

(b). *Hysteresis loops associated with developed compressive load.*

Figure 8. Typical results obtained from zero-displacement tests using a manufactured starter disbond.

The compressive force was attributed to the misalignment of fracture surfaces remaining on the underside of the face sheet and the topside of the core. The magnitude of these compressive forces ranged between 0.3 N and 3.0 N for all the baseline test specimens. The second load cycle typically produced the smallest compressive force, while the largest force was observed during the sixth load cycle.

The local detail of Figure 8a near zero load and zero displacement is depicted separated and enlarged in Figure 8b to illustrate the enclosed loops of dissipated energy, dU, associated with the compressive forces. The algorithm used to quantify the total dissipated energy treated the compressive loops additively when determining the total fracture toughness. This approach would only be valid if the disbond length increased accordingly; however, no measurable increase in length was detected. The magnitude of the largest sixth loop was found to be on the order of 1.36 J, and is small when compared to a typical total quantity of 473 J. For this reason, no alteration of the algorithm was made, and its effect was neglected. However, the compressive hysteresis loops should not be ignored, primarily when they are nearer in magnitude to their positive counterparts.

Growing the disbond from the *Teflon*® insert has the potential to cause difficulties during the first load cycle. For specimen 1-5-1-L-T-U-N-F-05-2, the load dropped by approximately 2.69 N when it reached a value of 122 N without a measurable change to the disbond length. This issue was attributed to the resin-rich zone directly behind the manufactured starter disbond. After growing the disbond through the resin-rich zone, a natural disbond front was formed and sudden decreases in load were associated with disbond growth within the core. The disbond quickly propagated into the core material once the natural disbond front was formed as shown in Figure 9a. The disbond continued along the specimen length on a plane parallel to the SCB fixture base as shown in Figure 9b. The through-the-thickness depth of the disbond maintained a level approximately equal to the size of the adhesive meniscus within the honeycomb cell. The disbond increased in length in a stable manner until a honeycomb cell wall, or node, was reached. The load then increased until enough energy was available to grow the disbond through this honeycomb node region.

The final three baseline test specimens differed from the first two only by the existence of a machined starter disbond. The starter disbond was introduced into the core of each specimen using a snap-off blade from a typical utility knife. The disbond exhibited semi-stable growth as shown by the peaks and valleys for a given load cycle in Figure 10a. The disbond stabilized at a level below the adhesive meniscus and maintained this level for the duration of the experiment, as shown in Figure 10b.

All five zero-displacement specimens initially displayed a linear load vs. displacement characteristic but quickly transformed into a non-linear, or concave upward, load vs. displacement behavior. This condition was attributed to the geometrical non-linear behavior associated with bending the relatively thin face sheet. During the first load cycle, the ratio of maximum crosshead deflection to corresponding disbond length had an average value of 0.30. These values increased for load cycles two through six, producing ratios of 0.37, 0.46, 0.52, 0.57, and 0.62, respectively. Additionally, the unloading portion of a cycle consistently overlapped by the subsequent loading of the next cycle.

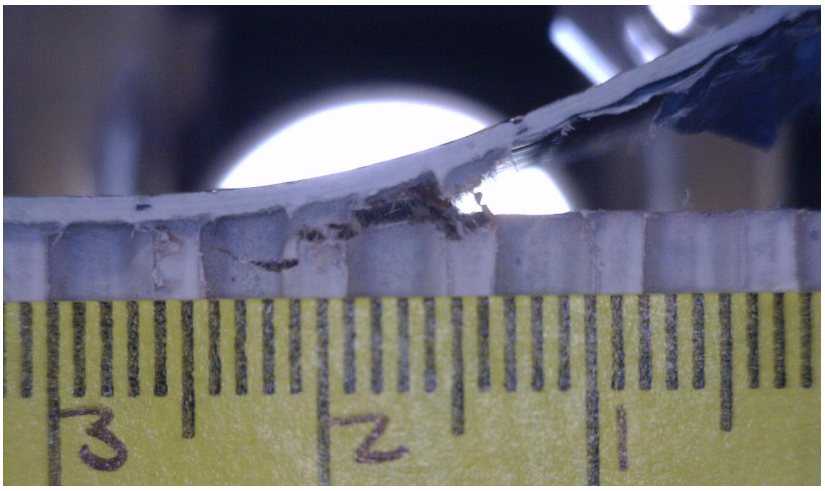

(a). *Initial disbond growth from manufactured starter crack into core material.*

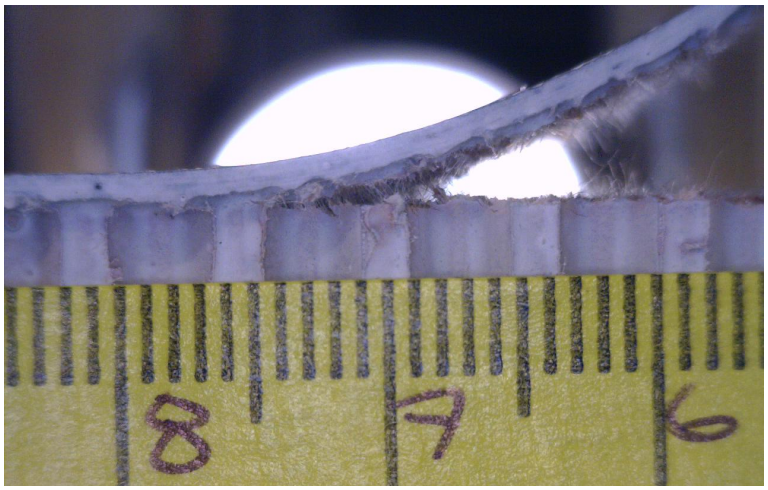

(b). *Maintained depth of disbond through to final load cycle.*

Figure 9. Through-the-thickness disbond location of zero-displacement specimens.

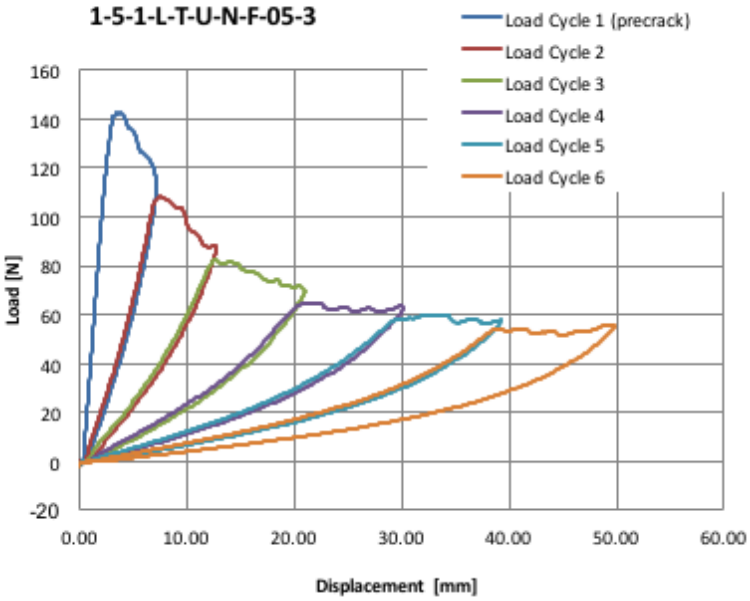

(a). *Load vs. displacement diagram*

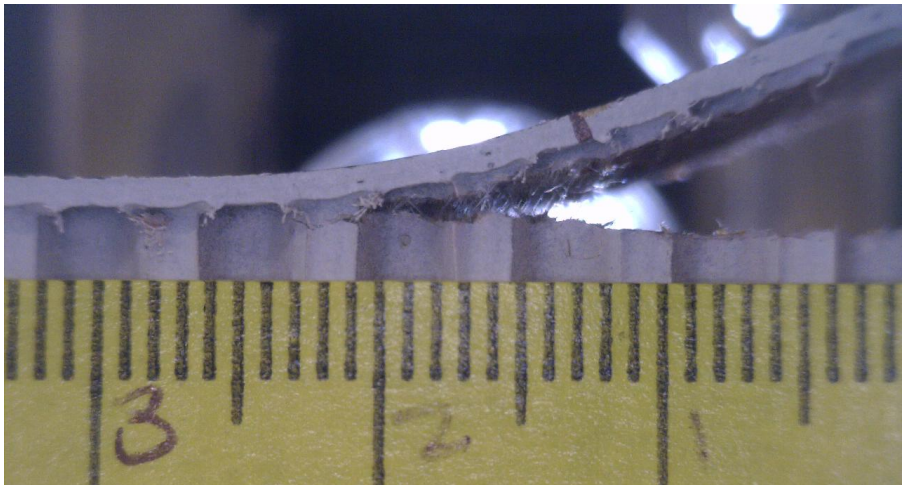

(b). *Stabilized depth of disbond*

Figure 10. Typical results obtained from zero-displacement testing from The University of Utah using a machined starter disbond.

As shown in Figure 11a, G_c for the first load cycle, 773±18.8 J/m^2, was significantly less than the remaining five loading cycles. The greatest G_c value was 933±67.8 J/m^2 and was produced during the third loading cycle. The value of G_c varied among all five baseline specimens for a given load cycle as shown in Figure 11b. The first cycle had the least amount of variation, even though it included the two different starter disbond types. This result illustrates the applicability of both starter disbond methods.

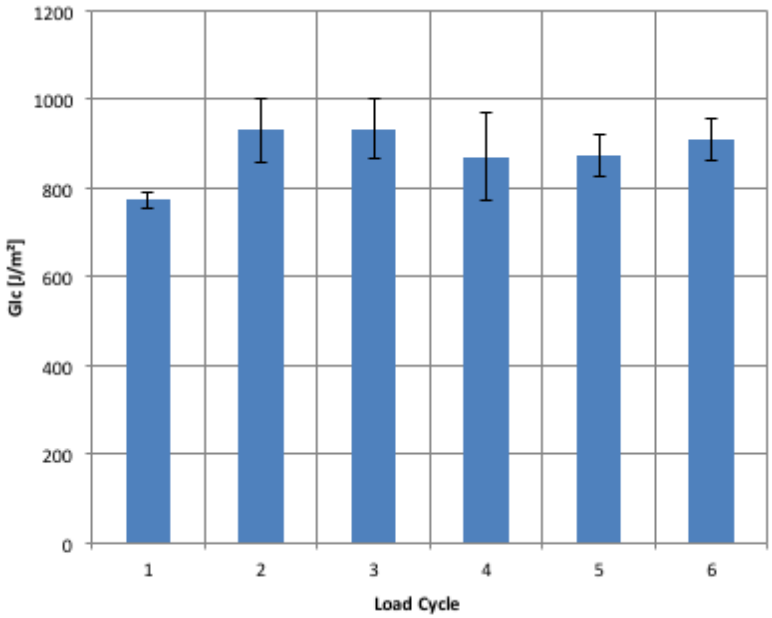

(a). *Average for all specimens at a given load cycle.*

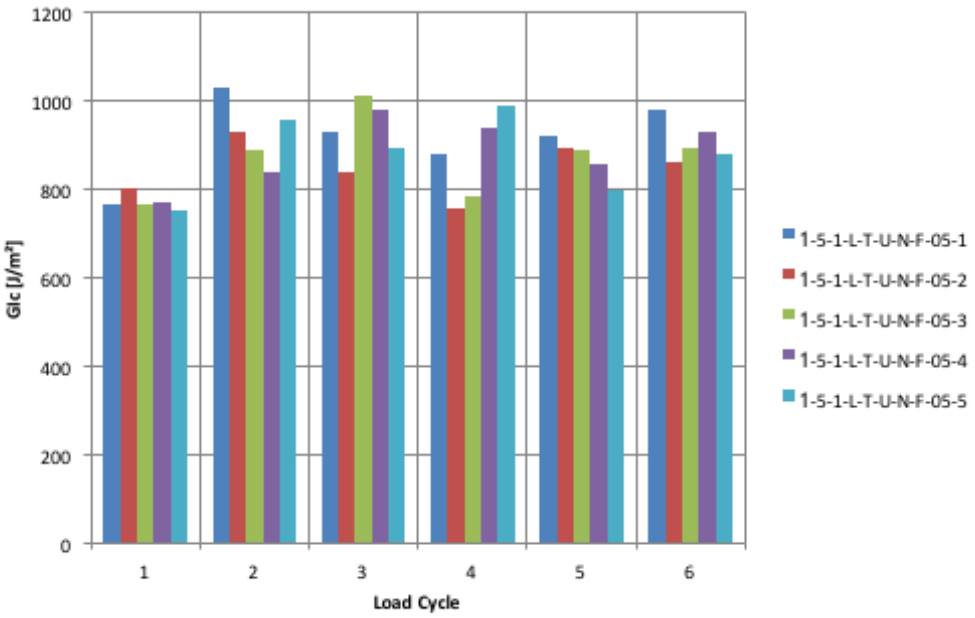

(b). *Specimens displayed individually for all load cycles.*

Figure 11. Interfacial fracture toughness of zero-displacement specimens determined using the area method.

Load-Rate Effects

The effect of loading and unloading rates on interfacial fracture toughness was investigated using the third set of supplied specimens. The load/unload rates for each specimen were held constant for all six load cycles, but the rate varied for each specimen. The first specimen was tested at a rate of 5 mm/min, while the second through fifth were tested at 10 mm/min, 20 mm/min, 30 mm/min, and 40 mm/min, respectively. The frequency of data collection increased along with the load/unload rate to ensure the total number of data points was kept constant (e.g., specimen one had a data collection frequency of 5 Hz, and the second specimen had a frequency of 10 Hz). All specimens were unloaded until zero force was reached. The initial disbond length, a_0, had an average value of 21.7 mm.

The disbond quickly stabilized at a through-the-thickness location just below the adhesive meniscus in the honeycomb core. Specimens exhibited semi-stable disbond growth, with the disbond growth rate controlled primarily by the honeycomb core cell walls as described previously. The load vs. displacement plot for all five specimens had similar features when compared to the baseline specimens as shown in Figure 12.

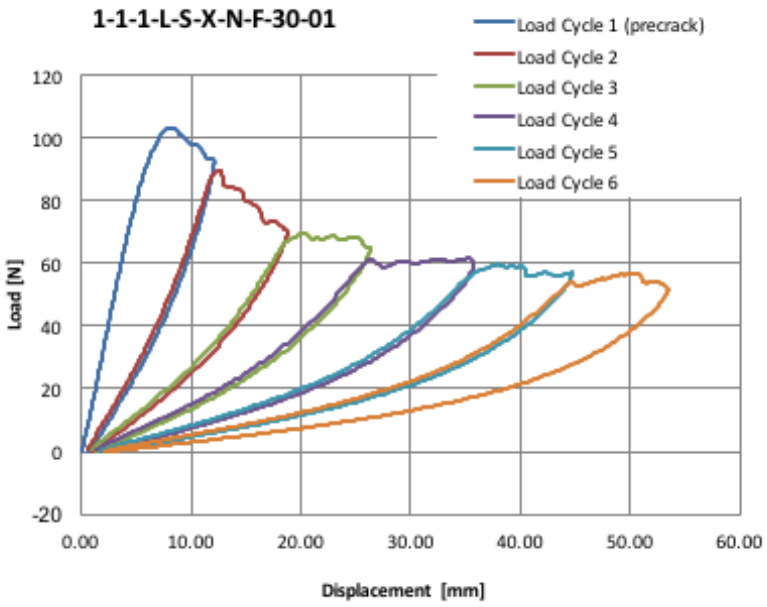

Figure 12. Typical load vs. displacement plot for the load-rate-effects specimens (example for 30 mm/min shown).

The average interfacial fracture toughness for all load cycles is shown in Figure 13. Load cycle three had the lowest values of G_c, 901±88.1 J/m^2, which differed from the zero-displacement tests in which the first load cycle had the lowest G_c magnitude. The largest interfacial fracture toughness values, 1067±137.5 J/m^2, occurred during loading cycle two.

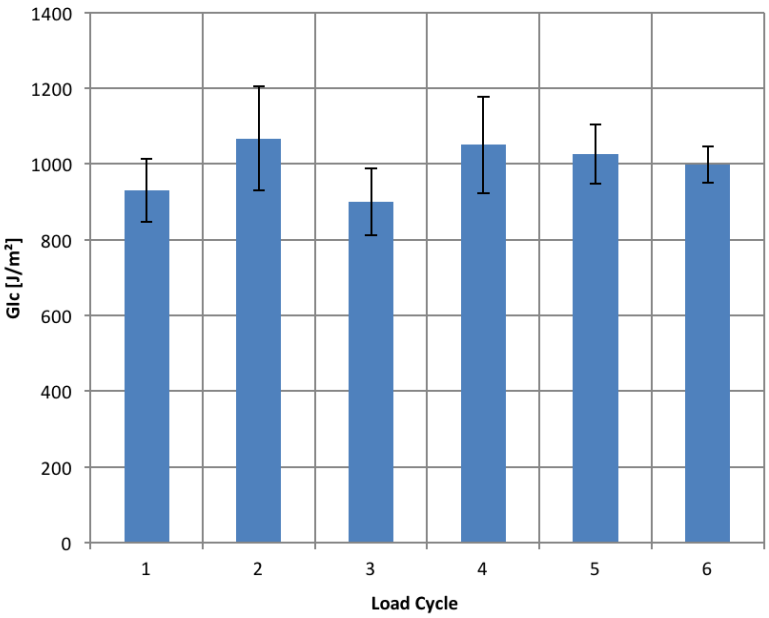

Figure 13. Average interfacial fracture toughness for load-rate-effect specimens found using the area method.

The two lower test rates of 5 mm/min and 10 mm/min produced nearly identical values of G_c, 957±65.7 J/m^2 and 958±60.7 J/m^2 respectively, as shown in Figure 14. The largest G_c values of 1055±176.0 J/m^2 were measured at the highest load/unload rate of 40 mm/min. In general, both the G_c values and standard deviations increased with the load/unload rate. However, within the range of one standard deviation, the greatest value of G_c obtained is within the range of the toughness measured from tests conducted at the standard loading rate of 5 mm/min.

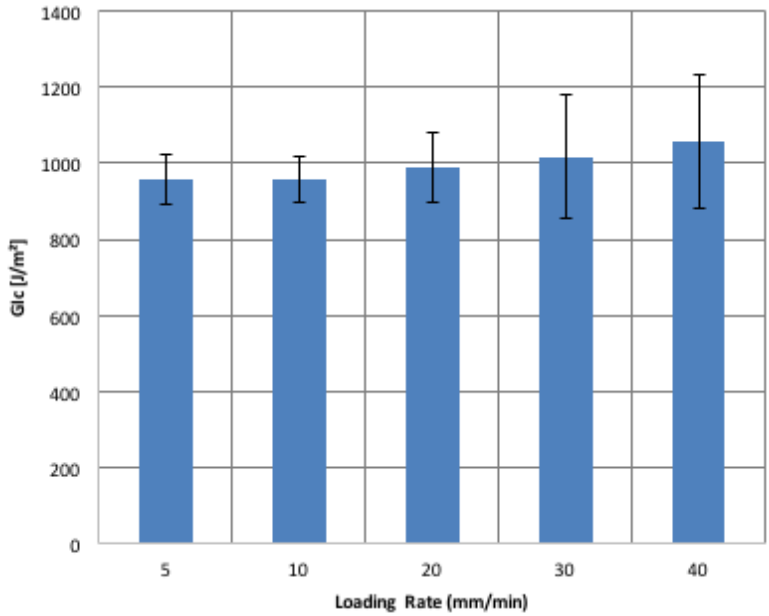

Figure 14. Effect of load/unload rate on the interfacial fracture toughness.

Based on these test results, a displacement rate of up to 40 mm/min appears to be feasible. However, testing using a 40 mm/min displacement rate appeared to be an upper limit when following the described procedure and resulted in higher scatter in G_c values. For such procedures, a lower maximum displacement rate such as 30 mm/min is recommended. Further reduced displacement rates of 20 mm/min, 10 mm/min, and 5 mm/min appear to have diminishing advantage due to the significant increase in the time required to complete the test. The approximate total time to complete six load/unload cycles for each of the displacement rates investigated is shown in Table VII. Note that these values do not include the time between cycles when cameras were reset by centering the disbond within the view frame.

5.2 Lab 2: NIAR, Wichita State University, Wichita, KS, USA

5.2.1 Baseline Testing

The baseline testing followed the test parameters shown in Table IV. The specimens were loaded until a disbond extension of approximately 10 mm from the initial disbond length and unloaded. Following that, loading-unloading cycles were repeated five times, each with a disbond extension of approximately 10 mm. The disbond propagated slightly into the core away from the original *Teflon*® or saw-cut pre-disbond and stayed on a path parallel to the top face sheet as shown in Figure 15a. The non-linearity of load-displacement curves continued to increase as the loading-unloading cycles continued due to large face sheet deformation. When the test specimens were unloaded to 0-load, the actuator displacement did not return to 0-displacement. This caused a small offset in actuator displacement for each subsequent loading cycle. Two of the baseline specimens were unloaded to 0-load as outlined in the test matrix in Table IV. Three of baseline test specimens were subsequently unloaded to 0-displacement to investigate the two different unloading styles. Both styles showed comparable results.

Both the method based on MBT and the area method were used to calculate G_c values. For the area method, the use of measured G_c values was preferred, as opposed to the straight G_c values, especially due to the non-linearity of load cycles 5 and 6. The area method also provided an average fracture toughness value for the entire disbond length.

5.2.2 Additional Testing

Saw-Cut Starter Disbond

The second set of specimens were fabricated without the *Teflon*® insert and the starter disbond was manually cut as shown in Figure 3c. These specimens were tested with a fixed base at a loading speed other than specified in Table IV (loading speed 2.5 mm/min, unloading speed of 5 mm/min) to study the different effects. Four specimens were unloaded to 0-load and one specimen to 0-displacement. Two specimens were only tested through four loading cycles to about 40 mm of disbond propagation due to a controller software malfunction which resulted in loss of data. In saw-cut specimens, the disbond propagated slightly more into the core compared to *Teflon*® (baseline) pre-disbond specimens and then stayed parallel to the top face sheet as shown in Figure 15b. This is likely due to the saw-cut disbond not being directly in between the core and the face sheet in the adhesive layer. These specimens also indicated the increase in non-linearity of load-displacement curves for each subsequent load cycle as well as a slight offset in actuator displacement. The average maximum load on the first load cycle was lower than that for the baseline specimens since the saw-cut starter disbond did not have to overcome as high static

friction as the *Teflon*® pre-disbond. The G_c values calculated using the area method for saw-cut specimens were lower than those of baseline specimens. However, the MBT method showed the opposite trend.

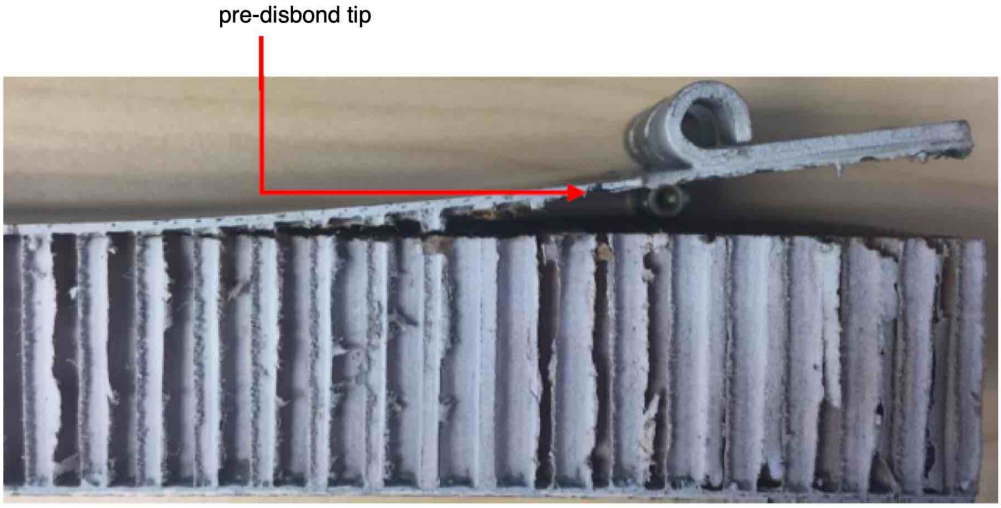

(a). *Teflon insert starter crack*.

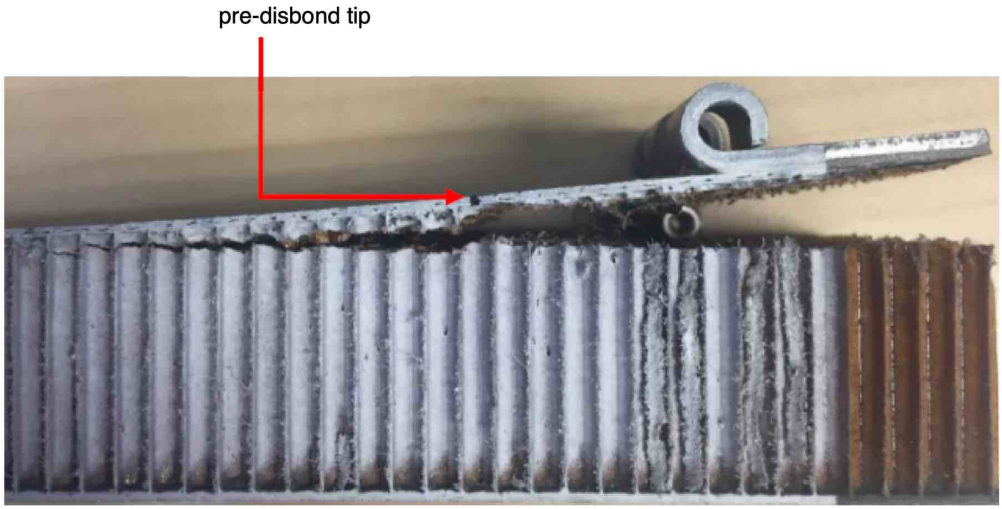

(b). *Saw cut starter crack*.

Figure 15. Disbond growth observed at NIAR.

Translating Fixture

The third set of specimens were tested with a saw-cut starter disbond using a translating base shown in Figure 2b and Figure 4b. These specimens were tested with a loading speed of 2.5 mm/min and an unloading speed of 25 mm/min. Three specimens were unloaded to 0-load and two specimens were unloaded to 0-displacement. The disbond growth behavior was similar to the previous saw-cut specimens. The loading curves showed the similar non-linear behavior, but the unloading curves indicated significantly different behavior compared to the results from fixed base; sudden changes were observed during unloading cycle possibly due to movement of sliding base when the static friction was overcome. The offset in actuator displacement was significantly higher than that with the fixed base. Approximately 92% of G_c values calculated for this set of specimens were higher than the fixed base set of specimens. The 0-load and 0-displacement for these specimens also yielded comparable results.

5.3 Lab 3: DuPont International Operations, Geneva, Switzerland

5.3.1 Results Summary:

As mentioned earlier in section *2.4 Test Matrix*, five specimens each were tested for three conditions: baseline testing, specimens where the disbond propagated in the W direction and accelerated testing where specimens were tested at 100 mm/min during loading and unloading. Detailed result data including single-specimen load curves, and G_c as a function of cycle are shown in the appendix (see Figures D3, E1, and J2). A summary of results is provided in Table VIII.

Table VIII. Results obtained at DuPont.

Condition	G_c (J/m^2)	SD (J/m^2)	CV (%)
Baseline L	840	30.2	3.6
Additional W	970	44.4	4.6
Additional Speed L	1154	26.2	2.3

5.3.2 Observations

Baseline Testing

- Fracture toughness was calculated using area method (AM).
- Large and non-linear face sheet deformation was experienced.
- First cycle led to higher variability. Disbond positioning occurred very likely during cycle 1 (10 mm disbond growth) and possibly beginning of cycle 2 (10 mm disbond increment) also.
- Fracture toughness average, G_c, as well as Standard Deviation, *SD,* and Coefficient of Variation, *CV,* as shown in Table VIII, were obtained from the five specimens taking cycles 2 to 6 into consideration and excluding cycle 1 data.
- Disbond propagated into the core below the face sheet and meniscus. None of the tested specimens showed either face sheet/core adhesive or face sheet failure.

Specimens Where the Disbond Propagated in W-Direction

- Other parameters such as conditioning, speed, and cycle length were similar to baseline testing.

- Power shut down occurred during a test (specimen 591WTUNF20-10) and invalidated results.
- Average G_c data generated along the W direction was about 15% higher than baseline data along the L direction.

Accelerated Test Speed

- Conditioning as well as test direction and cycle length were similar to baseline testing.
- The third set of specimens were tested at 100 mm/min load and unload.
- Automatic data acquisition (including P, δ, a and time) at 5 Hz was successfully evaluated up to 200 mm/min.
- Average G_c data generated at 100 mm/min was about 37% higher than baseline along the L direction.

5.4 Lab 4: NASA Langley Research Center, Hampton, VA, USA

5.4.1 Baseline Testing

The baseline test followed the testing parameters shown in Table IV. The load vs. displacement data of the first baseline test specimen, 4-5-2-L-T-U-N-F-05-06, is plotted in Figure 16a. The remaining specimens in this series were consistent with the first specimen in terms of disbond growth behavior. Disbond propagation was nominally 10 mm during each loading cycle. The initial *Teflon*®-induced disbond was located at the core/face sheet layer. However, the disbond propagated along the path of least resistance and dove into the core below the core/face sheet interface, adjacent to the meniscus layer. The disbond remained parallel to the base plate throughout the test. Due to the blunted disbond front created by the *Teflon*® insert and the disbond migrating through the meniscus layer, multiple peak forces were observed in the first load cycle at disbond growth initiation. The subsequent load cycles grew from natural pre-disbonds. Therefore, the point of the maximum load clearly indicated stiffness loss and typically corresponded to visually detectable disbond extension.

The first load cycle followed a linear loading curve. However, increased non-linearity was noted with increased disbond growth length. The observed non-linearity was caused by the large face sheet deformation during the later load cycles. To illustrate, the ratio of crosshead displacement to disbonded face sheet length was 0.27 at the end of the first load cycle and increased to 0.63 at the end of the last load cycle. Deflection of the face sheet in the last load cycle is shown in Figure 16b. Such a large deformation is well beyond the limit of geometric linearity assumed in the Euler-Bernoulli beam theory. Also, as the disbond propagated, the crosshead position for unloading was offset slightly, as shown in Figure 16a. The end of the first load cycle had the highest unload position offset, averaging to 0.46 mm. Subsequent load cycles had less offsets in the unload positions. The changing unload position could be due to the mismatching fracture surfaces at the core and face sheet. Fractured *Nomex*® core materials remained attached to the core and face sheet and created resistance against closing the disbond during unloading.

Figure 16c shows the fracture toughness for the baseline specimens. Both the area method (blue bars) and the MBT method results (green bars) are shown. The area method is the preferred method for the standard because it is not sensitive to the face sheet bending and the core fracture behaviors, unlike the MBT Method.

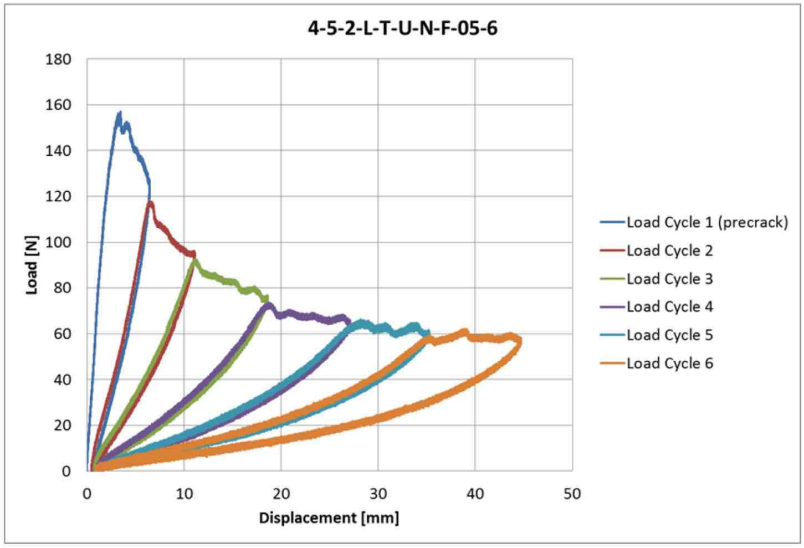

(a). *Typical load/displacement plot with six loading and unloading cycles.*

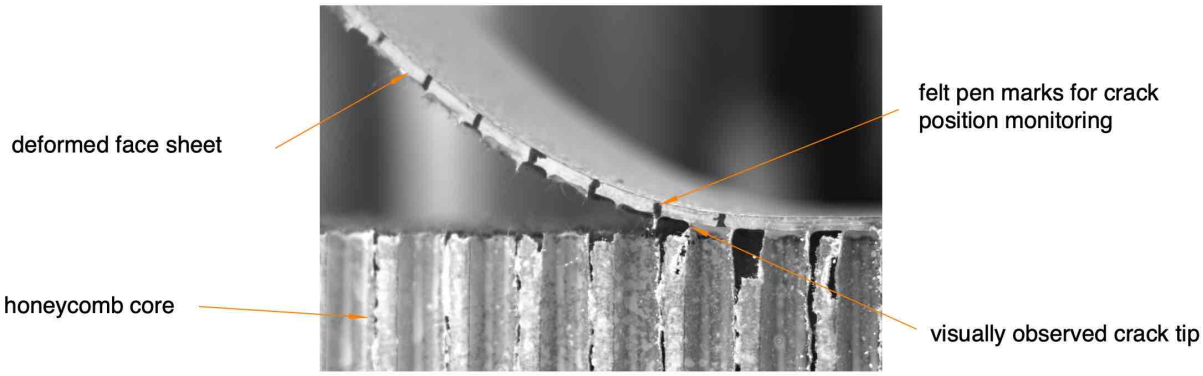

(b). *Observed local deformation near the crack tip.*

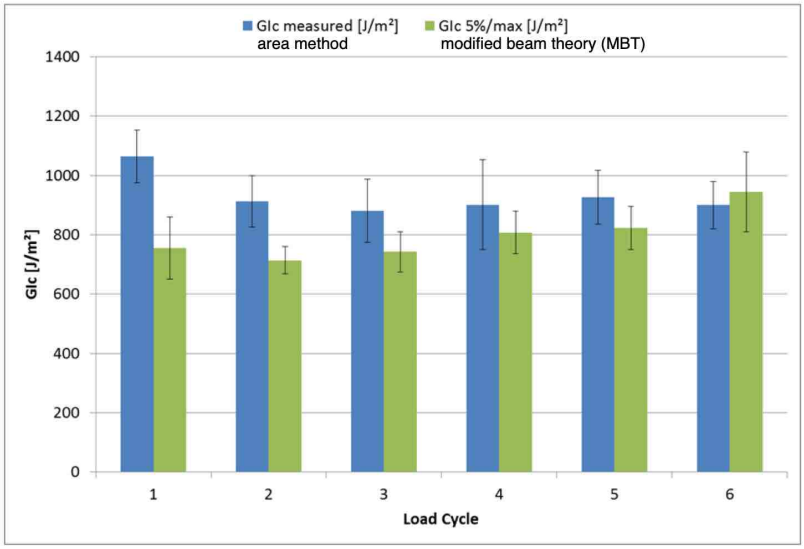

(c). *Fracture toughness values obtained from area method and modified beam theory.*

Figure 16. Typical results obtained from baseline testing at NASA Langley Research Center.

First, the MBT formulation assumed linear elastic face sheet bending. Since non-linear deformation was observed in thin face sheets, the MBT results were invalidated. Second, the first load cycle data often showed multiple peak forces due to the irregular disbond tip geometry. Identifying the force and displacement values to be used in the MBT method presents an additional challenge. The area method circumvents both of these problems. Additionally, the area method yields the average fracture toughness over a set disbond growth lengths. Thus, it eliminates variations in measuring G_c for the non-homogenous, repeating cells of the *Nomex*® core structure. Finally, results of the area method are reliable because the potential errors due to the hysteresis between the load cycles are negligible. The MBT typically yielded lower values of G_c than the area method.

Challenges in monitoring the disbond growth location came from the hexagonal core structure, where disbond growth paths branched at the hexagon angles. Also, slight eccentricity in load and variation in the core material could cause the visible disbonding on the edges of the specimen to grow unevenly, advancing faster on one edge than the other. In addition, visibility of the disbond could also be hindered by the hanging *Nomex*® material left from manufacturing the specimen. Thus, visible disbonds along the edges of the specimen did not always reflect the disbond front position inside the specimen.

5.4.2 Additional Tests

Unloading to Zero Displacement

The second set of specimens was unloaded to a position of zero crosshead displacement. Due to the mismatching fracture surfaces between the core and face sheet, a compressive force was observed at the end each load cycle. The compressive data served no purpose for a fracture test because it is an artifact of the remaining core material after fracture. Therefore, they were omitted in the fracture energy calculation. The force vs. displacement data for the first specimen in the zero-displacement test series, 4-2-2-L-T-U-N-F-05-1, is plotted in Figure 17a. This set of data was comparable to the baseline test specimens and followed the same trends. Figure 17b shows the fracture toughness values obtained from all tests where specimens were unloaded to the zero crosshead displacement position. As before, both the area method (blue bars) and the MBT results (green bars) are shown in Figure 17b. The difference in fracture toughness between the baseline series and the series where unloading was performed to zero displacement are less than their standard deviations. Both unloading methods are viable and produced similar results. Thus, the choice of unloading method should be dependent on the capability of the test equipment and the user.

Specimens with Doublers

The third set of specimens was reinforced with 3.18-mm-thick face sheet doublers, bonded to the upper face sheets to increase their bending and shear rigidity. The goals of using doublers were to:

- prevent non-linear face sheet deformation and obtain more reliable results using the MBT method, and
- induce a stronger mode-II shear stress component at the disbond tip and observe the changes in disbond growth behavior.

The doubler thickness was chosen to achieve an estimated 0.042% shear compliance in the face sheet, based on the SCB test sizing method [14]. In this series of tests, the crosshead displacement speed was reduced to 1 mm/sec to allow for measurement of the disbond tip position.

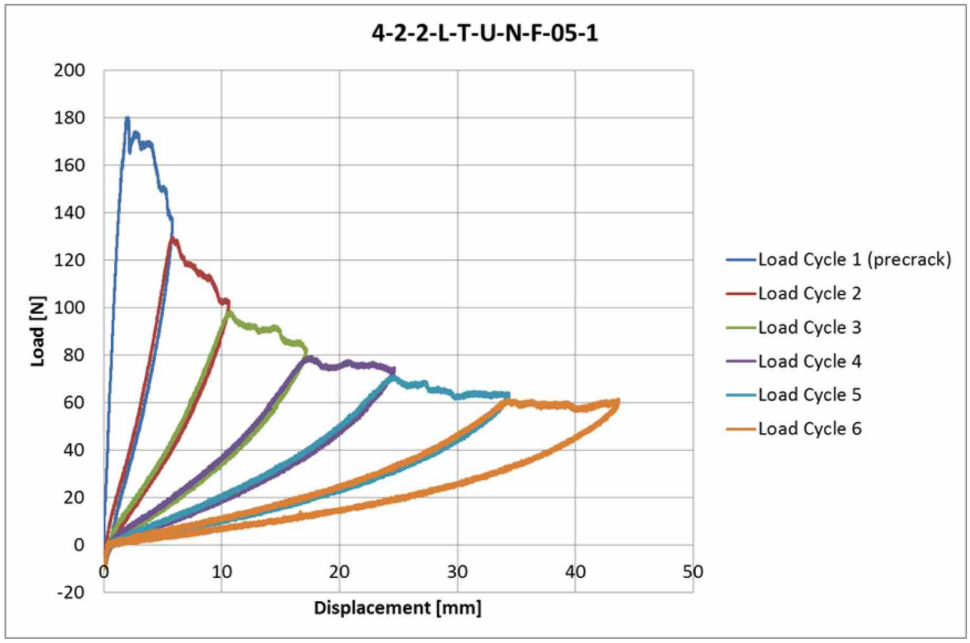

(a). *Typical load/displacement plot with six loading and unloading cycles*.

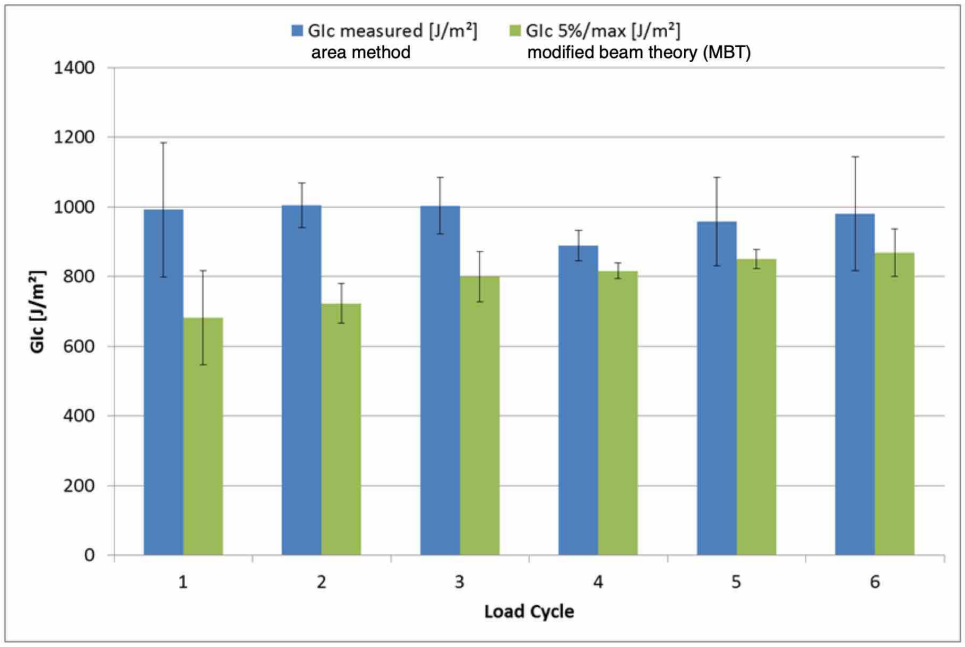

(b). *Fracture toughness values obtained from area method and modified beam theory.*

Figure 17. Results obtained at NASA LaRC for tests with an unloading cycle to zero displacement.

The load vs. displacement data for the first doubler specimen in the test series, 4-2-2-L-T-U-D-F-01-06, is plotted in Figure 18a. Note that the loads built up faster and disbond growth occurred at lower crosshead displacements compared to the baseline specimen. Fracture toughness results for both the area method (blue bars) and the MBT method (green bars) are shown in Figure 18b. From this figure, it can be seen that the addition of face sheet doubler improved the results obtained using the MBT method. While the MBT results were still consistently lower than the area method results, the difference was reduced.

In the doubler-bonded specimens, the disbond had a propensity to dive diagonally downwards into the core during the first load cycle and continue to propagate parallel to the base plate. Detailed photographs of the side of a doubler-bonded specimen near the disbond tip region are shown in Figure 18c and 18d. Figure 18c shows the disbond diving into the core. The local disbond growth pattern in the doubler specimen is clearly visible in Figure 18d. The disbond propagated approximately 2 mm below the meniscus layer. Under the influence of Mode-II shear stress, the disbond growth path was not straight and would sometimes oscillate above and below the 2 mm mark below the meniscus. In addition, rather than propagating at a single disbond tip, the disbond could move in a "smeared" process zone. Multiple visible disbonds could form on the edges of a specimen ahead of main disbond front. A disbond could jump ahead of the current disbond tip, and then remerge with the old disbond afterwards. It is not known if this trend is applicable to the inside of the specimen, which cannot be observed without a more complicated apparatus.

The use of a face sheet doubler either to improve the MBT method results or to change disbond tip stress mode mix was recommended. However, while choosing a shear loading contribution of less than 1% is considered to be acceptable by the SCB sizing method [14], the test results indicated that it can drastically increase the disbond tip shear stress. The disbond propagation depth was affected. The user must be aware of these affects. Tracking the disbond tip position was particularly difficult for the doubler-bonded specimens due to disbond oscillation and jumping. Potential load-rate sensitivity of the *Nomex*® core material was another issue related to changing the crosshead displacement speed from 5 mm/sec to 1 mm/sec. Load-rate sensitivity could explain the overall lowered average fracture toughness in the doubler-bonded specimen set.

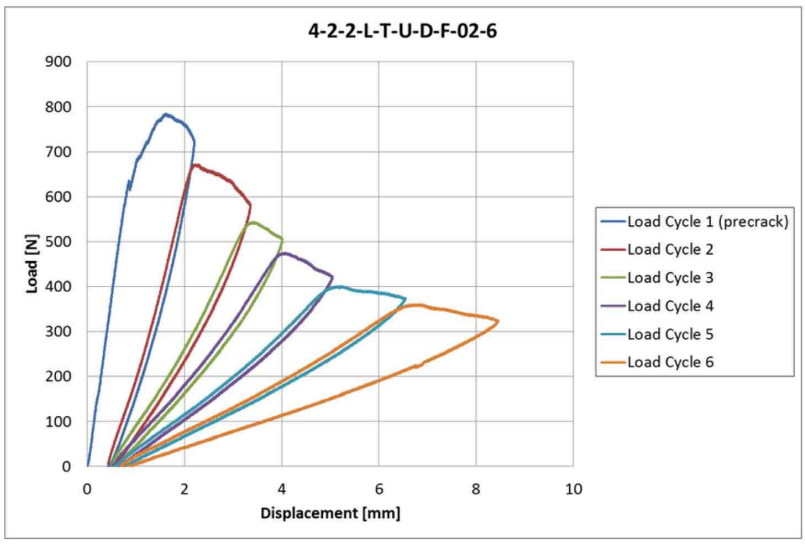

(a). *Typical load/displacement plot with six loading and unloading cycles.*

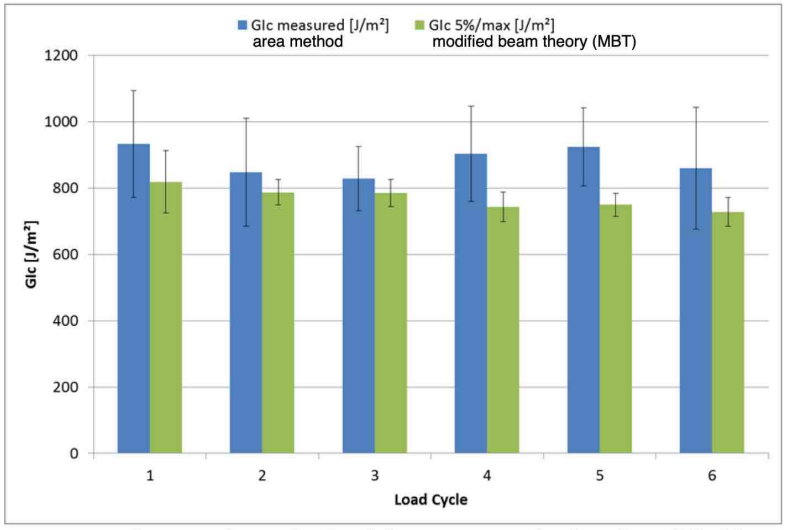

(b). *Fracture toughness values obtained from area method and modified beam theory.*

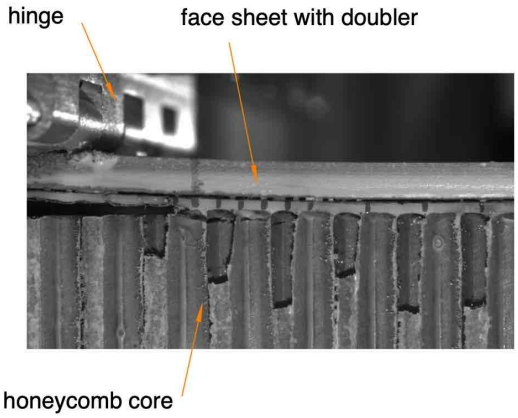

(c). *Observed local deformation.*

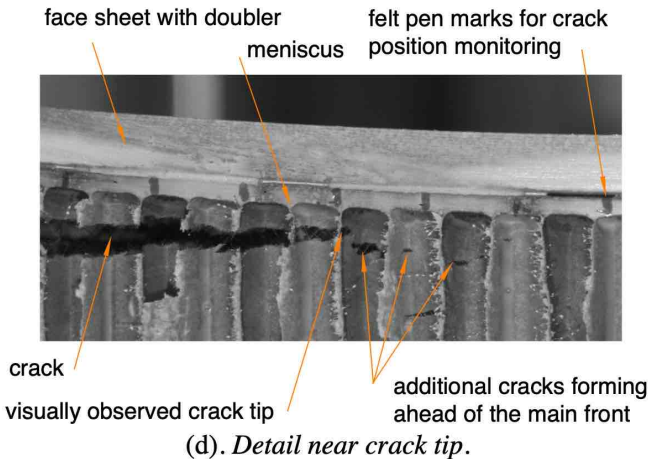

(d). *Detail near crack tip.*

Figure 18. Typical results obtained from specimens with doublers tested at NASA LaRC.

5.4.3 Comparison of Results

Figure 19 compares the G_c values, as measured by the area method, for all three series tested. It can be seen that the average fracture toughness in the doubler specimens is lower compared to the specimens tested without face sheet doubler.

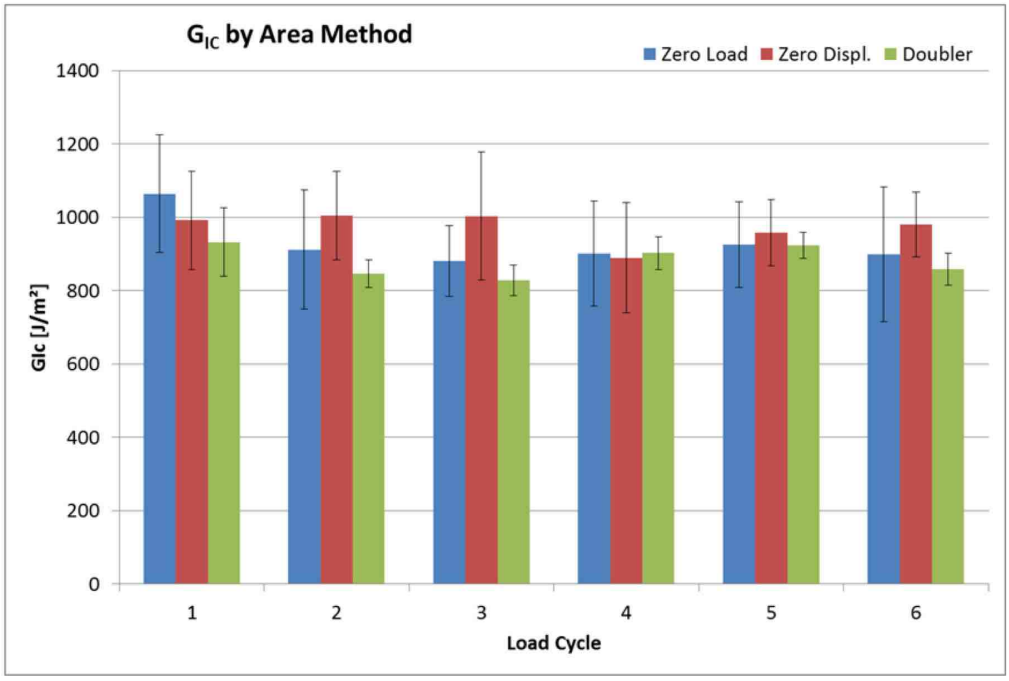

Figure 19. Typical results obtained from specimens with doublers tested at NASA LaRC.

5.5 Lab 5: Fraunhofer Institute for Microstructure of Materials and Systems IMWS, Halle, Germany

5.5.1 Baseline Testing

The baseline test series at lab 5 consists of the six specimens named 8-6-2-L-T-U-N-F-05-06 to 8-6-2-L-T-U-N-F-05-10. As shown in Table IV, the essential test parameters specify a loading at a constant crosshead speed of 5 mm/min and unloading at 30 mm/min down to a force of 0 N.

The test procedure starts from a 12.7-mm-long artificial pre-disbond, induced by the *Teflon*® film which was located exactly at the interface between the face sheet and the honeycomb core cells. During initial loading (cycle 1) and up to a disbond length of approximately 10 mm, the disbond developed into a natural position and shape. The disbond started exactly at the adhesive interface layer and ran towards the core, which represents the weakest path of the specific material under the prevailing test conditions. The initial cycle is followed immediately by cycles 2 to 6. The disbond runs below and close to the face sheet and the resin rich bond zone (meniscus zone) and continues to run parallel to the edge of the specimen. Figure 20 shows a representative disbond path and fracture surface of the baseline test series. The loading was manually stopped at a visual disbond propagation of around $\Delta a \approx 10$ mm per load cycle, immediately followed by unloading. The exact disbond length at the end of each cycle was determined after test completion in a post-

processing step averaging left and right disbond tip positions as described in section C5 of appendix C.

Within each loading cycle as well as between subsequent cycles, the load direction was reversed without significant pausing. The maximum holding time at reversal points was kept less than one second.

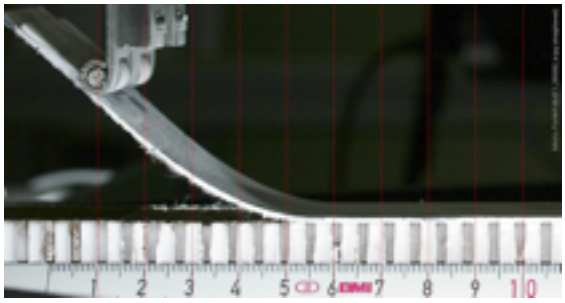

Figure 20. Left-side image with automatically generated auxiliary grid at Fraunhofer IWFM.

The test procedure starts at zero load and zero displacement in cycle 1. After unloading to a force of 0 N, recurrently in cycles 2 to 6, a displacement greater than 0 mm remains, due to a small amount of irreversible deformation at the disbond surfaces. Typically, a micro-scale ragged fringe made of broken aramid filament ends remains at the fracture surface of the cell wall material and inhibits a perfect closure of the entire disbond at a load of 0 N.

Data reduction was performed following the area method. The area enclosed in the loading and unloading curve of the load vs. displacement curve was calculated. Only portions of the load vs. displacement history with forces greater than zero were taken into account. The area represents the energy (in N-mm) necessary to generate the disbond surfaces. Division by the generated surface area results in the fracture toughness $G_{IC,\ AM,\ measured}$. Due to secondary energy dissipating effects, e.g., micro-damage as described above, the fracture toughness intrinsically will be overestimated to a certain amount. The overlapping area, enclosed by the unloading curve of cycle N and the loading curve of cycle N+1 gives a measure of this amount.

The load vs. displacement curves of the five specimens are shown in Figure D5a. Figure D5b gives a summary of the resulting fracture toughness, an average value of cycles 2 to 6 for each specimen and one average fracture toughness $G_{IC,\ AM,\ measured}$ for the set of all five specimens.

5.5.2 Testing with Disbond Propagation in W-direction

The test series consists of the six specimens named 5-9-1-W-T-U-N-F-20-01 to 5-9-1-W-T-U-N-F-20-05. The test conditions followed the baseline test specification except the orientation of the specimen or core, respectively. Consequently, the disbond propagation was in the W-direction of the core.

Due to insufficient clamping to the base plate, two of the specimens, namely 5-9-1-W-T-U-N-F-20-03 and -04, were slightly lifted up during testing and hence the results were considered to be invalid. Two additional tests were conducted using these specimens, starting disbond propagation from the opposite end of the specimen. Since no *Teflon*® foil was originally inserted at this position,

a saw cut was used instead. The load vs. displacement curves of the remaining specimens are shown in Figure E2a. Figure E2b gives a summary of the resulting fracture toughness, an average value of cycles 2 to 6 for each specimen and one average fracture toughness $G_{IC,\ AM,\ measured}$ for the series of all five specimen.

5.5.3 Testing at Accelerated Test Speed, Combined with Unloading to Zero Displacement
The test series consists of the six specimens named 3-2-1-L-T-U-N-S-20-06 to 3-2-1-L-T-U-N-S-20-10. A constant crosshead speed of 20 mm/min was applied while loading and 30 mm/min during unloading. Unloading was continued within each cycle until the original position of the load introduction point at 0 mm was reached. A negative force (pressure) is needed at the end of each cycle to return exactly to the original position at zero displacement. This is primarily caused by the disbond surface topology as discussed in section 5.5.1. Secondary effects, which yields remaining face sheet curvature after unloading, caused, e.g., by micro-damage of the deformed face sheet laminate itself or the resin rich meniscus layer, could intensify this behavior. The negative force applied via load introduction elements did not necessarily yield uniform pressure between the face sheet and the core along the disbond. The load distribution along the disbond propagation direction primarily is a function of the bending stiffness of the face sheet and the distance to the load introduction point and the disbond tip position, respectively. It can be assumed that unloading to zero displacement will cause only small impact on measured G_{Ic} since the immediate disbond tip vicinity will not be influenced. Area, or energy, respectively, introduced at negative forces is excluded from data reduction.

Accelerated test speed can slightly increase the resulting G_{Ic}. This effect likely is caused by visco-elastic behavior of the honeycomb core cell wall material which requires increased load to reproduce the same deflection as for lower speeds. Though, unloading to 0 mm does not seem to significantly affect the resulting fracture toughness value.

The load vs. displacement curves of the five specimens are shown in Figure I3a. Figure I3b gives a summary of the resulting fracture toughness. The graphs and the summary were duplicated in Figure J3 in appendix J, presenting data obtained under ‘accelerated load’ since accelerated speed and unloading to 0 mm were combined in the series under consideration.

5.6 Lab 6: Airbus Operations GmbH, Bremen

5.6.1 Test Performance
The specimens were loaded with a constant crosshead displacement rate of 5 mm/min and unloaded with 30 mm/min. After each loading cycle, the specimen was unloaded to 0 N. The specimens were loaded in six load cycles each of them provoking a disbond growth more than three times the honeycomb cell size or a minimum of 10 mm. In order to reach these target disbond lengths, the machine displacement, which correlates to these disbond lengths, needed to be identified.

Therefore Lab 1 tested the first three specimens by monitoring the disbond growth. The test was stopped manually for each loading cycle when a disbond growth of 10 mm was observed. The average values of the maximum machine displacement were calculated and communicated to the

other labs. These machine displacements were then used as reversal points for the loading cycles for the baseline and saw-cut tests.

Specimens with Doublers

For the first two specimens with doublers, the unloading point was set manually after the monitored disbond reached approximately the disbond lengths of the corresponding cycle of the baseline tests. For the remaining specimens, the displacements of those reversal points were used for the unloading point.

5.6.2 Incidents During Testing

The following incidents occurred during baseline testing:

- Specimen 6-6-1-L-T-U-N-F-05-7 / load cycle 1: Propagation data were not recorded.
- Specimen 6-6-1-L-T-U-N-F-05-10 / load cycle 1: Propagation data were not recorded.
- Specimen 6-6-1-L-T-U-N-F-05-9 / load cycle 2: Propagation data were not recorded.
- Specimen 6-6-1-L-T-U-N-F-05-10 / load cycle 1: Specimen slipped out of the fixture. Test data was invalid for the first load cycle. For the following load cycles, specimen was remounted. No slippage in cycles 2 to 6 (see also load-displacement curves in appendix A6).
- Specimen 6-6-1-L-T-U-N-F-05-10 / load cycles 4 and 5: Load cycle 4 was stopped at the displacement target value of load cycle 5. Therefore, load cycles 4 and 5 were tested in one single load cycle.

No incidents occurred for specimens tested with a saw cut as starter disbond.

Specimens with Doublers

The following incidents occurred for specimens tested with doublers:

- All specimens tested with doublers showed an irregularity in the first loading cycle between 100 N and 250 N. The root cause of this behavior could not be identified during the tests and as it was only affecting the first loading cycle, it was not considered as critical.
- Specimen 6-4-1-L-S-x-F-05-07 / load cycles 3 and 4: Load cycle 3 was stopped at the displacement target value of load cycle 4. Therefore, load cycles 3 and 4 were tested in one single load cycle.

5.6.3 Data Reduction

Zwick TestXpert I V9.04A was used for the data reduction. Additionally, the raw data was reduced using an *Excel* template provided to all participating labs. The initiation 5%/max G_{Ic} value was not calculated.

Data reduction in *TestXpert* including R-curve value calculation was done directly at the test machine by the tester after completing the test. Therefore, the recorded disbond propagation images, which include the current load and displacement of the test machine, were analyzed and the data was transferred into the corresponding input box of *TestXpert*. All test results following the different data reduction methods except initiation 5%/max G_{Ic} values were calculated automatically directly after test completion.

Detailed results are shown in the respective appendices. The results obtained from the five baseline specimens are shown in Figure D6. The results obtained from the five specimens with a starter saw cut are shown in Figure F2 and those obtained from specimens with doublers are shown in Figure G2, respectively.

5.7 Lab 7: Technical University of Denmark, Kgs. Lyngby, Denmark

5.7.1 Baseline Testing

The baseline testing was carried out for specimens with cells oriented in the L-direction. The testing parameters used are listed in Table IV. It was decided to achieve a disbond growth of ~10 mm for each load cycle. A test program was set up such that the machine stopped at a desired displacement level which corresponded to a 10 mm disbond growth. The target displacement level for each load cycle was provided from Lab 4 and was used to stop the loading. In total, five specimens were tested under baseline conditions (7-6-2-L-T-U-N-F-05-1 to 7-6-2-L-T-U-N-F-05-5), with each specimen having six load-unload cycles. Plots of load vs. displacement for the five tested specimens are provided in Figure 21a. A stable disbond growth with a disbond propagation path through the core just below the meniscus layer parallel to the base plate was observed.

The disbond growth during first load cycle started from the *Teflon*® pre-disbond and subsequently migrated to a level slightly beneath the meniscus layer. Such a pre-disbond followed by migration leads to multiple peak forces as evident in first load cycle for all five specimens. The first load cycle was not the same for all specimens. As seen in Figure 21a, the loading region of the curve for specimen 7-6-2-L-T-U-N-F-05-02, albeit having the same slope, does not follow the loading curve of other specimens. Moreover, with increasing load cycles, non-linearity was observed in the load/displacement plot. The non-linearity is associated with large lift-offs and subsequent damage of the face sheet.

During the test, each load cycle was unloaded to 0 N. For each specimen, with increasing load cycles the zero-load position did not correspond to a zero-displacement position. This offset during unloading is shown in Figure 21b. The offset in displacement, incurred at the unloaded position, can be attributed to the micro-mechanics of the *Nomex*® paper. Moreover, major strain maps obtained using digital image correlation revealed residual strain in the face sheet after unloading (see Figure 21c). This can be attributed to face sheet damage which occurred during loading.

Fracture toughness was calculated for baseline configuration specimens using the area method. The toughness was averaged across specimens for each load cycle and is shown as a bar chart in Figure 22. An error bar showing deviation from the mean for each load cycle is also presented. Maximum deviation is observed in the first cycle followed by the fifth and sixth cycles. There are challenges associated in determining the disbond front accurately which will in turn affect the fracture toughness computation. The white paint applied on both sides of the specimens was used as an aid to locate the disbond front. However, due to the nature of core material, it was observed that the disbond position varied on both edges. An average of the disbond front position from left- and right-side images was computed to determine the final disbond increment length. The discrepancy of the disbond front on both edges might be due to the nature of the core material.

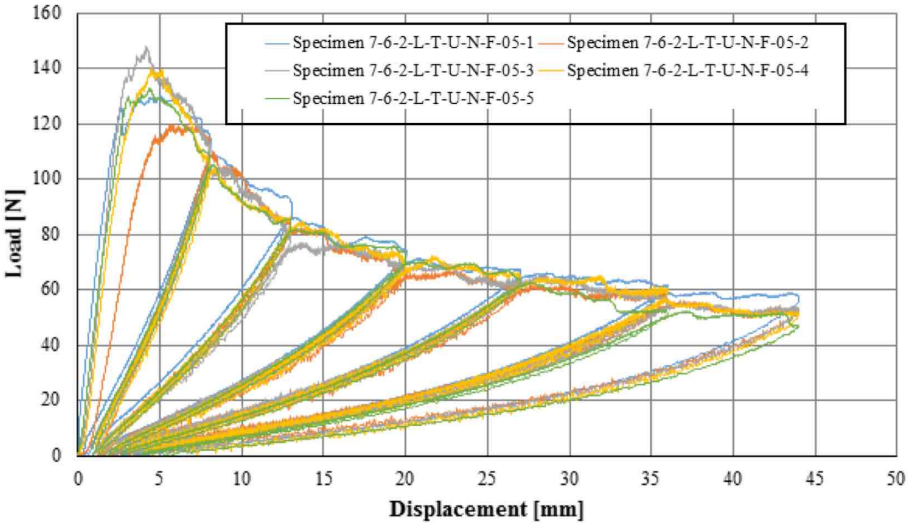

(a). *Load vs displacement plot for baseline specimens*

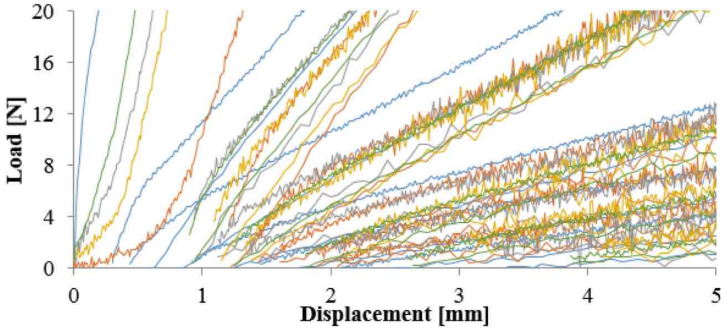

(b). *Zoomed in view showing an offset a 0 N load position in load vs displacement curves of baseline specimens*

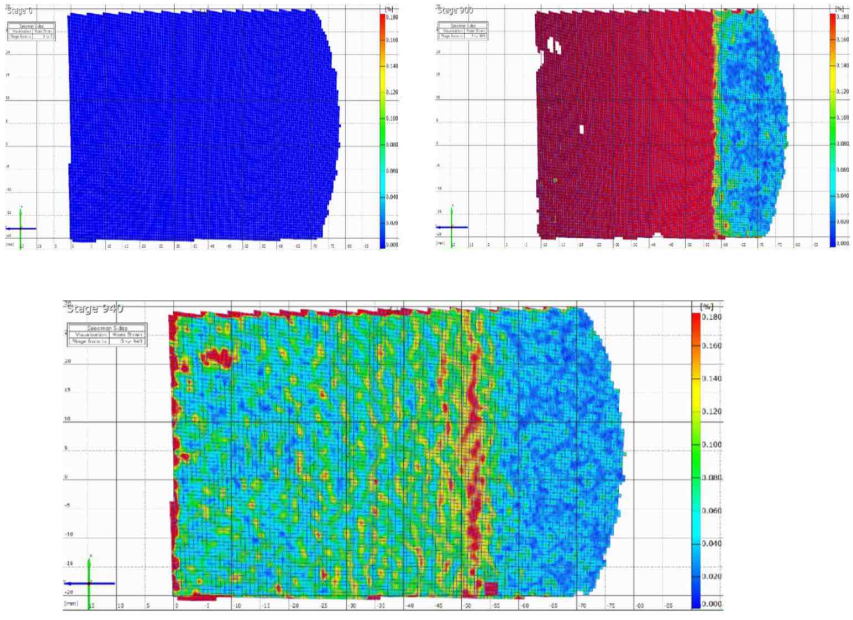

(c). *Major strain plot of face sheet loading/un-loading*

Figure 21. Results obtained for baseline configuration specimens tested at DTU.

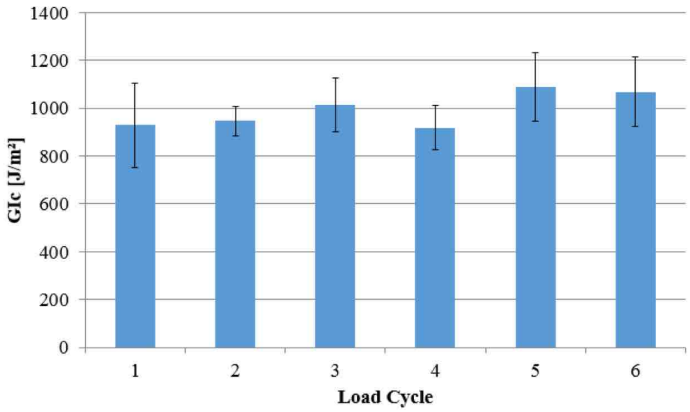

Figure 22. Fracture toughness values obtained using area method for baseline specimens presented for each load cycle averaged across specimens.

5.7.2 Additional Tests

Sliding Carriage

In the next set of tests, the influence of a sliding carriage plate was studied. By using a carriage that slides, effectively the boundary condition of the specimen is altered. During disbond propagation there exist both normal and shear components at the disbond tip. The primary aim of SCB test methodology is to perform fracture testing in mode-I or predominant mode-I conditions. There are several ways of mitigating the shear component thereby reducing mode II. One way is to use a long loading rod length, thereby ensuring that the load application remains vertical upon subsequent disbond propagation. It should also be noted that in sandwich composites, the disbond propagates along a face/core bimaterial interface with a huge elastic mismatch.

It was decided to use a sliding carriage such that sliding/rolling is initiated when the shear component was large enough to overcome the friction. To ensure relatively smooth sliding, the specimen plate is mounted atop sliders containing low friction roller bearings which slides on rods. Details of the test setup and the sliding arrangement are shown in appendix C. It should be noted that the same test setup was used for the baseline configuration tests as well. The SCB test rig was designed to have the possibility to lock and unlock the horizontal degree of freedom. This particular sliding table is free to slide when an M8-type bolt, placed exactly at the end of the slider, is unfastened. A fixed boundary condition is achieved by fixing the sliders containing the specimen plate by firmly securing the bolt onto the test bed.

A set of five specimens (7-4-2-L-T-U-N-S-05-01 to 7-4-2-L-T-U-N-S-05-05) were tested using a sliding carriage. The loading and unloading rate was kept similar to the baseline configuration tests with each specimen undergoing six load/unload cycles. However, prior data regarding displacement levels which corresponds to a 10-mm disbond length were unknown. Therefore, the first specimen was used to determine the displacement level required to attain a disbond length of ~10 mm. A typical load vs. displacement plot of a specimen with slider supports is shown in Figure 23a. Similar to baseline testing, non-linearity was observed with increasing load cycles which is related to the large displacement of the face sheet. Moreover, a higher loading peak was observed in the first loading cycle for all specimens, and a near face/core interface disbond propagation was observed.

The sliders inherently involve friction albeit they are equipped with low friction roller bearings. This implies that the sliding motion is at the cost of consuming energy which will be reflected in the load/displacement curve, thus leading to a higher fracture energy. However, sliding of specimen is initiated when the shear component becomes large. Hence, sliding will result in a reduction of fracture energy, which reduces the shear component. This effect is seen in the calculated fracture energy using the area method reported in a bar chart in Figure 23a. The average values computed for each load cycle are reported. It is seen that the fracture energy deviation across specimens is largest in load cycle 3.

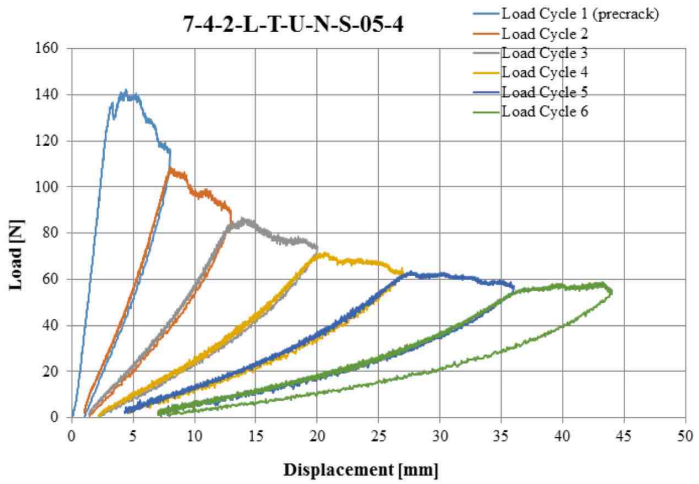

(a). *Typical load vs displacement plot for specimen tested on sliding carriage, specimen 7-4-2-L-T-U-N-S-05-4.*

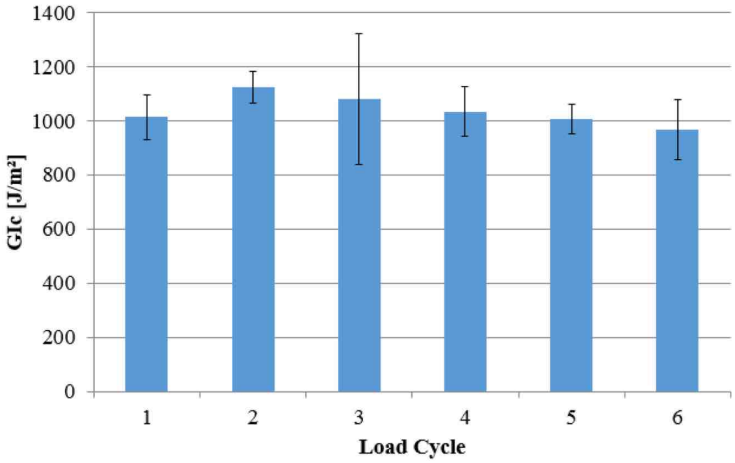

(b). *Fracture toughness values obtained using area method for specimens tested on slider carriage (averaged across specimens for each cycle).*

Figure 23. Results obtained from specimens tested with the sliding carriage performed at DTU.

Specimens with Doublers

The final set of tests were performed where the specimens were stiffened with reinforcement or "doubler" layers. A 2.38-mm (3/32-in) doubler material made of FR-4 (fiber glass sheet material) was bonded atop the top face sheet using *Araldite 2015*. The doubler layers were cut to specimen size and was supplied by Lab 1. First, the doubler material was bonded to the surface followed by bonding the specimen onto the specimen base plate. A curing time of 24 hours recommended by the supplier was used prior to bonding the hinge on top of the doubler layer. The FR-4 material comprises mainly of glass fiber sheet. Tensile and flexural properties (E_x = 14.89 GPa, X_t = 425.43 MPa, E_f = 536 MPa) were estimated using standard ASTM tests [24, 25].

The load/unload cycle parameter set was kept similar to the baseline specimen configuration. It was observed that the disbond propagated parallel to the specimen plate but grew in a layer slightly beneath the face sheet/core interface. This behavior is unlike that observed for baseline and specimens tested on the sliding carriage. The disbond showed a tendency to kink into the core. The disbond path is shown in Figure 24a. A typical load vs. displacement plot is shown in Figure 24b. Fracture toughness values computed using both MBT and the area method for each load cycle averaged across specimens is provided as a bar chart in Figure 24c. The MBT method can be applied here to calculated fracture energy as the huge lift-off of face sheets is restricted as they become stiffer due to the doubler layer. Furthermore, by adding doubler layers, the bending stiffness of the face sheet is increased which prevents damage of the thin face sheet. Therefore, the fracture toughness values computed will not be affected by energy consumed due to damage of the face sheet.

5.7.3 Comparison of Results

Fracture toughness values were obtained using the area method in three different test configurations, namely, baseline, sliding carriage and doubler configurations, and are presented in Figure 25. In the first load cycle, higher values were obtained for the sliding carriage configuration whereas, in the final cycle, the doubler configuration exhibited higher toughness values. An average fracture toughness of 1036.69 J/m^2 was obtained for specimens tested with slider, 994.66 J/m^2 for base-line configuration and 1051.41 J/m^2 for specimens reinforced with FR-4 doubler layers.

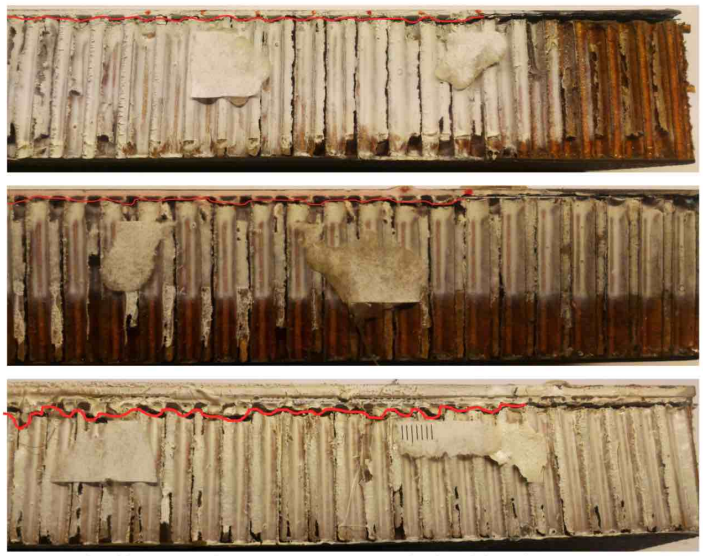

(a). *Disbond propagation path illustrated on specimen with doubler for specimens, 7-4-2-L-T-U-D-F-05-1, 7-4-2-L-T-U-D-F-05-2 and 7-4-2-L-T-U-D-F-05-3.*

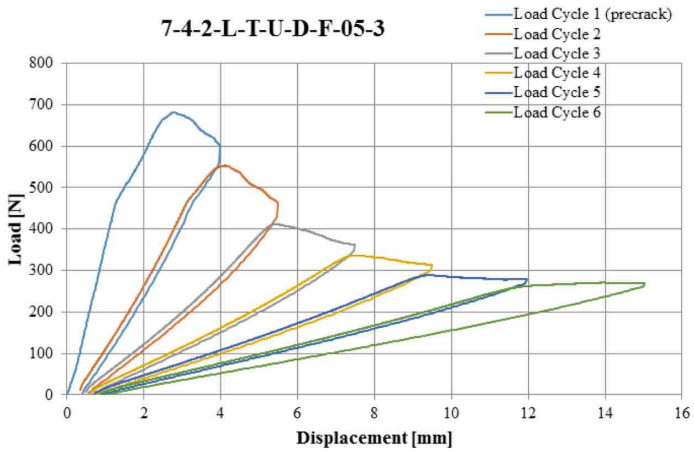

(b). *Typical load vs displacement plot for specimen bonded with doubler layer, specimen 7-4-2-L-T-U-D-F-05-3.*

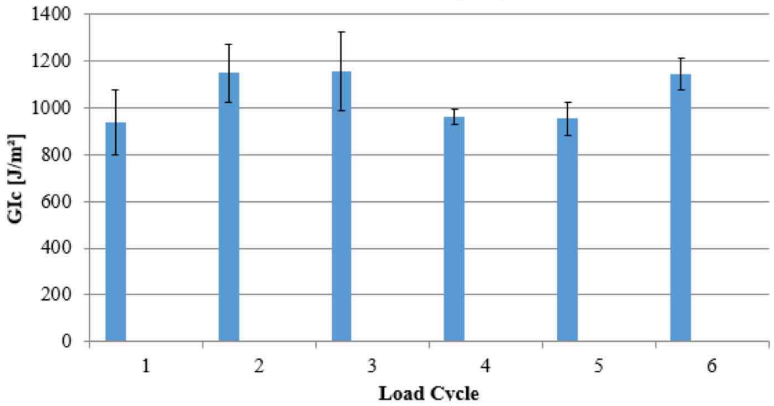

(c). *Fracture toughness of specimen bonded with doubler layers, obtained using area method (averaged across specimens for each cycle).*

Figure 24. Results obtained from specimens bonded with FR-4 doublers tested at DTU.

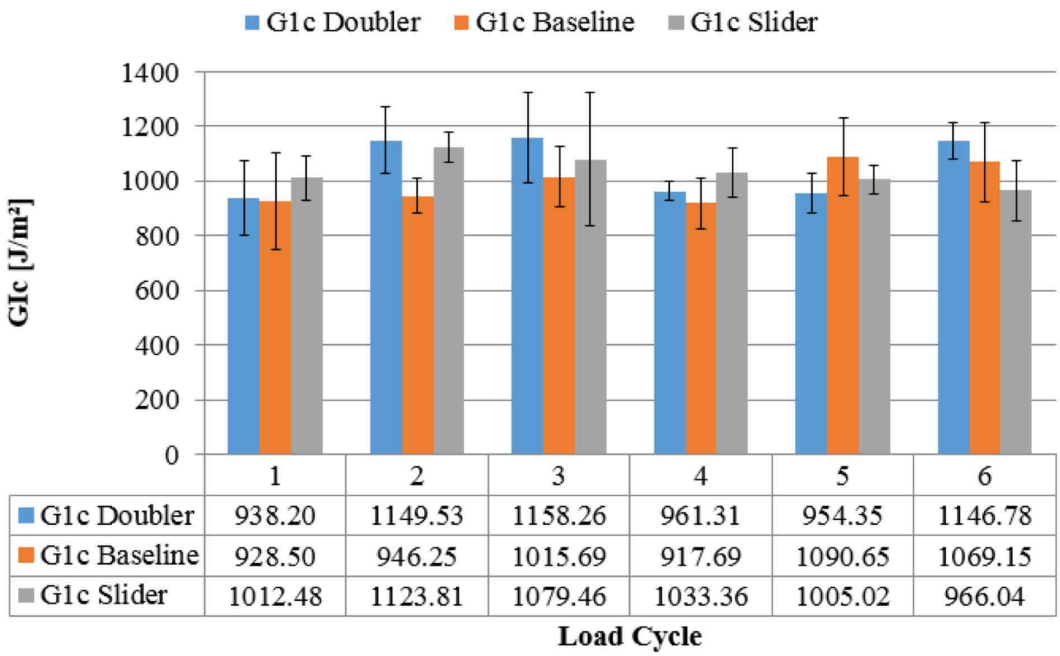

	1	2	3	4	5	6
G1c Doubler	938.20	1149.53	1158.26	961.31	954.35	1146.78
G1c Baseline	928.50	946.25	1015.69	917.69	1090.65	1069.15
G1c Slider	1012.48	1123.81	1079.46	1033.36	1005.02	966.04

Figure 25. Comparison of fracture toughness values obtained in three different specimen configurations.

5.8 Comparison of Results From All Labs

Fracture toughness values obtained across all participating labs for the baseline specimen configuration is compared and presented in Table IX. It should be noted that the comparison is carried out for toughness values obtained using the area method. For each lab, average fracture toughness of five specimens for each load cycle is presented. In addition, standard deviation for each cycle is reported in the row below. The baseline configuration specimens contained a pre-disbond introduced using a *Teflon*® film, which resulted in an artificial disbond. Therefore, the disbond propagates from an artificial disbond front in the first cycle. For the sake of comparison, an average value from cycle 2 – 6 for each lab is calculated and reported in Table IX.

A highest fracture toughness value of 1078 J/m^2 was obtained by Lab 2, which is 11% more than the average of 970 J/m^2 across all the labs. The lowest toughness of 841 J/m^2 was obtained by Lab 3, which is 13% lower than the average. The average toughness value computed using the DCB-UBM method was 1156 J/m^2, which is 19% higher than the average for the baseline configuration across all labs. A comparison of toughness values across various labs along with the DCB-UBM is provided in Figure 26.

Table IX. Fracture toughness values obtained using area method across all participating labs.

Lab	Load cycle	1	2	3	4	5	6	Average (2-6)
1	G1c [J/m^2]	990.97	1012.21	983.34	965.79	930.53	964.31	**971.24**
	STD	*92.62*	*35.40*	*64.95*	*59.41*	*104.71*	*71.74*	*67.24*
2	G1c [J/m^2]	872.58	1199.99	979.76	1002.43	1109.53	1096.01	**1077.54**
	STD	*151.10*	*367.36*	*130.88*	*129.85*	*70.97*	*298.34*	*199.48*
3	G1c [J/m^2]	1182.16	829.16	832.92	833.95	839.86	868.12	**840.80**
	STD	*66.83*	*62.23*	*33.01*	*31.03*	*39.71*	*18.25*	*36.85*
4	G1c [J/m^2]	1066.33	912.34	881.87	900.78	929.25	899.91	**904.83**
	STD	*90.47*	*85.81*	*107.65*	*151.07*	*88.16*	*80.22*	*102.58*
5	G1c [J/m^2]	1004.86	1059.17	979.26	1029.31	1066.84	1067.01	**1040.32**
	STD	*93.39*	*51.88*	*79.42*	*72.09*	*63.35*	*69.35*	*67.22*
6	G1c [J/m^2]	1380.60	1025.41	951.81	909.53	890.38	957.96	**947.02**
	STD	*857.73*	*64.38*	*120.78*	*97.38*	*17.00*	*122.11*	*84.33*
7	G1c [J/m^2]	928.50	946.25	1015.69	917.69	1090.65	1069.15	**1007.89**
	STD	*176.63*	*63.10*	*112.15*	*92.79*	*143.36*	*144.87*	*111.25*
Average	**G1c [J/m^2]**	**1060.85**	**997.79**	**946.37**	**937.06**	**979.57**	**988.92**	
	STD	*159.45*	*109.55*	*60.27*	*61.74*	*99.46*	*82.87*	

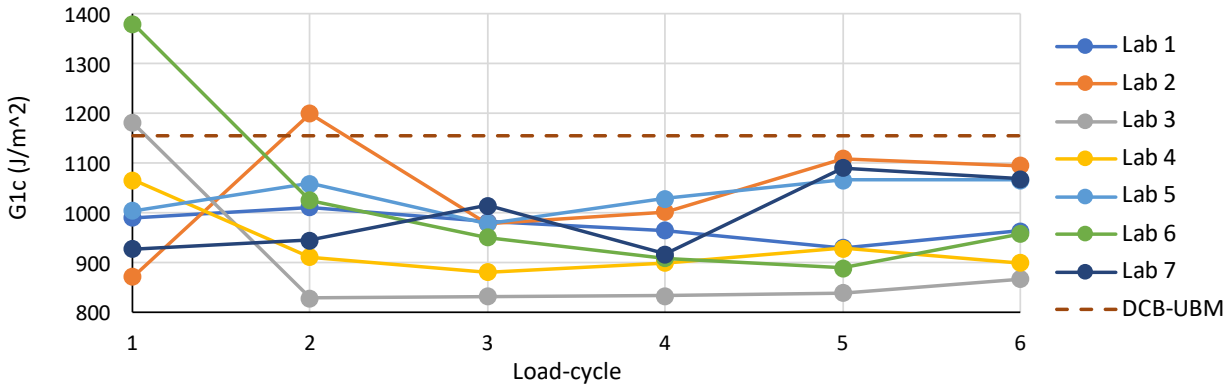

Figure 26. Fracture toughness values obtained using area method across all participating labs and using DCB-UBM test methodology

6. RECOMMENDATIONS FOR TEST STANDARD DEVELOPMENT

Although not investigated in these tests, the use of a manufactured starter disbond will be important for determining G_c corresponding to disbond initiation. However, for G_c measurements corresponding to disbond growth, the use of a machined starter disbond appears to be a suitable option. Potential advantages of using a machined starter disbond include allowing the test operator to make changes to the initial disbond length if needed as well as eliminating the need for the fabrication of specimens with *Teflon*® film inserts.

The maximum recommended displacement rate may be highly dependent on the test procedures used, particularly for measuring the disbond length. However, it may also be dependent on the experience level of the test operator as well as the experience level with a specific sandwich configuration. The first several test specimens may need to be performed at a lower displacement rate to establish efficient test procedures prior to increasing the displacement rate. As a result, the maximum recommended displacement rate will likely be based primarily on the ability of the test operator to accurately determine the location of the disbond tip during loading.

The use of multiple loading/unloading cycles may be replaced by a single disbond propagation cycle that includes a longer region of disbond growth. The elimination of multiple loading/unloading cycles will significantly reduce the time associated with testing and may allow for moderate test times with reduced displacement rates.

7. SUMMARY AND CONCLUDING REMARKS

The SCB test was used to characterize face sheet/core disbonding in sandwich components in an international round robin to support standard development. Each of the seven participating laboratories performed a set of five baseline tests with a fixed base using the same protocol, however, using their own specific equipment. In addition, each laboratory performed two sets of tests with altered test conditions which included using a test fixture with a translating (sliding) carriage and performing the tests with different loading and unloading speeds. The orientation of the disbond front with respect to the honeycomb core cells was varied and the effect on the fracture toughness was also studied. Additional factors that could influence test results were investigated, such as the use of a saw cut starter disbond as an alternative to *Teflon*® release film, and the effects of using a face sheet doubler to increase the bending stiffness. For each set of tests, summary results such as load/displacements plots, observed disbond growth location and calculated energy release rates were reported and a comparison of results between labs were presented.

Regarding test standard development, the following observations were made:

- The use of the area method appears to be well suited for measuring G_c associated with disbond propagation.
- The use of multiple loading/unloading cycles may be replaced by a single disbond propagation cycle that includes a longer region of disbond growth.
- The use of the MBT method for measuring G_c associated with disbond initiation requires further assessment and follow-on testing will be necessary. Limits of applicability of the MBT need to be established, especially with regard to the thickness and flexural rigidity of the face sheet.

Suggestions and recommendations based on the results of this round robin have been included in the latest ASTM draft standard [26].

ACKNOWLEDGEMENTS
Research performed at NASA Langley Research Center was originally supported by NASA's Subsonic Rotary Wing Program. Most recent support was provided by the Revolutionary Vertical Lift Technology Project (RVLT) as part of NASA's Advanced Air Mobility Mission within the Aeronautics Research Mission Directorate (ARMD).

The National Institute of Aerospace (PI Ronald Krueger) was supported by the Federal Aviation Administration (FAA). Funding through the Aviation Research Grants Program, Research Grant Number 16-G-006 and task order 692M15-21-F-00229 is gratefully acknowledged.

The Technical University of Denmark (PI Christian Berggreen) conducted research under the scope of the *Disbond of Sandwich Structures* (DoSS) project, funded by the European Aviation Safety Agency (EASA).

Fraunhofer (PI Ralf Schäuble) conducted research under the ambit of the DoSS project, funded by EASA, as well as in collaboration with the *Thin Face Sheet Sandwich Disbond* (TFSanDis) project, supported with funds from the Federal Ministry for Economics and Energy, Germany.

NIAR (PI Waruna Seneviratne) received funding support from both, the FAA and the Kansas Aviation Research & Technology Growth Initiative (KART). Face sheet and core materials were donated by both Cessna and Beechcraft (now incorporated into Textron Aviation).

The University of Utah (PI Dan Adams) performed research funded by the FAA through the Joint Advanced Materials & Structures (JAMS) Center of Excellence, Cooperative Agreement No. 12-C-AW-UU.

REFERENCES

[1] "Loss of Rudder in Flight - Air Transat, Airbus A310-308, C-GPAT, 06 March 2005," Transportation Safety Board of Canada, Aviation Investigation Report A05F0047, 2007.

[2] "Air Accident Investigation Branch. AAIB Bulletin 8/92 Ref: EW/A92/5/1: Air Accident Investigation," United Kingdom, 1992.

[3] E. H. Glaessgen, J. R. Reeder, D. W. Sleight, J. T. Wang, I. S. Raju, and C. E. Harris, "Debonding Failure of Sandwich-Composite Cryogenic Fuel Tank with Internal Core Pressure," *J. Spacecr. Rockets*, vol. 42, no. 4, pp. 613–627, 2005.

[4] R. Hilgers, "Substantiation of Damage Growth within Sandwich Structures," presented at the FAA Workshop for Composite Damage Tolerance & Maintenance, Tokyo, Japan, 2009.

[5] S. Prasad and L. A. Carlsson, "Debonding and Crack Kinking in Foam Core Sandwich Beams—II. Experimental Investigation," *Eng. Fract. Mech.*, vol. 47, no. 6, pp. 825–841, Apr. 1994, doi: 10.1016/0013-7944(94)90062-0.

[6] M. Rinker, J. Ratcliffe, D. Adams, and R. Krueger, "Characterizing Facesheet/Core Disbonding in Honeycomb Core Sandwich Structure," NASA/CR-2013-217959, NIA report no. 2013-0115, 2013.

[7] C. Lundsgaard-Larsen, B. F. Sørensen, C. Berggreen, and R. C. Østergaard, "A Modified DCB Sandwich Specimen for Measuring Mixed-Mode Cohesive Laws," *Eng. Fract. Mech.*, vol. 75, no. 8, pp. 2514–2530, 2008.

[8] A. Quispitupa, C. Berggreen, and L. A. Carlsson, "Design Analysis of the Mixed Mode Bending Sandwich Specimen," *Journal of Sandwich Structures & Materials*, vol. 12, no. 2. pp. 253–272, 2010.

[9] R. P. Zarda and R. E. Fields, "Analysis and Test Methodology for Fracture Mechanics of Unbonded Sandwich Structures," Martin Marietta, Studies Task Report EDF No. MM0TKR 10722739-001, 1994.

[10] W. J. Cantwell, R. Scudamore, J. Ratcliffe, and P. Davies, "Interfacial Fracture in Sandwich Laminates," *Compos. Sci. Technol.*, vol. 59, pp. 2079–2085, 1999.

[11] X. Li and L. A. Carlsson, "The Tilted Sandwich Debond (TSD) Specimen for Face/Core Interface Fracture Characterization," *Journal of Sandwich Structures & Materials*, vol. 1, no. 1. pp. 60–75, 1999.

[12] A. T. Nettles, E. D. Gregory, and J. R. Jackson, "Using the Climbing Drum Peel (CDP) Test to Obtain a GIC Value for Core/Face Sheet Bonds," *J. Compos. Mater.*, vol. 41, no. 24, pp. 2863–2876, 2007.

[13] C. Weaver, "Evaluation of Mode I Fracture Mechanics Test Methods for Sandwich Composites," M.Sc Thesis, University of Utah, Salt Lake City, UT, 2009.

[14] J. G. Ratcliffe and J. R. Reeder, "Sizing a Single Cantilever Beam Specimen for Characterizing Facesheet-Core Debonding in Sandwich Structure," *J. Compos. Mater.*, vol. 45, no. 25, pp. 2669–2684, 2011.

[15] X. Li and L. A. Carlsson, "Elastic Foundation Analysis of Tilted Sandwich Debond (TSD) Specimen," *Journal of Sandwich Structures & Materials*, vol. 2, no. 1. pp. 3–32, 2000.

[16] Bent F. Sørensen, Kenneth Jørgensen, Torben K. Jacobsen, and Rasmus C. Østergaard, "DCB-Specimen Loaded with Uneven Bending Moments," *Int. J. Fract.*, vol. 141, no. 1–2, pp. 163–176, 2006.

[17] M. F. Kanninen, "An Augmented Double Cantilever Beam Model for Studying Crack Propagation and Arrest," *Int. J. Fract.*, vol. 9, no. 1, pp. 83–92, 1973.

[18] V. Saseendran, C. Berggreen, and R. Krueger, “Mode Mixity Analysis of Face/Core Debonds in a Single Cantilever Beam Sandwich Specimen,” *J. Sandw. Struct. Mater.*, vol. 22, no. 6, pp. 1879–1909, 2020, doi: https://doi.org/10.1177/1099636218788223.
[19] J. W. Hutchinson and Z. Suo, “Mixed Mode Cracking in Layered Materials,” *Adv. Appl. Mech.*, vol. 29, pp. 64–191, 1992.
[20] “Cytec Cycom 5320-1 T650 3k-PW Fabric Qualification Material Property Data Report,” Wichita, KS, NIAR, Wichita State University, CAM-RP-2012-017 Rev NC, 2015.
[21] “HexWeb® HRH-10®, Product data sheet,” Hexcel Corporation, Stamford, CT, USA, 2014.
[22] G. A. Irwin and J. A. Kies, “Critical Energy Rate Analysis of Fracture,” *Weld. J. Res. Suppl.*, vol. 33, pp. 193–198, 1954.
[23] C. Berggreen, B. C. Simonsen, and K. K. Borum, “Experimental and Numerical Study of Interface Crack Propagation in Foam-cored Sandwich Beams,” *J. Compos. Mater.*, vol. 41, no. 4, pp. 493–520, 2007.
[24] “ASTM D7264 - Standard Test Method for Flexural Properties of Polymer Matrix Composite Materials,” ASTM International, West Conshohocken, PA, USA, 2017.
[25] “ASTM D3039 - Standard Test Method for Tensile Properties of Polymer Matrix Composite Materials,” West Conshohocken, PA, USA, 2018.
[26] “ASTM WK56166 Standard Test Method for Mode I Dominant Facesheet-to-Core Fracture Toughness of Sandwich Constructions,” ASTM International, West Conshohocken, PA, USA, Work Item, 2021.

APPENDIX A – SPECIMEN MANUFACTURING[4]

A list of all specimens manufactured and used for baseline testing is shown in Table AI. The specimen's name is based on:

- Lab number
- Panel number from specimen fabrication
- Subpanel number
- Test direction: W or L
- Starter disbond: *Teflon*® (T) or saw cut (S)
- Disbond location: Near upper face sheet (U) or bottom face sheet (B)
- Use of doubler during testing: Use of doubler (D) or no doubler (N)
- Type of fixture used: Fixed (F) or sliding carriage (S)
- Test Speed in mm/min

It was agreed that participating labs could change the specimen's name to reflect the final test configuration and condition, while keeping a record of the original name for tracking purposes. Specimens used for additional testing are listed in Table AII.

Table AI: First set of SCB specimens manufactured at NIAR[4]

Lab #	L/W	Teflon / Saw cut	Doubler (Y/N)	Fixture (Fixed / Translate)	Test Speed	SPECIMEN NAME	AVG THICKNESS [in]	AVG WIDTH [in]	AVG INSERT LENGTH [in]	LENGTH [in]
Lab 1	W	T	N	F	05	1-5-1-W-T-U-N-F-05-1	1.056	2.003	1.547	12.022
						1-5-1-W-T-U-N-F-05-2	1.057	2.010	1.510	12.014
						1-5-1-W-T-U-N-F-05-3	1.058	2.003	1.518	12.023
						1-5-1-W-T-U-N-F-05-4	1.058	2.008	1.466	12.035
						1-5-1-W-T-U-N-F-05-5	1.058	2.001	1.539	12.027
Lab 2	W	T	N	F	05	2-5-1-W-T-U-N-F-05-6	1.059	2.007	1.544	12.030
						2-5-1-W-T-U-N-F-05-7	1.058	2.003	1.511	12.035
						2-5-1-W-T-U-N-F-05-8	1.058	2.006	1.479	12.027
						2-5-1-W-T-U-N-F-05-9	1.058	2.009	1.487	12.029
						2-5-1-W-T-U-N-F-05-10	1.058	2.006	1.408	12.040
Lab 3	W	T	N	F	05	3-5-2-W-T-U-N-F-05-1	1.054	2.007	1.540	12.034
						3-5-2-W-T-U-N-F-05-2	1.056	2.011	1.528	12.030
						3-5-2-W-T-U-N-F-05-3	1.057	2.000	1.522	12.032
						3-5-2-W-T-U-N-F-05-4	1.056	2.004	1.553	12.030
						3-5-2-W-T-U-N-F-05-5	1.056	2.001	1.551	12.022
Lab 4	W	T	N	F	05	4-5-2-W-T-U-N-F-05-6	1.056	2.007	1.537	12.002
						4-5-2-W-T-U-N-F-05-7	1.056	2.004	1.515	12.021
						4-5-2-W-T-U-N-F-05-8	1.056	2.007	1.545	12.007
						4-5-2-W-T-U-N-F-05-9	1.057	2.009	1.550	12.021
						4-5-2-W-T-U-N-F-05-10	1.058	2.008	1.553	12.014
Lab 5	L	T	N	F	05	5-6-1-W-T-U-N-F-05-1	1.056	2.003	1.549	12.027
						5-6-1-W-T-U-N-F-05-2	1.058	2.003	1.493	12.019
						5-6-1-W-T-U-N-F-05-3	1.061	2.005	1.565	12.006
						5-6-1-W-T-U-N-F-05-4	1.058	2.002	1.562	12.003
						5-6-1-W-T-U-N-F-05-5	1.057	2.001	1.555	12.000
Lab 6	W	T	N	F	05	6-6-1-W-T-U-N-F-05-6	1.057	2.004	1.482	12.001
						6-6-1-W-T-U-N-F-05-7	1.056	2.000	1.531	12.006
						6-6-1-W-T-U-N-F-05-8	1.055	2.001	1.485	12.003
						6-6-1-W-T-U-N-F-05-9	1.056	2.001	1.517	12.010
						6-6-1-W-T-U-N-F-05-10	1.055	2.000	1.527	12.026
Lab 7	W	T	N	F	05	7-6-2-W-T-U-N-F-05-1	1.059	2.004	1.526	12.045
						7-6-2-W-T-U-N-F-05-2	1.058	1.999	1.530	12.030
						7-6-2-W-T-U-N-F-05-3	1.061	2.003	1.520	12.017
						7-6-2-W-T-U-N-F-05-4	1.062	2.005	1.501	12.023
						7-6-2-W-T-U-N-F-05-5	1.059	2.003	1.542	12.015

[4] Sandwich panels were fabricated and specimens were cut using processes, specifications and dimensions in US customary units.

Table AII: Second set of SCB specimens manufactured at NIAR[4]

Lab #	L/W	Teflon / Saw cut	Doubler (Y/N)	Fixture (Fixed / Sliding)	Test Speed	SPECIMEN NAME	AVG THICKNESS [in]	AVG WIDTH [in]	AVG INSERT LENGTH [in]	LENGTH [in]
Lab 1	W	S	N	F	30	1-1-1-W-S-X-N-F-30-01	1.055	2.001	N/A	12.056
						1-1-1-W-S-X-N-F-30-02	1.056	1.999	N/A	12.059
						1-1-1-W-S-X-N-F-30-03	1.057	1.998	N/A	12.050
						1-1-1-W-S-X-N-F-30-04	1.058	1.997	N/A	12.043
						1-1-1-W-S-X-N-F-30-05	1.058	1.996	N/A	12.048
						1-1-1-W-S-X-N-F-30-06	1.057	1.998	N/A	12.053
						1-1-1-W-S-X-N-F-30-07	1.059	1.994	N/A	12.055
						1-1-1-W-S-X-N-F-30-08	1.058	1.999	N/A	12.056
						1-1-1-W-S-X-N-F-30-09	1.057	1.996	N/A	12.064
						1-1-1-W-S-X-N-F-30-10	1.058	1.995	N/A	12.062
Lab 2	W	S	N	S	05	2-1-2-W-S-X-N-S-05-01	1.053	2.000	N/A	12.041
						2-1-2-W-S-X-N-S-05-02	1.054	2.002	N/A	12.035
						2-1-2-W-S-X-N-S-05-03	1.054	2.001	N/A	12.029
						2-1-2-W-S-X-N-S-05-04	1.056	2.003	N/A	12.026
						2-1-2-W-S-X-N-S-05-05	1.055	2.000	N/A	12.023
						2-1-2-W-S-X-N-S-05-06	1.055	2.003	N/A	12.024
						2-1-2-W-S-X-N-S-05-07	1.057	2.000	N/A	12.023
						2-1-2-W-S-X-N-S-05-08	1.056	2.002	N/A	12.034
						2-1-2-W-S-X-N-S-05-09	1.056	2.006	N/A	12.033
						2-1-2-W-S-X-N-S-05-10	1.056	2.001	N/A	12.034
Lab 3	W	T	N	S	20	3-2-1-W-T-U-N-S-20-01	1.060	1.994	1.598	12.041
						3-2-1-W-T-U-N-S-20-02	1.060	2.001	1.555	12.048
						3-2-1-W-T-U-N-S-20-03	1.062	2.000	1.545	12.036
						3-2-1-W-T-U-N-S-20-04	1.063	2.000	1.545	12.041
						3-2-1-W-T-U-N-S-20-05	1.064	1.997	1.581	12.038
						3-2-1-W-T-U-N-S-20-06	1.062	1.998	1.567	12.048
						3-2-1-W-T-U-N-S-20-07	1.061	2.006	1.550	12.035
						3-2-1-W-T-U-N-S-20-08	1.061	2.000	1.543	12.038
						3-2-1-W-T-U-N-S-20-09	1.061	2.003	1.490	12.047
						3-2-1-W-T-U-N-S-20-10	1.059	2.001	1.562	12.065
Lab 4	W	T	Y	S	05	4-2-2-W-T-U-D-S-05-01	1.060	1.995	1.441	12.073
						4-2-2-W-T-U-D-S-05-02	1.062	1.998	1.459	12.057
						4-2-2-W-T-U-D-S-05-03	1.060	2.000	1.449	12.043
						4-2-2-W-T-U-D-S-05-04	1.062	1.997	1.441	12.025
						4-2-2-W-T-U-D-S-05-05	1.062	1.999	1.479	12.026
						4-2-2-W-T-U-D-S-05-06	1.062	2.004	1.489	12.028
						4-2-2-W-T-U-D-S-05-07	1.061	1.996	1.476	12.028
						4-2-2-W-T-U-D-S-05-08	1.061	1.997	1.469	12.029
						4-2-2-W-T-U-D-S-05-09	1.061	1.997	1.489	12.041
						4-2-2-W-T-U-D-S-05-10	1.059	1.997	1.487	12.047
Lab 5	L	T	N	F	20	5-9-1-L-T-U-N-F-20-01	1.058	1.999	1.562	12.013
						5-9-1-L-T-U-N-F-20-02	1.061	2.007	1.615	12.010
						5-9-1-L-T-U-N-F-20-03	1.062	2.003	1.582	12.008
						5-9-1-L-T-U-N-F-20-04	1.061	2.007	1.531	12.003
						5-9-1-L-T-U-N-F-20-05	1.061	2.002	1.564	12.002
						5-9-1-L-T-U-N-F-20-06	1.061	2.006	1.550	12.005
						5-9-1-L-T-U-N-F-20-07	1.062	2.006	1.485	12.010
						5-9-1-L-T-U-N-F-20-08	1.061	2.009	1.548	12.008
						5-9-1-L-T-U-N-F-20-09	1.060	2.008	1.539	12.011
						5-9-1-L-T-U-N-F-20-10	1.059	2.007	1.558	12.020
Lab 6	W	S	Y	F	05	6-4-1-W-S-X-D-F-05-01	1.060	2.001	N/A	12.058
						6-4-1-W-S-X-D-F-05-02	1.060	2.005	N/A	12.061
						6-4-1-W-S-X-D-F-05-03	1.060	2.003	N/A	12.044
						6-4-1-W-S-X-D-F-05-04	1.061	2.005	N/A	12.055
						6-4-1-W-S-X-D-F-05-05	1.062	2.005	N/A	12.026
						6-4-1-W-S-X-D-F-05-06	1.061	2.003	N/A	12.033
						6-4-1-W-S-X-D-F-05-07	1.060	2.006	N/A	12.035
						6-4-1-W-S-X-D-F-05-08	1.060	2.004	N/A	12.040
						6-4-1-W-S-X-D-F-05-09	1.060	2.002	N/A	12.048
						6-4-1-W-S-X-D-F-05-10	1.057	2.004	N/A	12.050
Lab 7	W	T	Y	S	05	7-4-2-W-T-U-D-S-05-01	1.055	2.003	1.515	12.048
						7-4-2-W-T-U-D-S-05-02	1.059	2.003	1.547	12.046
						7-4-2-W-T-U-D-S-05-03	1.058	2.007	1.559	12.039
						7-4-2-W-T-U-D-S-05-04	1.058	2.003	1.573	12.039
						7-4-2-W-T-U-D-S-05-05	1.058	2.005	1.474	12.038
						7-4-2-W-T-U-D-S-05-06	1.060	2.001	1.474	12.035
						7-4-2-W-T-U-D-S-05-07	1.059	2.003	1.533	12.027
						7-4-2-W-T-U-D-S-05-08	1.060	1.997	1.558	12.032
						7-4-2-W-T-U-D-S-05-09	1.060	2.001	1.548	12.048
						7-4-2-W-T-U-D-S-05-10	1.059	2.006	1.551	12.073

APPENDIX B – TEST PROTOCOL

B1 Required test setup

Following the procedure, an upwards, vertical load is applied to the specimen via a piano hinge or block connected to the testing machine crosshead, causing a peel loading of the disbonded face sheet. For the test, a properly calibrated test machine shall be used that can be operated in a displacement-control and force-control mode with a constant displacement rate in the range from 0.5 mm/min to 10.0 mm/min. The testing machine load-sensing device shall be capable of indicating the total load carried by the test specimen. This device shall be essentially free from inertial lag at the specified rate of testing and shall indicate the load with an accuracy over the load range(s) of interest of within ±1% of the indicated value.

For the SCB test, a loading rod is required to offset the load application point from the surface of the specimen if a fixed base plate (see Figure 2a and Figure 4a) is to be used. This serves to ensure that load point rotation is minimized to levels that do not adversely affect the test loading conditions. The loading rod shall be connected to the piano hinge or pinned to the loading block bonded onto the specimen on one end, while the remaining end of the loading rod is connected to the crosshead of the test machine. A base plate shall contain a clamping mechanism to apply a clamping force to the sides of the lower face sheet, holding the specimen stationary during testing. For the translatable carriage fixture shown in Figure 2b and Figure 4b, the base plate shall perform the same functions as those stated above with the additional function of being translatable in a horizontal direction via a pair of linear bearings.

To conduct the test, the testing machine heads shall be capable of being attached to the loading rod and the base plate assembly. The loading rod must be attached to the crosshead via a pinned connection that prevents the development of a moment arm in the loading rod. The connection of the base plate to the machine must maintain perpendicularity to the line of loading and the flat surface to which the specimen is attached. During the test, the opening displacement may be estimated as the crosshead separation, provided the deformation of the test system (test machine and fixture), with the specimen grips attached, is less than 2% of the opening displacement of the test specimen. If not, then the opening displacement shall be obtained from a properly calibrated external gage or transducer attached to the specimen. The displacement indicator shall indicate the disbond opening displacement with an accuracy of within ±1% of the indicated value once the disbond occurs. A digital record of force vs. load point displacement shall be stored for subsequent post-processing.

For visual disbond monitoring, a travelling optical microscope with a magnification no greater than 70×, or an equivalent magnifying device, shall be positioned on one side of the specimen to observe the disbond front as it extends along one edge during the test. This device shall be capable of pinpointing the disbond front with an accuracy of at least ±0.5 mm (±0.02 in.). A mirror may be used to determine visually any discrepancy in disbond onset from one side of the specimen to the other. Other methods, such as disbond length gages bonded to a specimen edge, may be used to monitor disbond length, provided their accuracy is as good as the optical microscope so that disbond length may be measured to the accuracy specified above. In the test setup shown in Figure 4a, video cameras were used on both sides of the specimen and the disbond location was observed via a computer monitor.

B2 Step-by-step test procedure

A step-by-step procedure was developed and shared with the participating labs to ensure that tests would be conducted in a consistent manner:

- Measure the width of each specimen to the nearest 0.05 mm (0.002 in.) at the midpoint and at 25 mm (1 in.) from either end. The variation in thickness along the length of the specimen shall not exceed 0.1 mm (0.004 in.). The average values of the width and thickness measurements shall be recorded.
- Estimate load and displacement at the onset of disbond growth using

$$\delta_c = \sqrt{\frac{8G_c^{est}}{3E_f t_f^3}}\left(a_0 + \left[\frac{t_c t_f^3 E_f}{3E_c}\right]^{\frac{1}{4}}\right)^2, \quad P_c = \sqrt{\frac{E_f b^2 t_f^3 G_c^{est}}{6}} \Bigg/ \left(a_0 + \left[\frac{t_c t_f^3 E_f}{3E_c}\right]^{\frac{1}{4}}\right) \qquad \text{(B-1)}$$

where the values and properties in Tables II and III are used to estimate:

1. load and displacement at disbond growth onset at $a=a_0$,
2. load-displacement response over the five 10-mm disbond growth increments (discussed below).

The resulting data are shown in Figure B2-1a and B2-1b corresponding to $G_c^{est} = \min G_c^{est}$ and $G_c^{est} = \max G_c^{est}$, respectively. These data may be used to anticipate the load and displacement ranges expected during a test on a baseline SCB specimen.

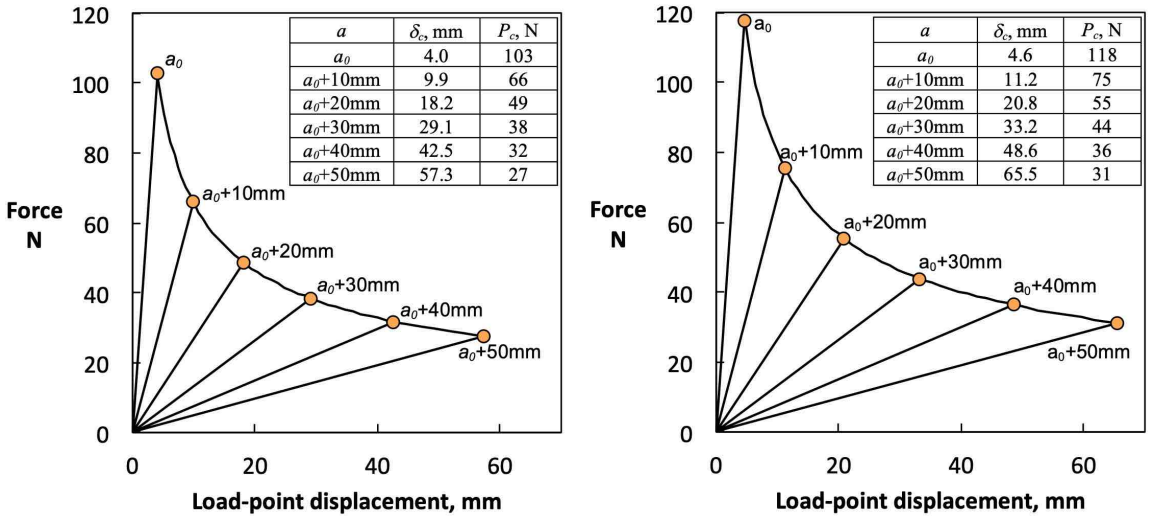

(a). *Response for G_c^{est}=0.69 kJ/m²* (b). *Response for G_c^{est}=0.9 kJ/m²*

Figure B2-1. Estimated force/displacement responses.

- Apply a coat of white aerosol paint to the edge of the specimen, including the disbonded face sheet and core, to aid the visual detection of disbond initiation. Afterwards, mark the first 10 mm (0.2 in.) from the initial disbond tip towards the expected direction of disbond growth with thin vertical lines every 1 mm (0.04 in.). Mark the remaining amount of disbond growth with thin vertical lines every 5 mm (0.2 in.). Other methods including the application of adhesive-backed scales can also be used when applicable. The disbond length is the sum of the distance from the loading line to the end of the initial disbond

(measured in the undeformed state) plus the increment of growth determined from the tick marks.

- Connect one end of the loading rod to the upper head of the test machine using the aforementioned connection types.
- Mount the base plate onto the lower head of the test machine followed by clamping of the specimen onto the base plate using the side clamps. Care must be taken to ensure the load block or hinge on the specimen is aligned and centered with the loading rod.
- Connect the remaining end of the loading rod to a wedge grip, if hinges are being used, or if load blocks are being used, a yoke compatible with the block.
- Two values of disbond initiation from the non-adhesive insert front shall be reported:
    1. at the point of deviation from linearity in the load-displacement curve (NL) and
    2. at the point at which the compliance has increased by 5% or the load has reached a maximum value (5%/max) depending on which occurs first along the load-displacement curve (see Figure B2-2).

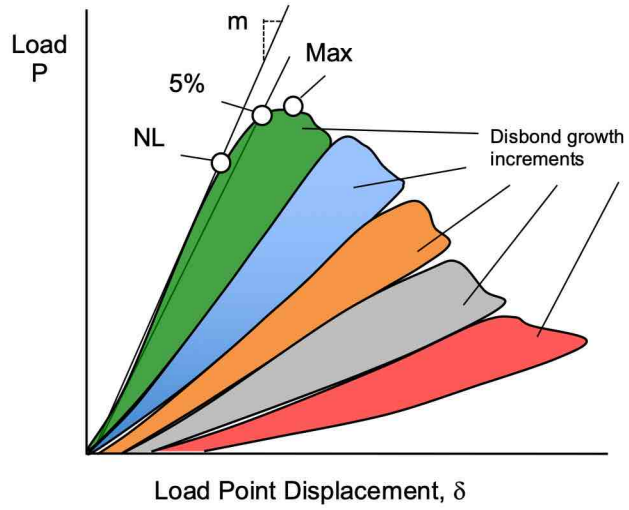

Figure B2-2. Anticipated load/displacement response of SCB Test.

Each definition of disbond initiation is associated with its own value of G_c calculated from the load at the corresponding critical point.

- Load specimen in displacement control at a rate of 5 mm/min until approximately 10 mm of disbond growth has occurred and unload at 5 mm/min. Note the load and displacement at the onset of disbond growth and after completion of the 10-mm growth increment. Record specimen load-displacement response during the entire loading cycle using a sample rate of no less than 4 Hz. Repeat this procedure five times.
- Values for toughness shall not be calculated for any specimen that fails by breaking in some manner other than disbond advance, such as breaking at some obvious flaw, unless such flaw constitutes a variable being studied. Acceptable failure modes for G_c are those resulting in disbond growth occurring either at or in the vicinity of the face sheet/core interface, or within the core material, parallel to the plane of the face sheet/core interface. Retests shall be performed for any specimen on which values are not calculated.

B3 Interfacial Fracture Toughness Calculations

Two data reduction methods for calculating G_c values were evaluated for use in this test method [6, 9, 12, 15]. These consist of a modified beam theory method (MBT) and an area method (AM). The MBT method will enable calculation of G_c associated with disbond initiation and propagation, while the area method yields propagation values of G_c corresponding to the disbond growth increment used in the AM method.

The beam theory expression for the compliance solution of the SCB specimen modeled as a cantilever beam supported on an elastic foundation is given by [9, 12]:

$$C_{SCB} = \frac{\delta}{P} = D_f \left[a + \Delta\right]^3 \tag{B3-1}$$

where D_f is the compliance coefficient related to the bending rigidity of the disbonded face sheet,

$$D_f = \frac{4}{E_f b t_f^3} \tag{B3-2}$$

and Δ is the effective disbond extension due to disparity between the core and cantilever beam stiffness,

$$\Delta = \frac{1}{\lambda} = \left[\frac{t_c t_f^3 E_f}{3E_c}\right]^{\frac{1}{4}} \tag{B3-3}$$

which may be determined experimentally by generating a least squares plot of the cube root of compliance, $C^{1/3}$, as a function of disbond length (Figure B3-1a). The compliance, C, is the ratio of the load point displacement to the applied load, δ/P. The values used to generate this plot should be the loads and displacements corresponding to the visually observed disbond onset on the edge and all the propagation values. Calculate the interfacial fracture toughness as follows:

$$G_c = \frac{3P\delta}{2b\left(a + |\Delta|\right)} \tag{B3-4}$$

Calculate values of G_c corresponding to disbond growth initiation from the non-adhesive insert as described above. Repeat this procedure for each loading cycle. Report the values of G_c from the last four loading cycles.

Using the area method, the interfacial fracture toughness is calculated as follows:

$$G_c = \frac{dU}{dA} \tag{B3-5}$$

where the energy dissipated, *dU*, during a disbond growth increment, *da*, is given by the shaded area depicted in Figure B3-1b. The area, *dA,* of a disbond created during a growth increment,

$$dA = b\left(a_2 - a_1\right) \tag{B3-6}$$

is the difference between the disbond length, a_1, at the start of a growth increment and the final disbond length, a_2, at the end of the growth increment, as illustrated in Figure B3-1b.

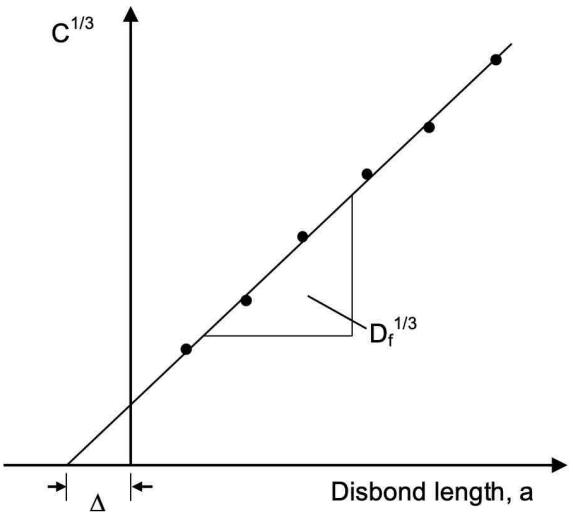

(a). *Modified Beam Theory.*

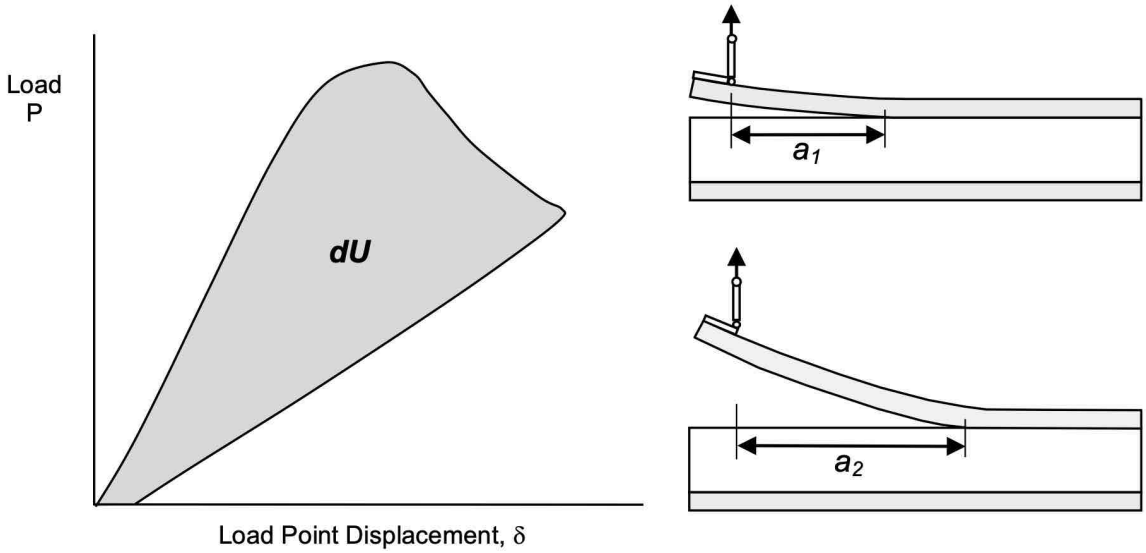

(b). *Area Method.*

Figure B3-1. Data reduction methods.

For each series of tests, the average value, standard deviation and coefficient of variation (in percent) are calculated for each property determined:

$$\bar{x} = \left(\sum_{i=1}^{n} x_i \right) / n \tag{B3-7}$$

$$S_{n-1} = \sqrt{\left(\sum_{i=1}^{n} x_i^2 - n\bar{x}^2 \right) / \left(n-1 \right)} \tag{B3-8}$$

$$CV = 100 \times S_{n-1} / \bar{x} \tag{B3-9}$$

where $\bar{x}$ is the sample mean (average), S_{n-1} is the sample standard deviation, CV is the sample coefficient of variation (in percent), n is the number of specimens, and x_i is the measured or derived property.

B4 Reporting

For reporting, it was recommended to include coupon data such as specimen thickness and width. Further, it was suggested to document the type of load introduction (piano hinges or blocks), base plate configuration, drying procedure, relative humidity, test temperature, and loading rate. With respect to test results, it was recommended to document:

- Load vs. displacement curves indicating load and displacement as shown in Figure B2-2.
- Curve fitting parameters pertaining to the MBT compliance solution as shown in Figure B3-1.
- The calculated fracture toughness (see equations B3-4 and B3-5).
- The number of specimens tested and the mean, standard deviation, and coefficient of variation of each version of G_c calculated (see equations B3-7 to B3-9).

Additionally, it was suggested to report any deviations from the round robin test procedure and alteration to the specimen configuration. A recommended data reporting sheet was provided in reference [14].

APPENDIX C – ROUND ROBIN LABORATORY SCB TEST PARAMETERS

C1 Lab 1: University of Utah, Salt Lake City, UT, USA

The test setup used at The University of Utah is shown in Figure C1. The lower (non-tested) face sheet of the specimen was clamped onto the adjustable, non-translating carriage base as shown in Figure C1a. The fixture accommodates specimen widths between 20 mm and 81 mm. A leaf from a commercial piano hinge was bonded onto the face sheet as shown in Figures C1b and C1c. The second leaf of the hinge was removed to allow a clevis-type attachment, Figure C1, without the mechanical interference of a complete hinge.

The bond surfaces associated with the hinge interface was prepared using a standard abrade and solvent wipe protocol. A machinist file was used to abrade the steel hinge, and 240 grit aluminum-oxide sandpaper was used on the face sheet. The abrasion of the face sheet was performed carefully and ceased when exposed carbon fibers were detected. Both surfaces were wiped thoroughly using acetone until no residue remained on the cloth. The bond was completed using a two-part adhesive, *Loctite Hysol 907*, and allowed to fully cure at room temperature per the manufacturer's data sheet. A specified bond line thickness was not maintained during this bond procedure.

The hinge was connected to one end of a 610-mm loading rod while the remaining end was connected to the test frame through an integrated load cell. A similar clevis-type attachment was used to connect the loading rod to the test machine. The rod itself consisted of a 12.7-mm (1/2-in.) -long section of all-thread and a pair of jam nuts. The jam nuts were used at both clevis attachments to eliminate rotation around the longitudinal axis of the rod. The jam nuts also ensured the rod remained perpendicular to the clevises by removing the fit-up clearance of the threaded joint.

The specimens were tested in an unconditioned (as-received) state with the exception of missing starter disbonds on some specimens that required an altered test condition. In these instances, the starter disbond was machined into the core of the specimen, just below the face sheet-adhesive interface using either a paring knife or snap-off blade from a utility knife. A 250-kN-capable *Instron* electromechanical test frame was used to test all 15 specimens. The crosshead displacement was used to measure the load point deflection, δ, of the test specimen at a rate of 5 Hz. An integrated load cell with capacity equal to 1 kN was used to measure the load, P, at the same rate.

Prior to testing, loose segments of the honeycomb core on the edge of each test specimen were trimmed back to the continuous edge to improve detection of disbond growth. Additionally, a thin coat of flat white enamel paint was applied to the edge of each test specimen to facilitate disbond tip detection. A high-contrast adhesive-backed yellow scale with black lettering spaced at 1-mm intervals was applied to each side of the test specimen. The disbond length, a, was measured using each scale and two universal serial bus (USB) digital microscope cameras with 10× to 50× zoom. The disbond length and test frame load were noted during each image capture of the disbond. The images were then reanalyzed to estimate the position of the disbond tip to within ±0.5 mm for reporting. All corresponding data, disbond lengths, and test specimen widths were subsequently used to calculate G_c using the area method. The energy dissipated, dU, was verified using the *Instron* software.

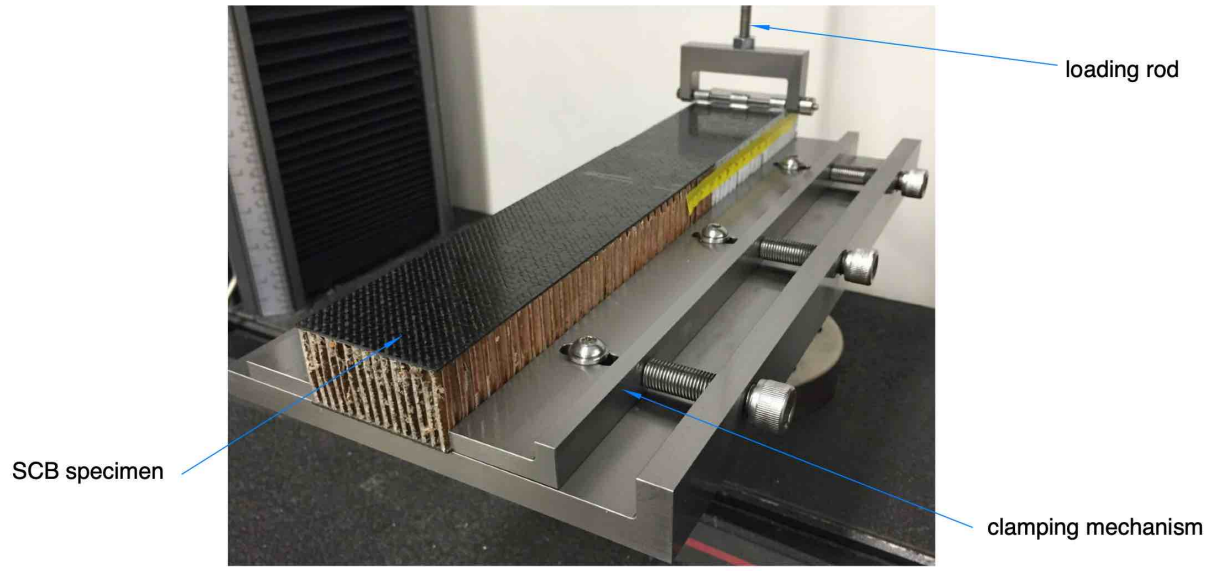

(a). *SCB Test Fixture*.

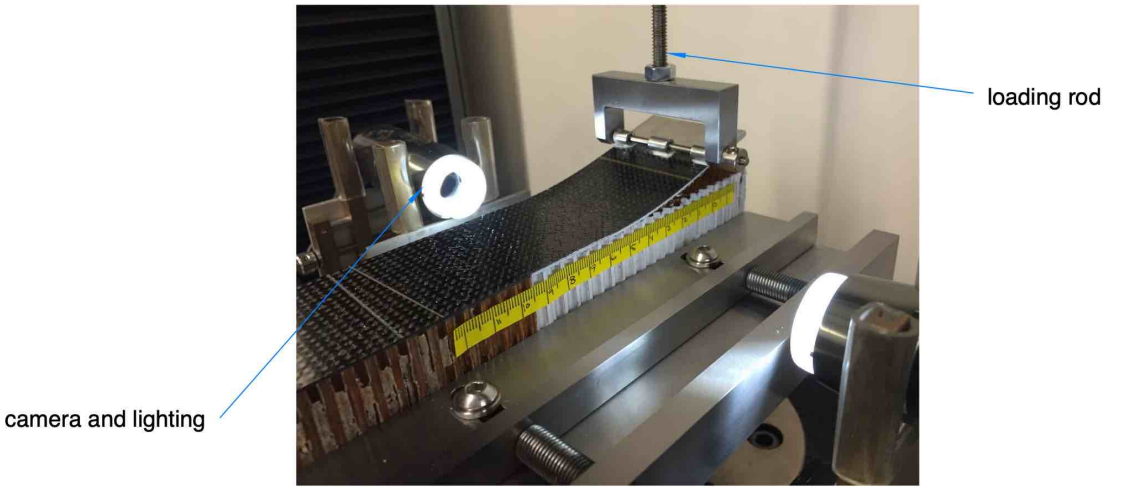

(b). *Detail of test fixture*.

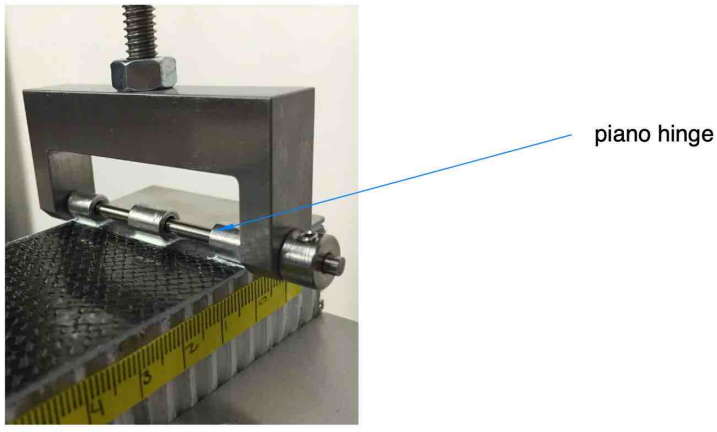

(c). *Detail of hinge assembly*.

Figure C1. Test setup at The University of Utah.

Testing was performed under displacement control at a specified displacement rate. A pseudo fatigue test method protocol was created to control the test frame's up and down movement. This protocol ensured that data was collected during both the loading and unloading portions of the test. One-half of the fatigue cycle was executed before unloading was initiated for the remaining portion of the cycle.

C2 Lab 2: NIAR, Wichita State University, Wichita, KS, USA

The test setup used at NIAR is shown in Figure C2. The lower face sheet of the specimen was clamped into the translatable fixture as shown in Figure C2b. Translation of the sliding mechanism was suppressed for baseline testing. A piano hinge was bonded to the top face sheet as shown in Figures C2. The hinges are connected to the load cell and to the upper part of the test machine via an approximately 610-mm (24-in) loading rod.

The specimens were tested in an unconditioned (as-manufactured) condition. The disbond opening displacement, δ, was measured continuously during the test (minimum of one data point per second) using the actuator displacement of the test machine. The load, P, was measured continuously during the test (minimum of one data point per second) using the integrated load cell.

Two digital microscopes were mounted to traveling stages on both sides of the test specimen for monitoring disbond propagation throughout the test. A thin layer of white spray paint was applied to both sides of the specimen and a printed paper scale was then placed approximately 3.2 mm (1/8 in) from the top face sheet for measuring the disbond extension. Disbond propagation was observed and recorded manually. A video camera was also setup in order to be able to review the disbond growth data as a backup.

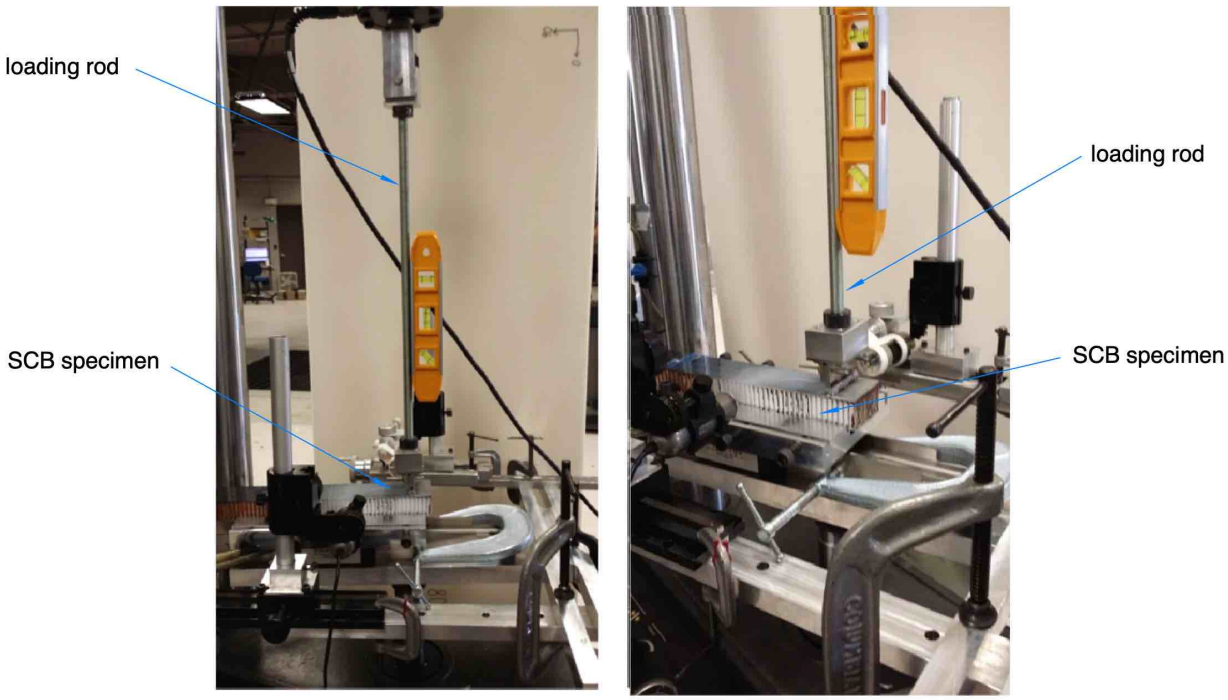

(a). *Test Machine and SCB Test Fixture.*

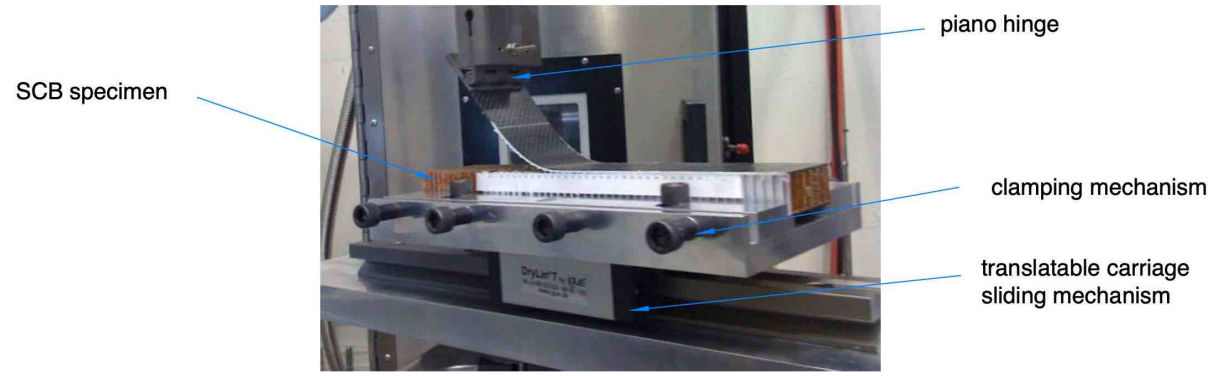

(b). *Detail of test fixture.*

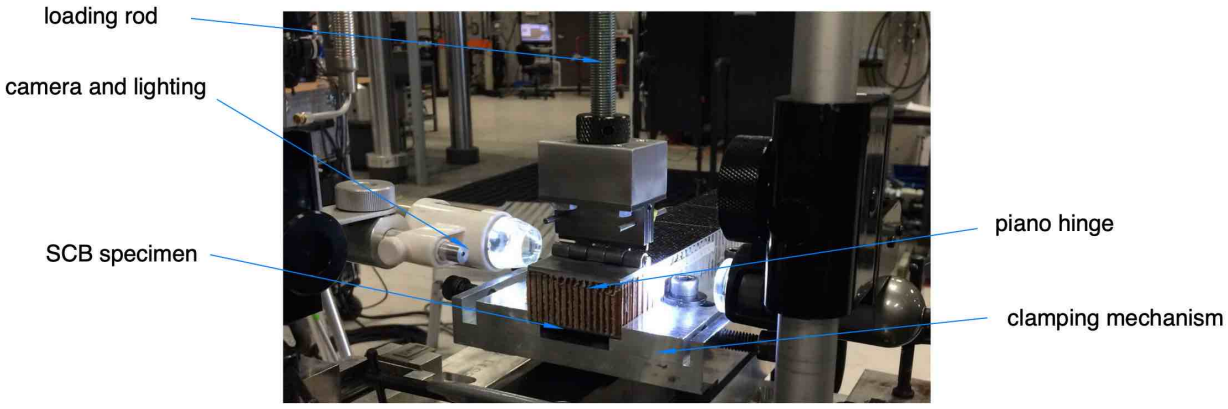

(c). *Detail of clamping mechanism and hinge assembly.*

Figure C2. Test setup at NIAR.

C3 Lab 3: DuPont International Operations, Geneva, Switzerland

The test setup used at DuPont is shown in Figure C3. The lower face sheet of the specimen was adhesively bonded to a steel base plate using two-component room-temperature curing epoxy adhesive (*Loctite® 9461* or *Hysol® 9461*). The steel base plate was screwed onto a translatable fixture which was mechanically fastened to a tensile machine fixed table as shown in Figure C3a. Translation of the sliding mechanism was suppressed in lab 3 for this international round robin campaign.

The upper loading chain includes a loading block, clevis assembly, rod and load cell. Details of the loading block design and dimensions are shown in Figure C3b. The loading block was adhesively bonded to the upper face sheet using two-component epoxy adhesive and connected to loading rod using a clevis assembly as shown in Figures C3c and C3d. The clevis was bolted to the 500-mm-long loading rod (see Figure C3d). The loading cell was installed on top, between the loading rod and tensile machine-driven crosshead.

The specimens were conditioned for at least 1 day at 20°C and 60% relative humidity and also tested under these conditions.

Load, P, and load point deflection, δ, were continuously measured with integrated tensile machine load cell and crosshead positioning device and recorded at 5 Hz frequency. Disbond length, a, was continuously measured with an optical extensometer 5 times per second. The optical extensometer camera was positioned perpendicular to the specimen cross section as shown in picture C3e. The camera was connected to a computer that analyzed pixel color to track the upper face sheet vertical position and then monitor disbond position and a. Accuracy ranging from 50 μm to 150 μm may be obtained using a 5M-pixel sensor.

The software continuously stored test video and data including P, δ, a and time. It calculated fracture toughness G_c at the end of each cycle, as well as specimen average G_c, standard deviation SD and coefficient of variation CV at the end of each test. The optical extensometer was periodically calibrated using a test video and applied ruler.

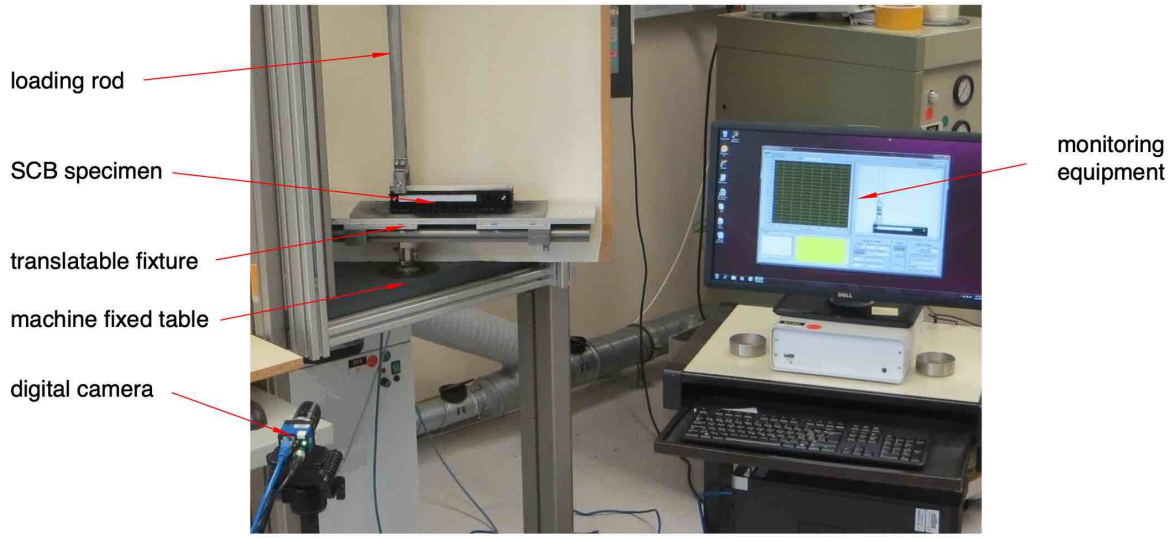

(a). *Test Machine and SCB Test Fixture*.

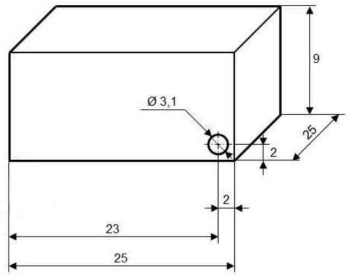

(b). *Loading block (dimensions in mm)*

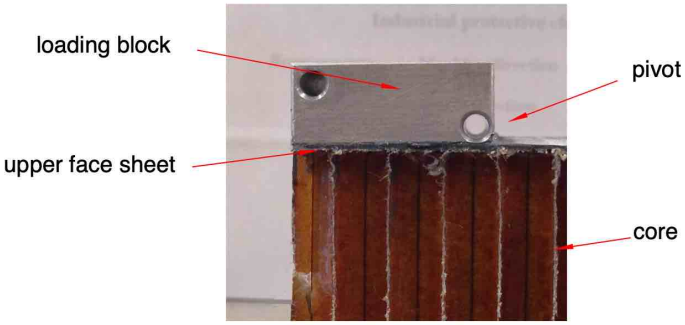

(c). *Detail of loading block*

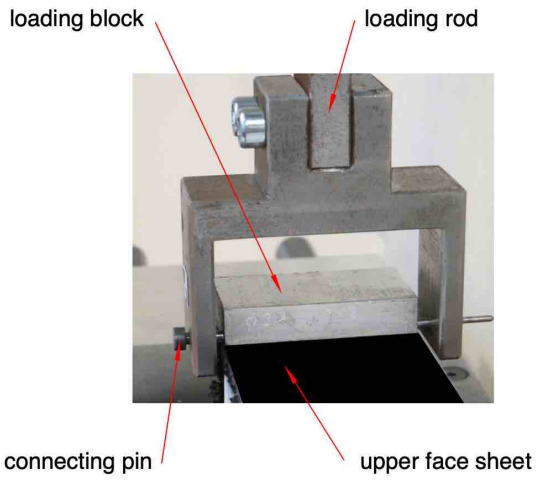

(d). *Detail of clevis assembly*

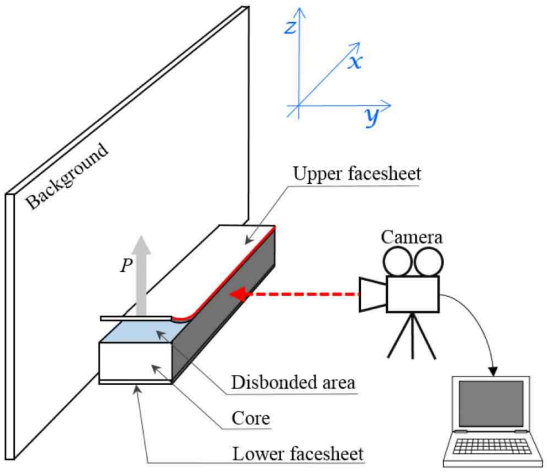

(e). *Schematic of optical extensomter setting*

Figure C3. Test setup at DuPont.

C4 Lab 4: NASA Langley Research Center, Hampton, VA, USA

The test setup used at NASA Langley Research Center is shown in Figure C4. A two-component epoxy adhesive *Hysol 9460* was used to adhesively bond the specimen to the test setup. The bottom face sheet of the specimen was adhesively bonded to a steel base plate, while the upper face sheet was adhesively bonded to a piano hinge for load application. For the set of specimens tested with face sheet doublers, a 3.18-mm-thick fiberglass sheet was first bonded to the upper face sheet, and the piano hinge was bonded to the fiberglass sheet. To achieve high bond quality, surface preparation was performed before bonding. The face sheet and piano hinge surfaces were sand blasted, and the bonding surfaces were treated with isopropyl alcohol. Then, the adhesive was applied and cured at room temperature for 24 hours.

The bonded specimen was then mechanically fastened to the test machine. First, the steel base plate was bolted onto a steel fixture, which was connected to the load cell at the bottom of the test frame as shown in Figure C4a. Second, the piano hinge was screwed into a loading plate, which was connected to a 500-mm-long loading rod as shown in Figures C4b and C4c. Finally, the loading rod was connected to a ball joint, which was connected to the actuator via a clevis and ping rod assembly as shown in Figure C4a. The specimen was aligned with the test fixture such that the base plate of the specimen was initially perpendicular to the loading rod. The piano hinge, ball joint, and clevis setup removed the moment in the loading rod due to small misalignments.

The specimens were tested in an unconditioned state (as received). Testing was performed using an *MTS 858 Table Top System*. The crosshead displacement of the test machine was used to measure the disbond opening displacement, δ, during the test. A 25-kN load cell was used to measure the load, P. Both the load and crosshead displacement were measured continuously at 20 Hz to ensure accurate data collection. Displacement commands were manually input to initiate the test, reverse the crosshead displacement direction at the desired disbond growth length, and stop the test after unloading. The crosshead displacement speed was constant at 5 mm/min for both loading and unloading.

The disbond growth position was collected using two *Point Grey GRAS-50S5M-C* optical cameras with 50-mm *Schneider* compact lenses. The cameras were mounted on travelling rails that were setup to provide clear views of the disbond along the sides of the specimen, as shown in Figure C4b. Each camera had a resolution of 2448 x 2048 pixels. To highlight the disbond growth position, the specimens were coated with a thin layer of white spray paint. A fine, felt tip pen was used to mark the top face sheet at the desired increments behind the disbond tip. The markings were placed at 2-mm increments for the first 10 mm and 5-mm increments for next 50 mm behind the disbond tip. During the test, the disbond was monitored live using the *VIC-Snap* software. As the disbond propagated to the marked increments, the cameras were manually triggered to capture images, along with a stamp of the corresponding load and crosshead displacement. The recorded data were then post-processed using the area method and MBT.

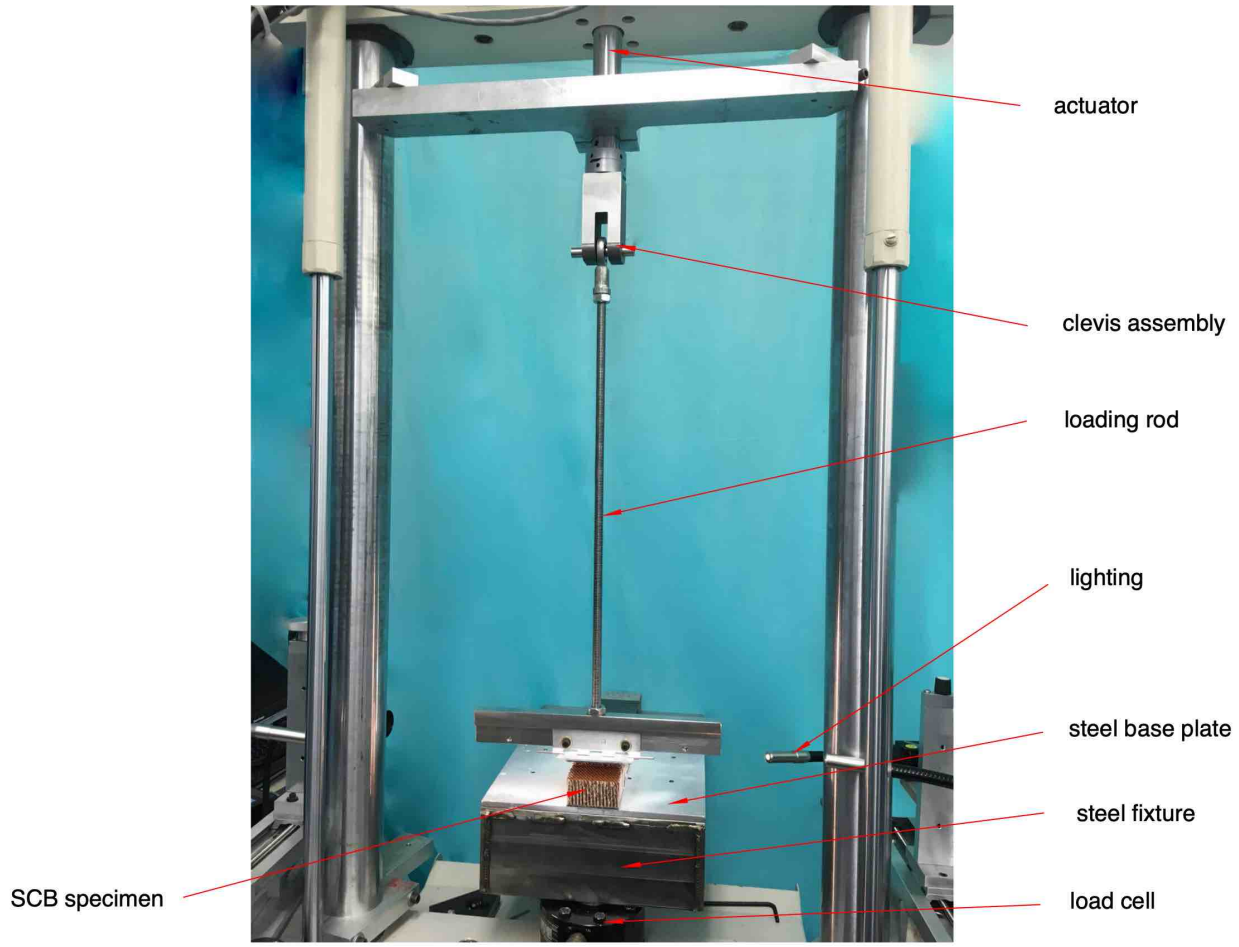

(a). *Test Machine and SCB Test Fixture*.

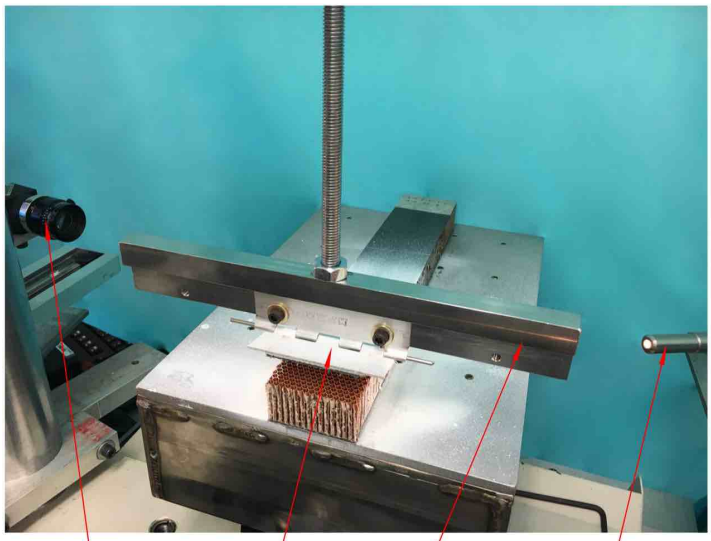

(b). *SCB Test Fixture*.

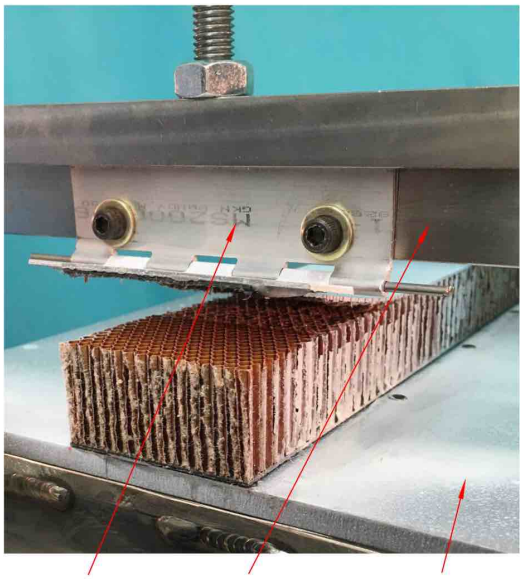

(c). *Detail of hinge assembly*.

Figure C4. Test setup at NASA Langley Research Center.

C5 Lab 5: Fraunhofer Institute for Microstructure of Materials and Systems IMWS, Halle, Germany

The test setup used at IMWS is shown in Figure C5a. The lower (non-tested) face sheet of the specimen was clamped into the fixture as shown in Figures C5b and C5c. A piano hinge was bonded to the face sheet to be tested using a room-temperature-curing structural adhesive (*HUNTSMAN Araldite® 2012*). The upper part of the hinge was screwed into a pulling plaque which was rigidly connected to the lower end of the loading rod, as shown in Figure C5c. In order to keep the load direction as perpendicular as possible with respect to the base plate and specimen, the effective length of the movable loading rod was chosen to be 520 mm, measured as the distance between the pivot point of the piano hinge and joint head at the upper end of the pulling rod.

The specimens were tested in the unconditioned state (as received). The disbond opening displacement, δ, was measured using the crosshead displacement of the electro-mechanical universal testing machine *Instron 5566*. The load, P, was determined by means of the integrated 1-kN load cell. Both δ and P were measured continuously during the test. Data points were acquired two times per second. The disbond was observed during the test and the propagation lengths were recorded. To track the disbond, images on both the left and right specimen side were recorded using two single-lens reflex cameras with 3888 x 2592 pixels each. Mirrors were used to enable unobstructed and clear views simultaneously on the disbond tip at both specimen sides. The camera and mirror setup is shown in Figure C5b. Furthermore, as a result of using the specific mirror assembly, the experimental setup is fully applicable within a climatic chamber while placing the two cameras outside in front of the window. The visible image detail was adjusted to have a resolution of 16 pixel per 1 mm at least. Image recording was carried out based on time-controlled triggering. The actual disbond length, a_i (appertaining to the disbond opening displacement, δ_i, and the load, P_i), was determined to be the average of the visible disbond lengths at both sides of the specimen detected from the recorded pairs of images. To enhance image contrast and increase detail detectability, a thin white paint was applied to the specimen edges. A ruler was positioned at the bottom of each specimen side and vertical auxiliary lines were automatically generated by image processing to assist exact disbond length measuring and avoid possible reading errors which might be caused by perspective image distortion, see Figure C5d.

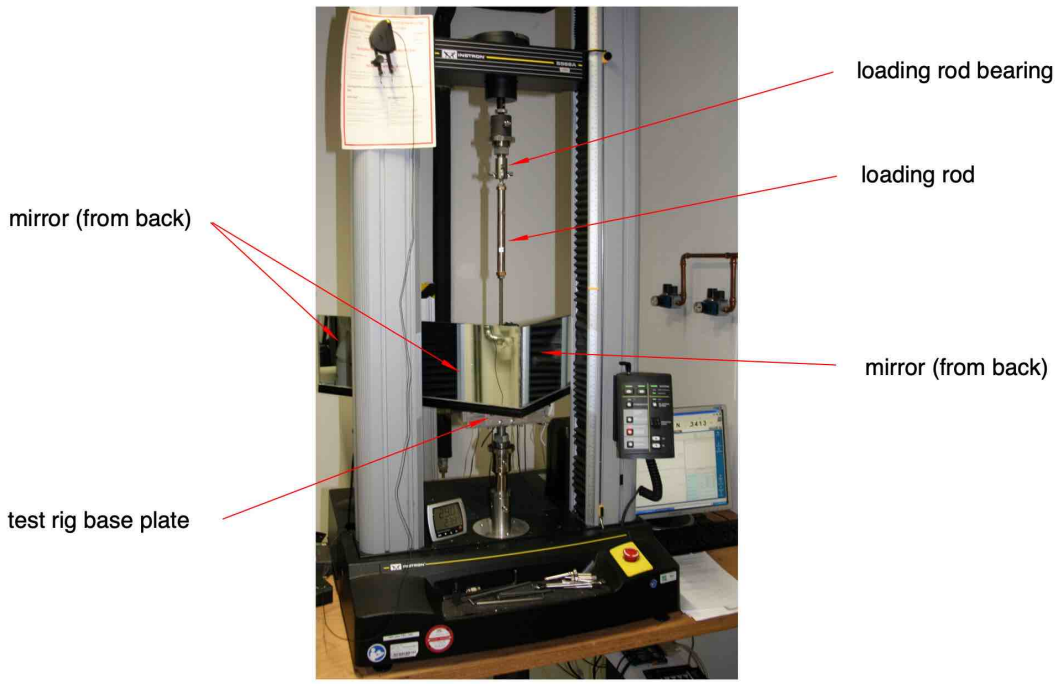

(a). *Instron table-top testing machine with SCB test rig; view from back*

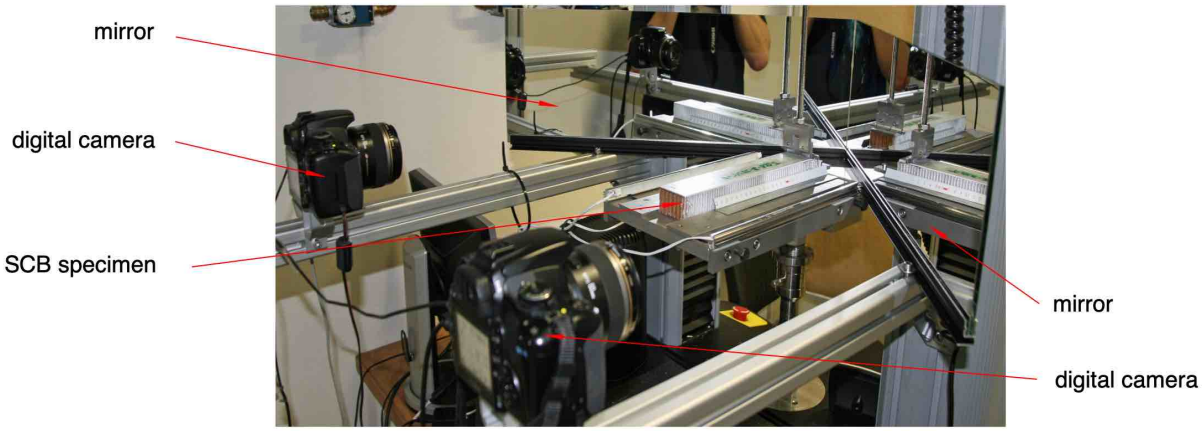

(b). *Mirror set up*

(c). *Detail of SCB test and base plate*

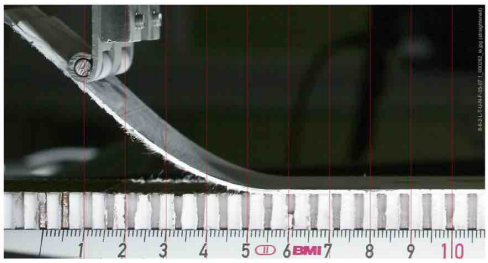

(d). *Left side image with automatically generated auxiliary grid*

Figure C5. Test setup at Fraunhofer IWFM.

C6 Lab 6: Airbus Operations GmbH, Bremen

The test setup used at Airbus is shown in Figure C6a. The lower (non-tested) face sheet of the specimen was clamped into the test fixture as shown in Figure C6b. On the face sheet to be tested, a load block, identical to the one used by Lab 3, was applied as shown in Figure C6c. The dimensions of the load blocks are shown in Figure C3b. The load blocks were applied to the SCB specimens with *HBM X60* adhesive. This adhesive is a two-component room-temperature-curing adhesive. Before bonding, the surface was roughened with sandpaper without damaging any fibers of the laminate. The blocks were connected via a loading rod and load cell to the upper part of the test machine. Due to the large deflection of the face sheet and the fixation of the specimen, a lateral movement of the loading point occurs. In order to keep the load direction as perpendicular as possible, the effective length of the movable loading rod was 326 mm, measured as the distance between the pivot point of the load block and joint head at the upper end of the leverage.

For a subset of specimens, a starter disbond of 40 mm in length was cut into the opposite side of the specimen. All specimens were tested in an unconditioned state (as received). The disbond opening displacement, δ, was measured continuously during the test (one data point per second at least). Crosshead displacement of the test machine was used. The load, P, was measured continuously during the test (one data point per second at least) using the integrated load cell. The disbond lengths for propagation were observed during the test. Images on the right specimen side were recorded by a single optical microscope with a resolution of 1024 x 780 pixels as shown in Figure C6a. To measure the disbond length, a transparent measurement foil was applied to the side of the specimen as shown in Figures C6b and C6d. Image recording was carried out by the test operator. The mean disbond length was determined as the visible disbond length of the right side of the specimen for each of the recorded images. In order to allow proper disbond tip monitoring during the test, the honeycomb cells at the edge of the specimen must be open to the side where the disbond is observed. Otherwise, optical shadows will lead to improperly measured disbond lengths. Therefore, the residues of adjacent cells were cut as shown in Figure C6e.

Before and after the test, the disbond length was measured outside the test fixture on both sides of the specimen again using a microscope with 25× magnification. Therefore, initial disbond length of load cycle 1 and the final disbond length of load cycle 6 is the average value of the left- and right-side measurements.

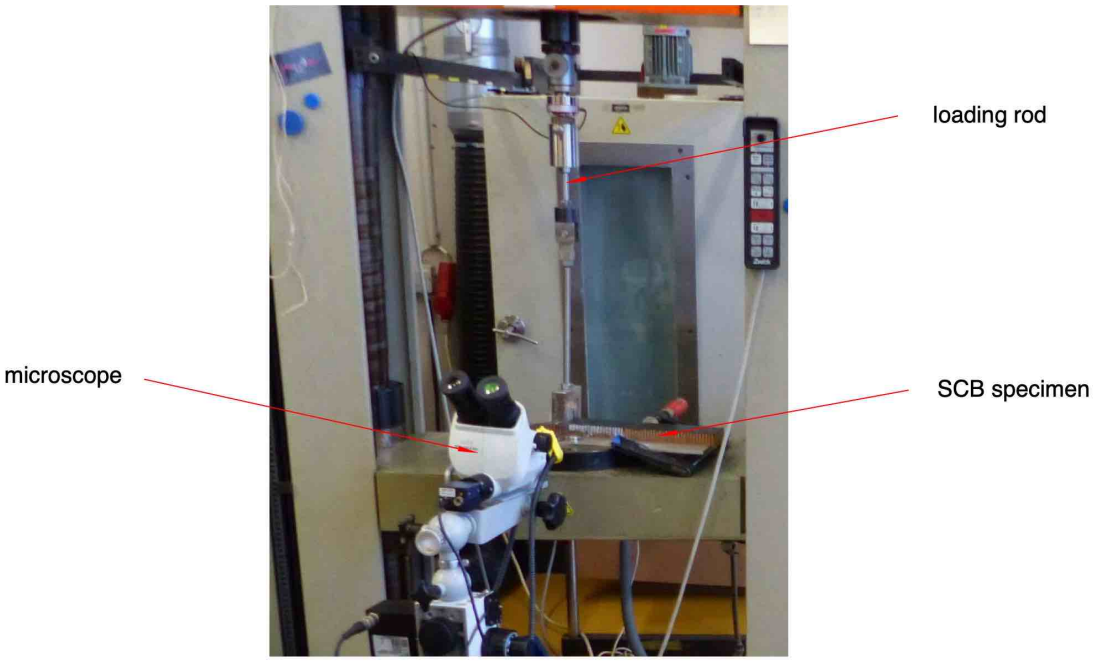

(a). *Test Machine and SCB Test Fixture*.

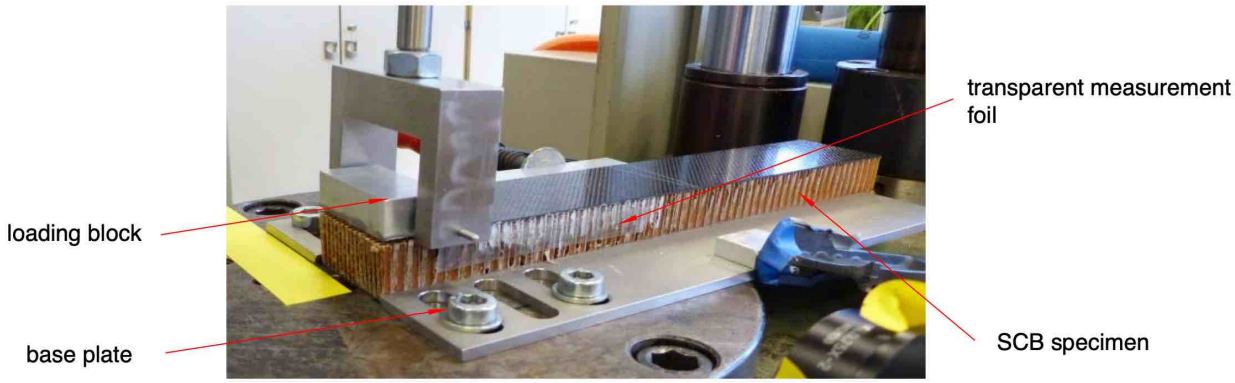

(b). *SCB Test Fixture*.

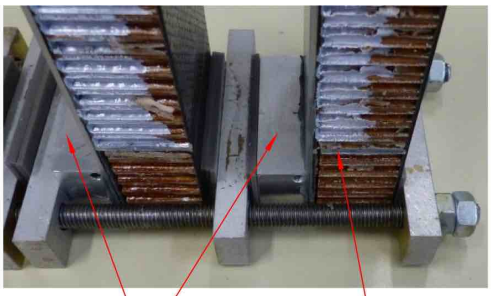

(c). *Application of loading block*

(d). *Detail of measurement foil*

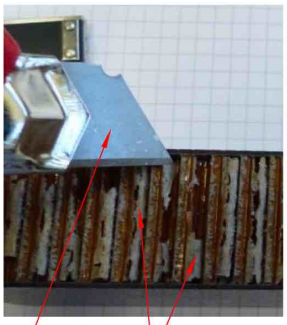

(e). *Cell wall removal*

Figure C6. Test setup at Airbus Bremen.

C7 Lab 7: Technical University of Denmark, Kgs. Lyngby, Denmark

The SCB test setup used at DTU is shown in Figure C7a. Details of the fixture are shown in Figure C7b. The lower (non-tested) face sheet of the specimen was bonded to the test fixture as shown in Figure C7a. On the face sheet to be tested, a hinge (see Figure C7c) was adhesively bonded using *Araldite 2015* adhesive which was cured at room temperature for 24 hours. This process resulted in an adhesive thickness of 0.05 mm to 0.10 mm. The hinge was fitted with a roller bearing to ensure smooth rotation of the loading arm as shown in Figure C7c. The hinges were connected via the hinge housing and the rod/hinge link to the actual loading rod and the load cell located near the upper part of the test machine as shown in Figures C7a and C7c. The primary purpose of hinge mechanism is to avoid friction during loading of the face sheet. Therefore, bearings were introduced in the design (*SKF W6301* and *SKF W619/9*).

Due to the large deflection of the face sheet and the fixation of the specimen, a lateral movement of the loading point occurs. In order to keep the load direction as perpendicular as possible, the effective length of the movable loading rod was 620 mm, measured as the distance between the pivot point of the piano hinge and joint head at the upper end of the leverage. Testing was performed on an *MTS 810* four-column load frame (Model 319.25).

All specimens were tested in the unconditioned state (as received). The disbond opening displacement, δ, was measured continuously during the test (one data point per second at least). Crosshead displacement of the test machine is used. The load, P, was also measured continuously during the test (one data point per second at least) using the integrated load cell. A 5-kN load cell was used, which was calibrated to class 1 accuracy (1% accuracy). The disbond tip location was monitored using a high-resolution camera (*Nikon D3100*) on both sides of the specimen. A mirror was placed to monitor the disbond on the back side. The average of the disbond lengths from front and back side was used in the data reduction. The images were gathered at a rate of 5 Hz for all tests. Prior to mounting of the specimen on the specimen plate, white paint was applied on both sides of the specimen to aid in determining the disbond front. In addition, rulers (scale 1:1) were printed and bonded to the specimen edges to accurately determine the disbond increment during post-processing.

The tests were conducted using vertical displacement levels that, during pilot studies, had shown a disbond growth of approximately 10 mm. Therefore, the *MTS* controller was programmed to begin the test from a 0-mm-displacement, unloaded (0-N) position, and pull the face sheet vertically at a rate of 5 mm/min up to the first displacement level. At the target displacement, the machine would stop, and, as the last picture is captured, the operator would press a button and the unloading cycle would start. The unloading cycle ended when the load cell recorded a zero-load signal.

This process was repeated six times per specimen. Data such as vertical displacement, force and horizontal displacement (during the ‘sliding table’ parametric study) were recorded at a rate of 10 Hz.

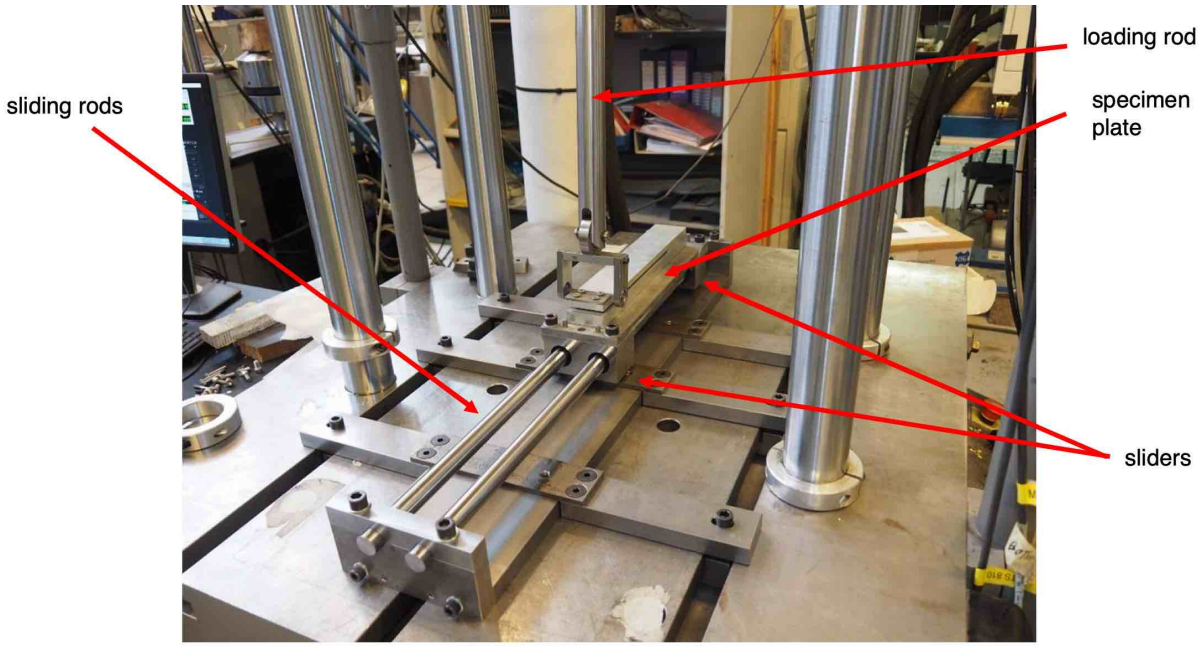

(a). *Test Machine and SCB Test Fixture*.

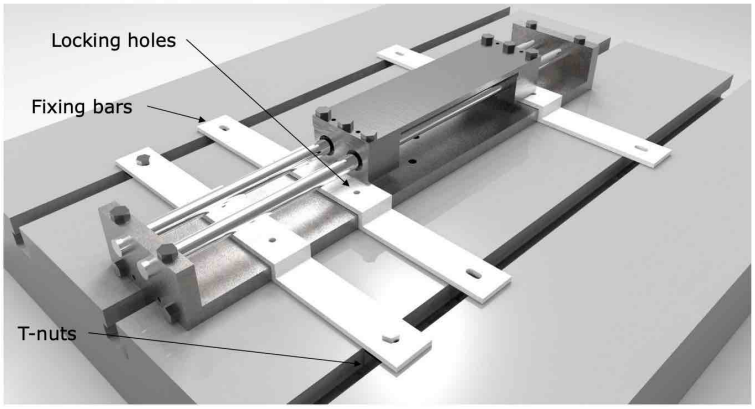

(b). *SCB Test Fixture*.

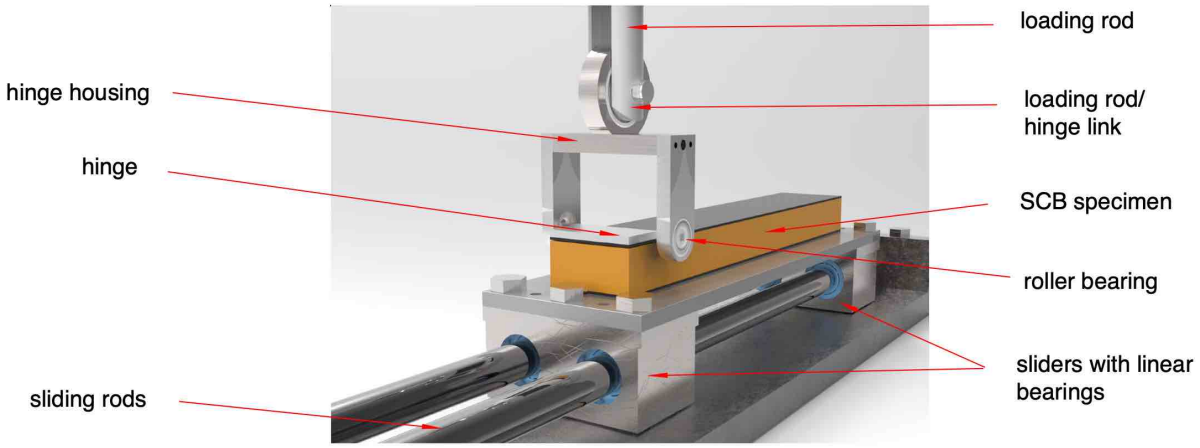

(c). *Detail of test fixture and load application*

Figure C7. Test setup at DTU.

MTS Multipurpose Testware software was used to program the controller. The test was programmed to start from a 0-mm position and then unload to 0 N, which marked the first step. Such a step was included to remove the weight of the loading rod assembly from the load cell. The program subsequently loaded the specimen by pulling the face sheet at a rate of 5 mm/min, up until the first displacement level. The first displacement level was the target displacement which corresponded to a disbond increment of 10 mm. After the last picture was captured at the target displacement level, the unloading cycle started. The controller was programmed such that a "button" was implemented which enabled the operator to initiate the unloading cycle as desired. Data signals from both load cell and cross head displacement were acquired at a rate of 10 Hz. Prior to the start of a test, a laser level gauge was used to ensure that the loading rod remained vertical and perpendicular to the face sheet.

APPENDIX D – RESULTS FROM BASELINE TESTING *(INDIVIDUAL PLOTS FOR THE TESTS FROM ALL LABS)*

D.1 Lab 1: University of Utah, Salt Lake City, UT, USA

Results from the baseline tests performed at The University of Utah (specimens 1-1-1-L-S-X-N-F-30-06, 1-1-1-L-S-X-N-F-30-07, 1-1-1-L-S-X-N-F-30-08, 1-1-1-L-S-X-N-F-30-09 and 1-1-1-L-S-X-N-F-30-06) are shown in Figure D1. The load vs. displacement data obtained are plotted in Figure D1a. Fracture toughness results for individual baseline test specimens are shown in Figure D1b.

D.2 Lab 2: NIAR, Wichita State University, Wichita, KS, USA

Results from the baseline tests performed at NIAR (specimens 2-5-1-L-T-U-N-F-05-06, 2-5-1-L-T-U-N-F-05-07, 2-5-1-L-T-U-N-F-05-08, 2-5-1-L-T-U-N-F-05-09, and 2-5-1-L-T-U-N-F-05-10) are shown in Figure D2. The load vs. displacement data obtained are plotted in Figure D2a. Fracture toughness results are shown in Figures D2b.

D.3 Lab 3: DuPont International Operations, Geneva, Switzerland

Results from the baseline tests performed at DuPont (specimens 3-5-2-L-T-U-N-F-05-01, 3-5-2-L-T-U-N-F-05-02, 3-5-2-L-T-U-N-F-05-03, 3-5-2-L-T-U-N-F-05-04 and 3-5-2-L-T-U-N-F-05-05,) are shown in Figure D3. The load vs. displacement data obtained are plotted in Figure D3a. Fracture toughness results, obtained from the area method, are shown in Figures D3b.

D.4 Lab 4: NASA Langley Research Center, Hampton, VA, USA

Results from the baseline tests performed at NASA Langley Research Center (specimens 4-5-2-L-T-U-N-F-05-07, 4-5-2-L-T-U-N-F-05-08, 4-5-2-L-T-U-N-F-05-09 and 4-5-2-L-T-U-N-F-05-10,) are shown in Figure D4. The load vs. displacement data obtained are plotted in Figure D4a. Fracture toughness results, obtained from the area method and MBT, are shown in Figures D4b and D4c, respectively.

D.5 Lab 5: Fraunhofer IMWS, Halle, Germany

Results from the baseline tests performed at Fraunhofer IMWS (specimens 8-6-2-L-T-U-N-F-05-06, 8-6-2-L-T-U-N-F-05-07, 8-6-2-L-T-U-N-F-05-08, 8-6-2-L-T-U-N-F-05-09, 8-6-2-L-T-U-N-F-05-10) are shown in Figure D5. The load vs. displacement data obtained are plotted in Figure D5a. Fracture toughness results, obtained from the area method, are shown in Figure D5b.

D.6 Lab 6: Airbus Operations GmbH, Bremen

Results obtained at Airbus Operations GmbH, Bremen for the baseline test specimens (6-6-1-L-T-U-N-F-05-06, 6-6-1-L-T-U-N-F-05-07, 6-6-1-L-T-U-N-F-05-08, 6-6-1-L-T-U-N-F-05-09, 6-6-1-L-T-U-N-F-05-10) are shown in Figure D6. The load vs. displacement data obtained are plotted in Figure D6a. Fracture toughness results, obtained from the area method, are shown in Figure D6b. Average results from different data reduction techniques are shown in Figure D6c.

D.7 Lab 7: Technical University of Denmark, Kgs. Lyngby, Denmark

Results obtained at Technical University of Denmark for the baseline test specimens (7-5-2-L-T-U-N-F-05-01, 7-5-2-L-T-U-N-F-05-02, 7-5-2-L-T-U-N-F-05-03, 7-5-2-L-T-U-N-F-05-04 and 7-5-2-L-T-U-N-F-05-05) are shown in Figure D7. The load vs. displacement data obtained are plotted in Figure D7a. Fracture toughness results, obtained from the area method, are shown in Figure D7b.

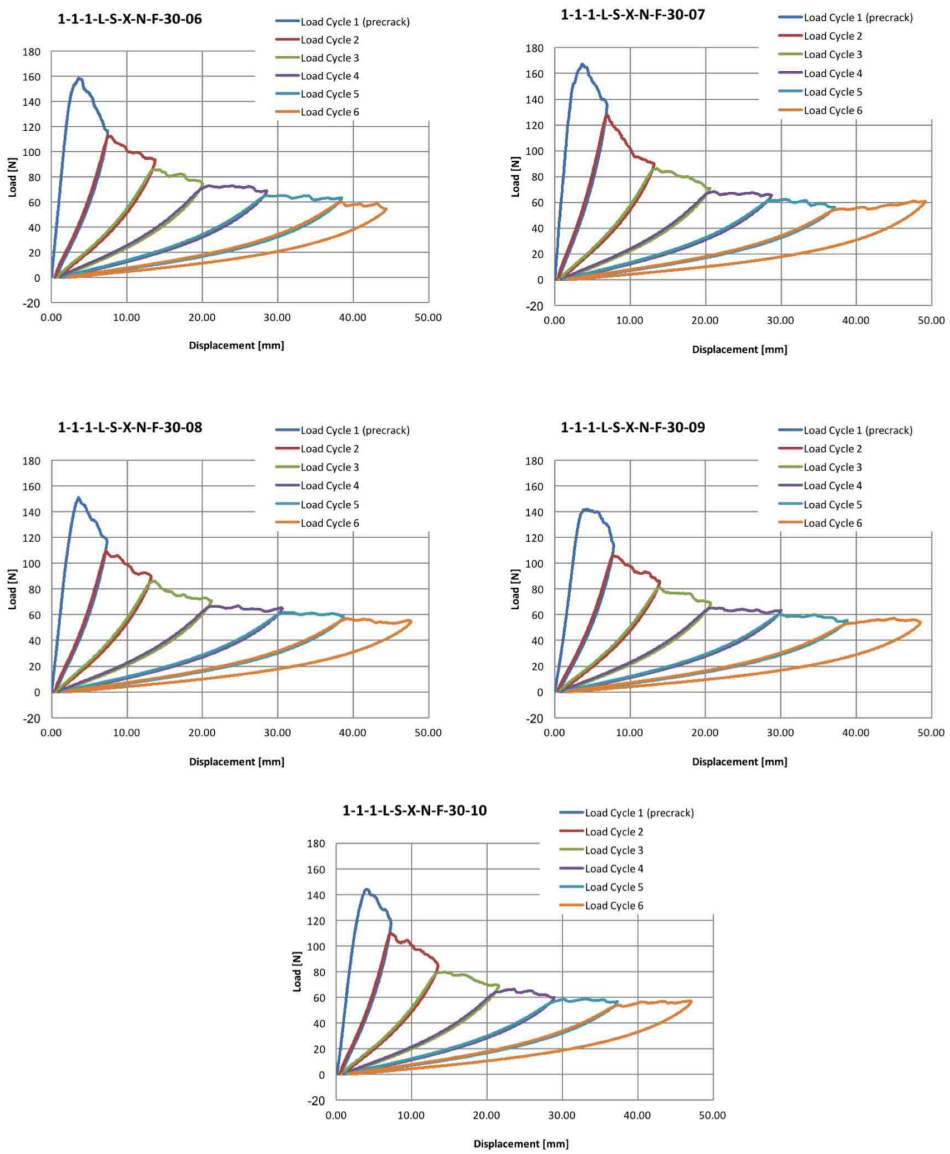

(a). *Load/displacement plots with six loading and unloading cycles for five specimens.*

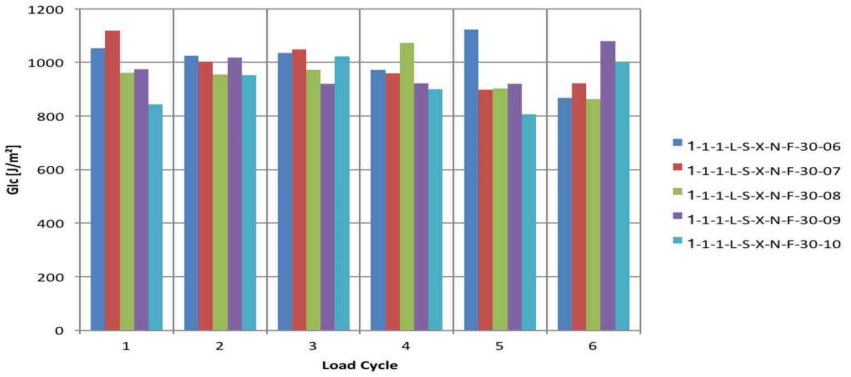

(b). *Measured G_c for individual baseline test specimens*

Figure D1. Results obtained from baseline configurations tested at The University of Utah.

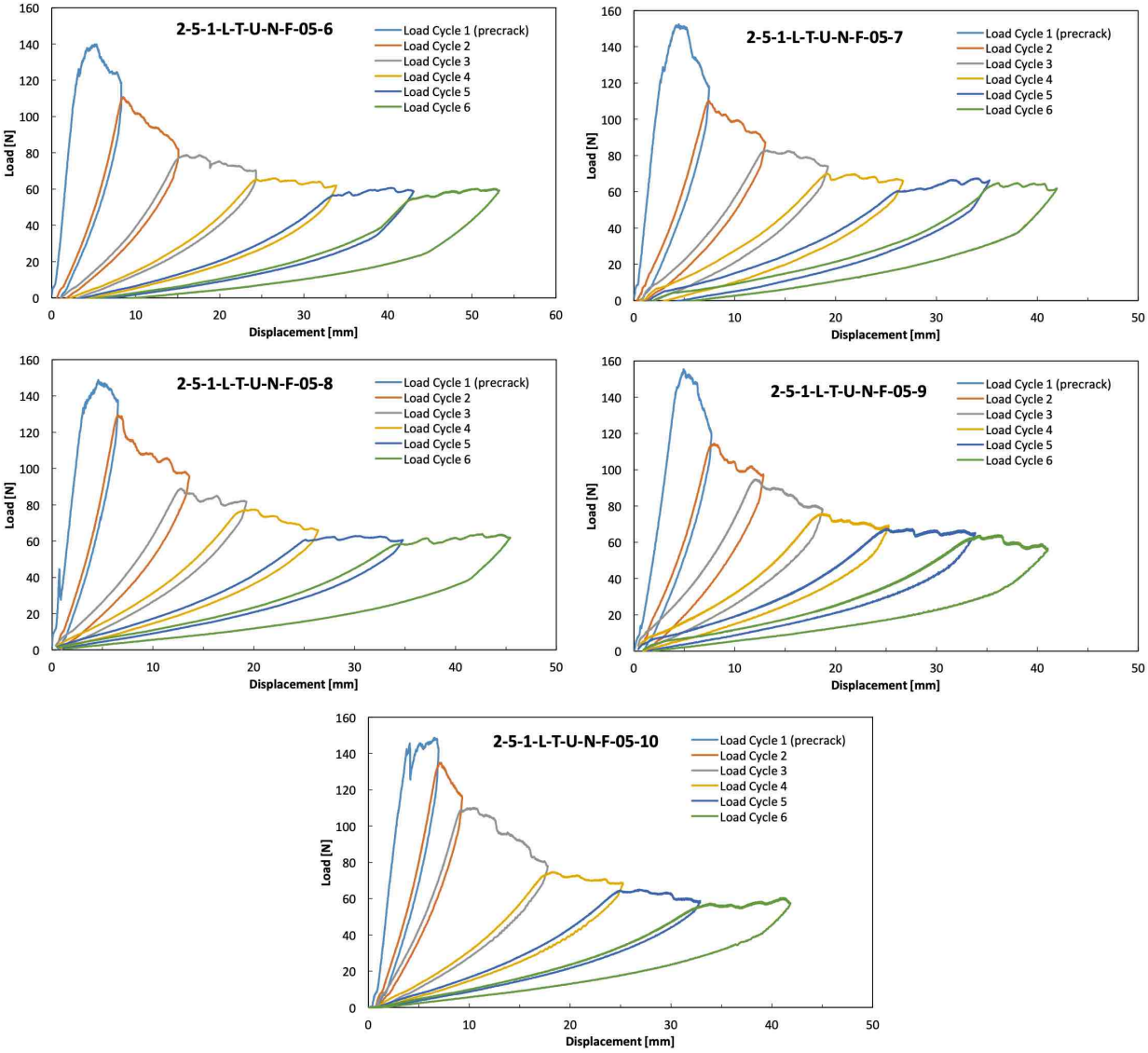

(a). *Load/displacement plots with six loading and unloading cycles for five specimens.*

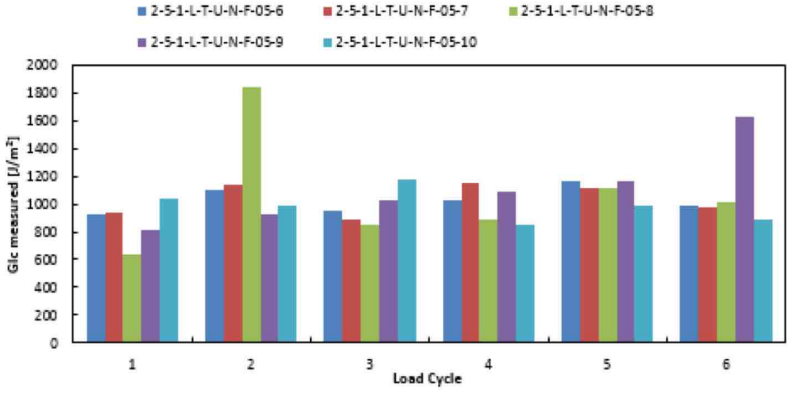

(b). *Fracture toughness values obtained from area method for all five specimens tested.*

Figure D2. Results obtained from baseline configurations tested at NIAR.

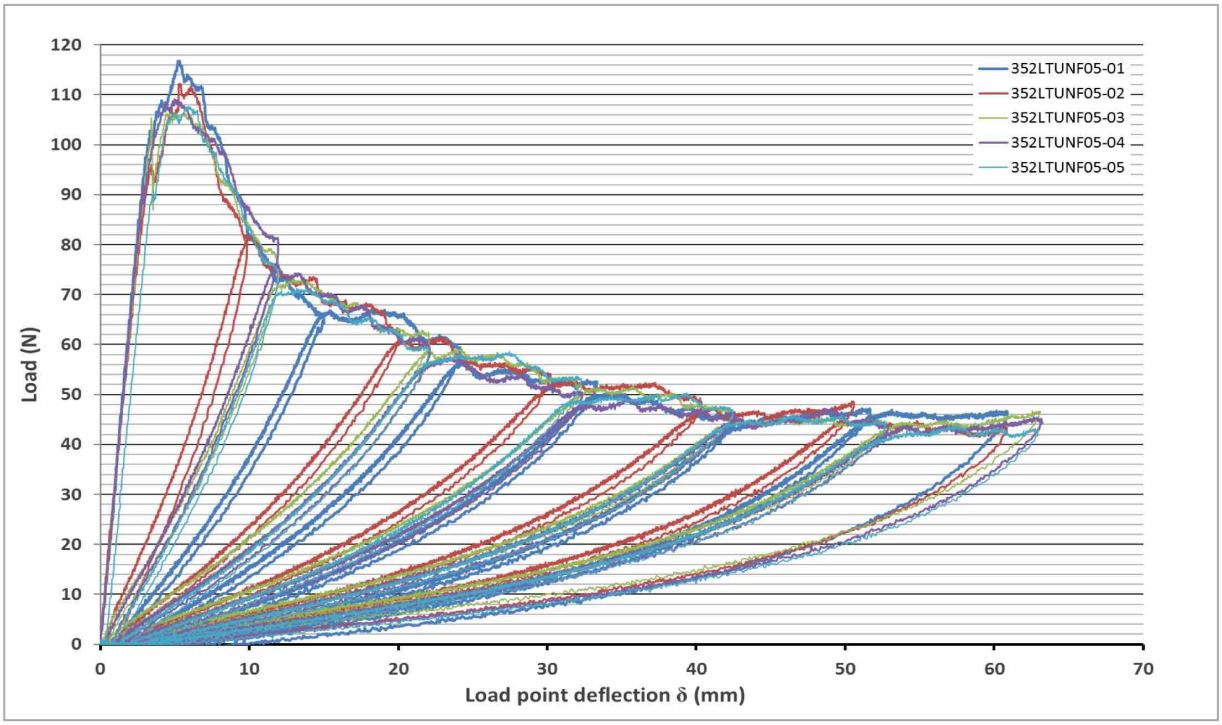

(a). *Load/displacement plots with six loading and unloading cycles for five specimens.*

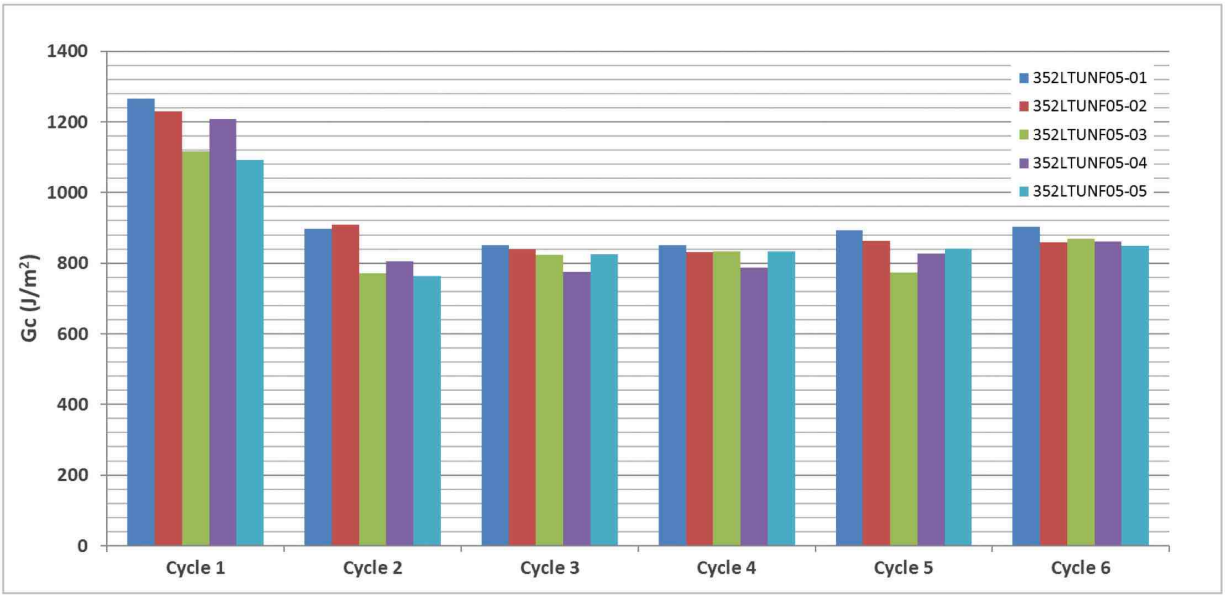

(b). *Fracture toughness values obtained from area method for five specimens tested.*

Figure D3. Results obtained from baseline configurations tested at DuPont.

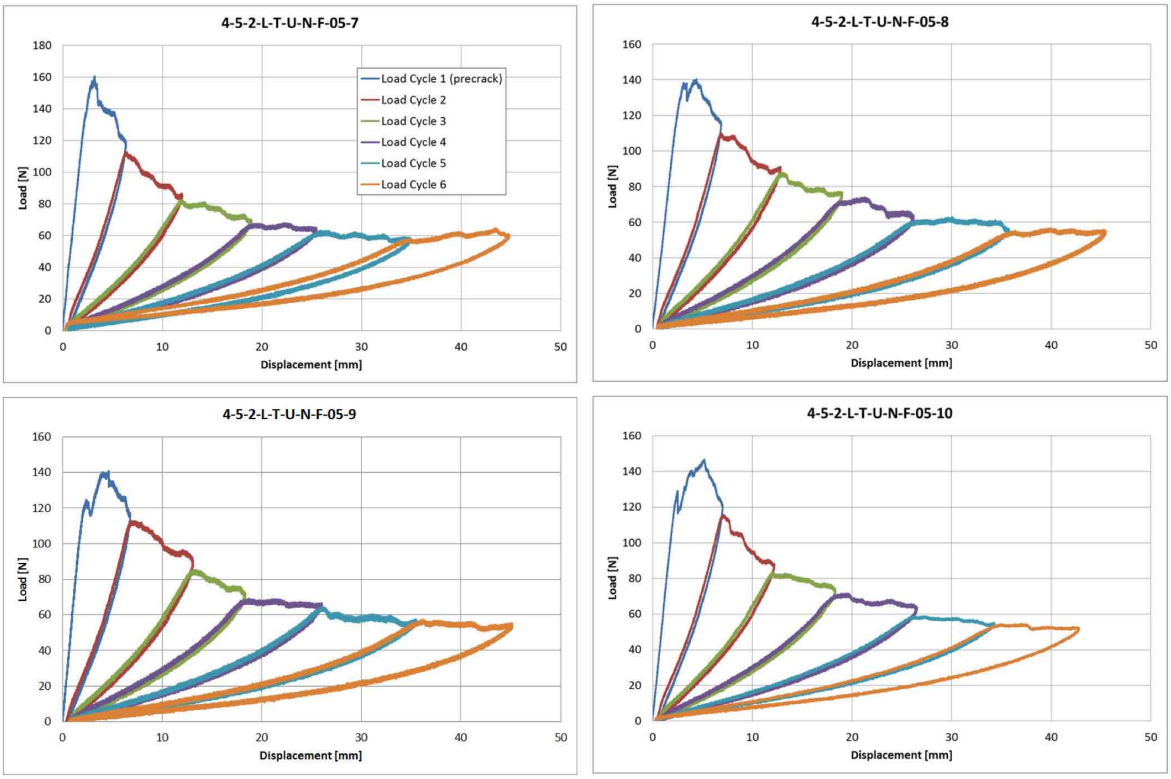

(a). *Load/displacement plots with six loading and unloading cycles for four specimens.*

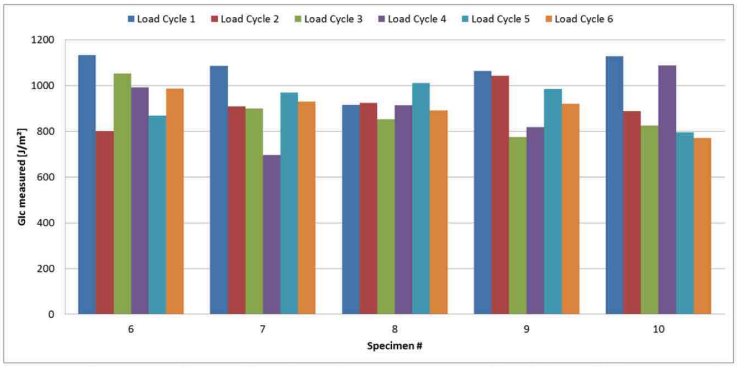

(b). *Fracture toughness values obtained from area method for all five specimens tested.*

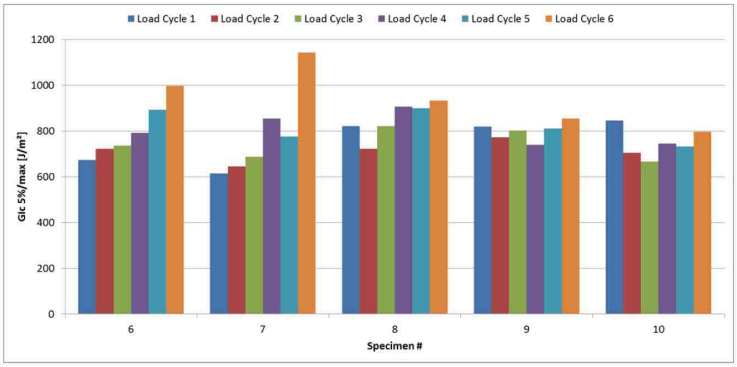

(c). *Fracture toughness values obtained from modified beam theory for all five specimens tested.*

Figure D4. Results obtained from baseline configurations tested at NASA LaRC.

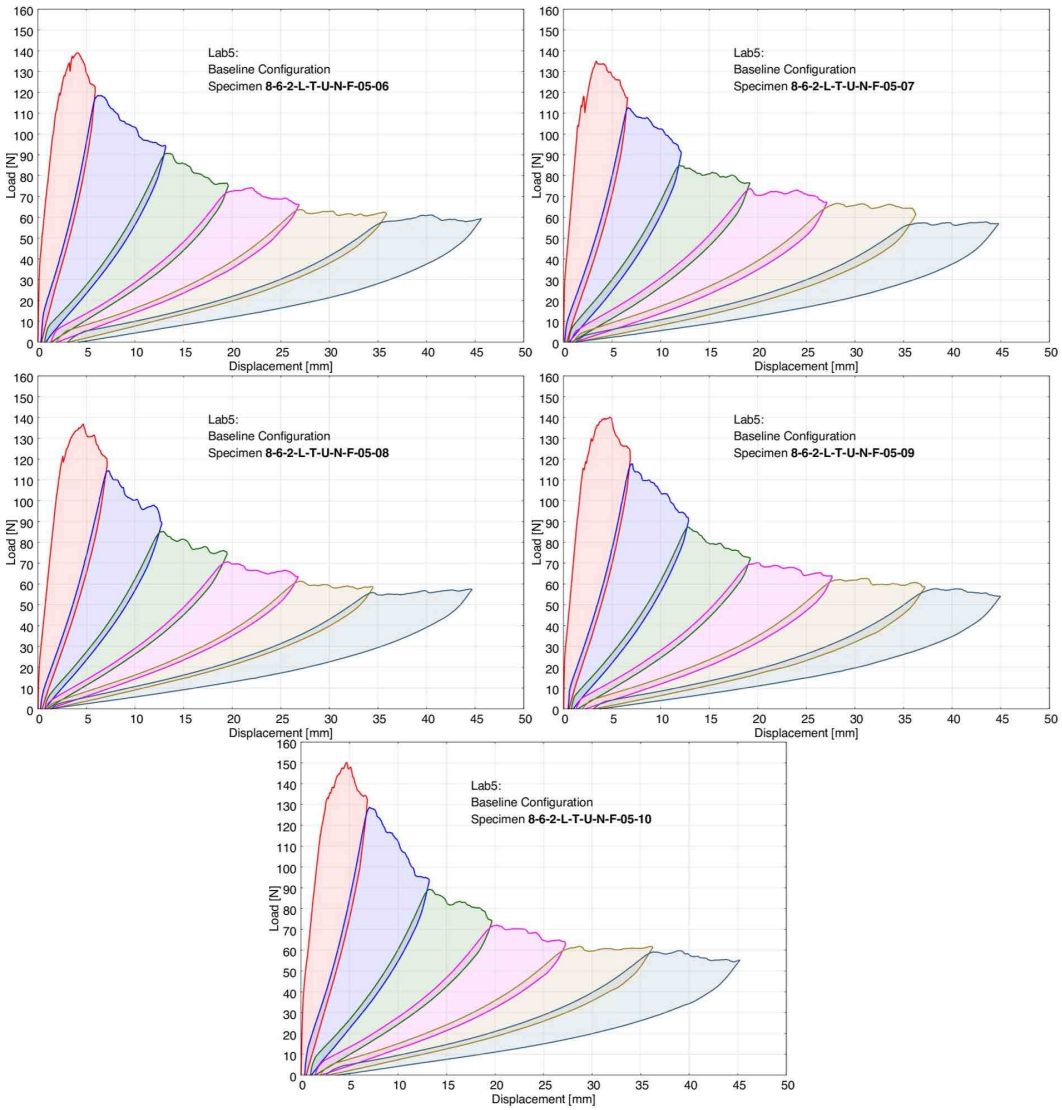

(a). *Load/displacement plots with six loading and unloading cycles for five specimens.*

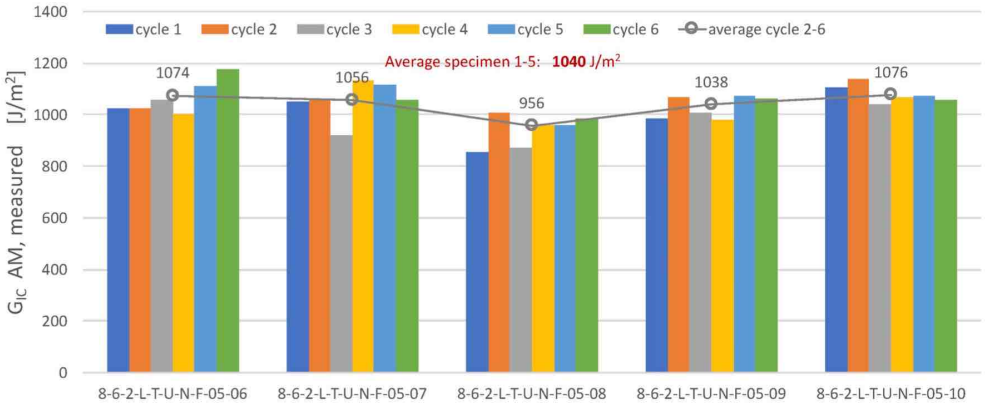

(b). *Fracture toughness values obtained from area method for all five specimens tested.*

Figure D5. Results obtained from baseline configurations tested at Fraunhofer IMWS.

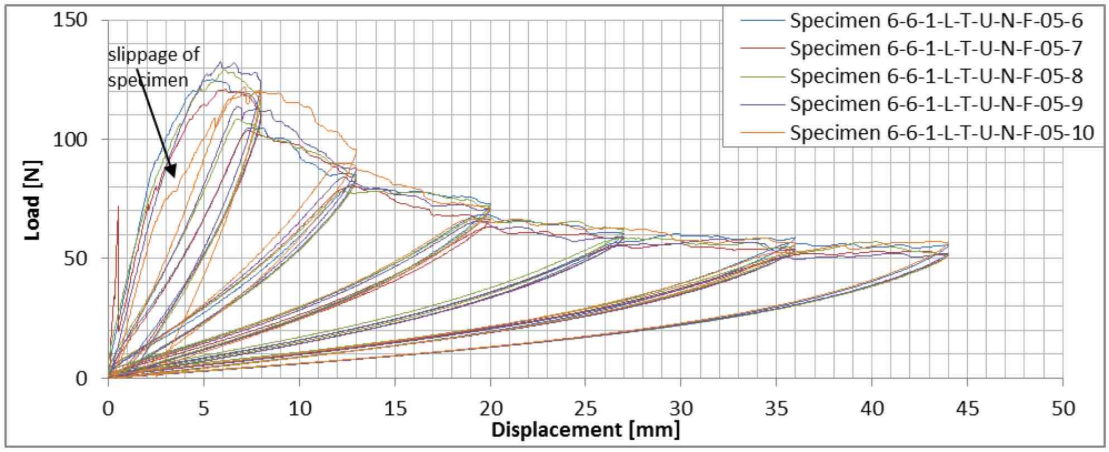

(a). *Load/displacement plots with six loading and unloading cycles for five specimens.*

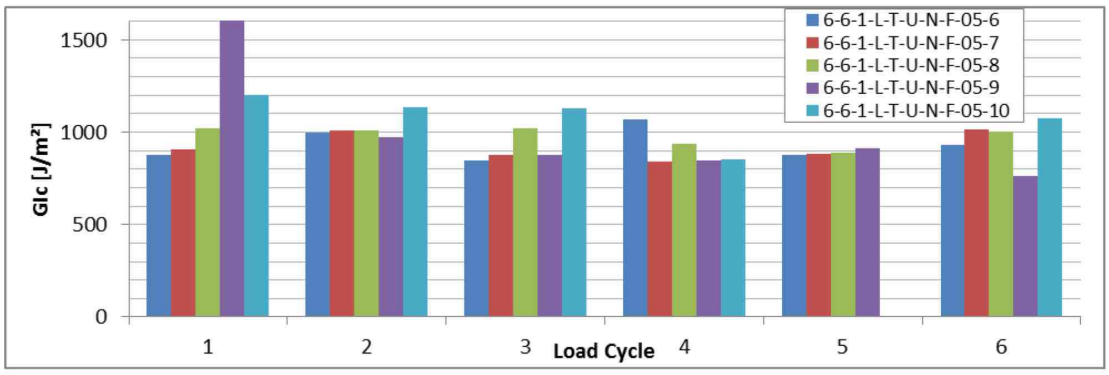

(b). *Fracture toughness values obtained from area method for all five specimens tested.*

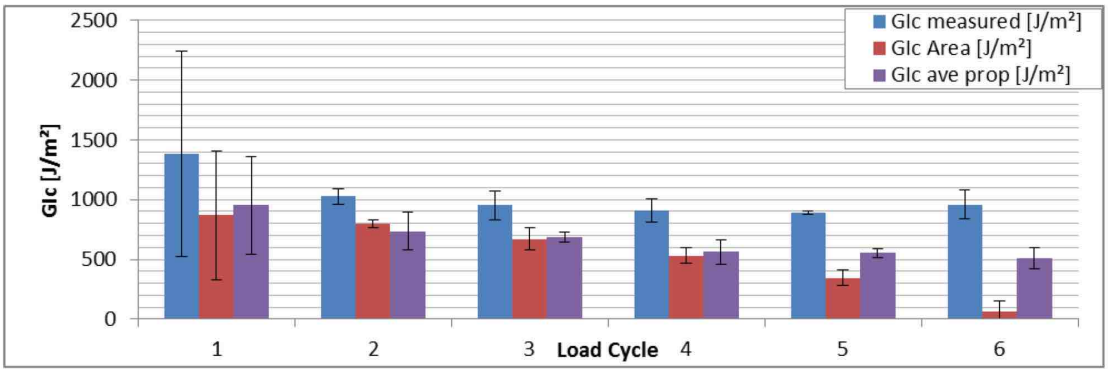

(c). *Average fracture toughness values obtained from different data reduction methods.*

Figure D6. Results obtained from baseline configurations tested at Airbus Bremen.

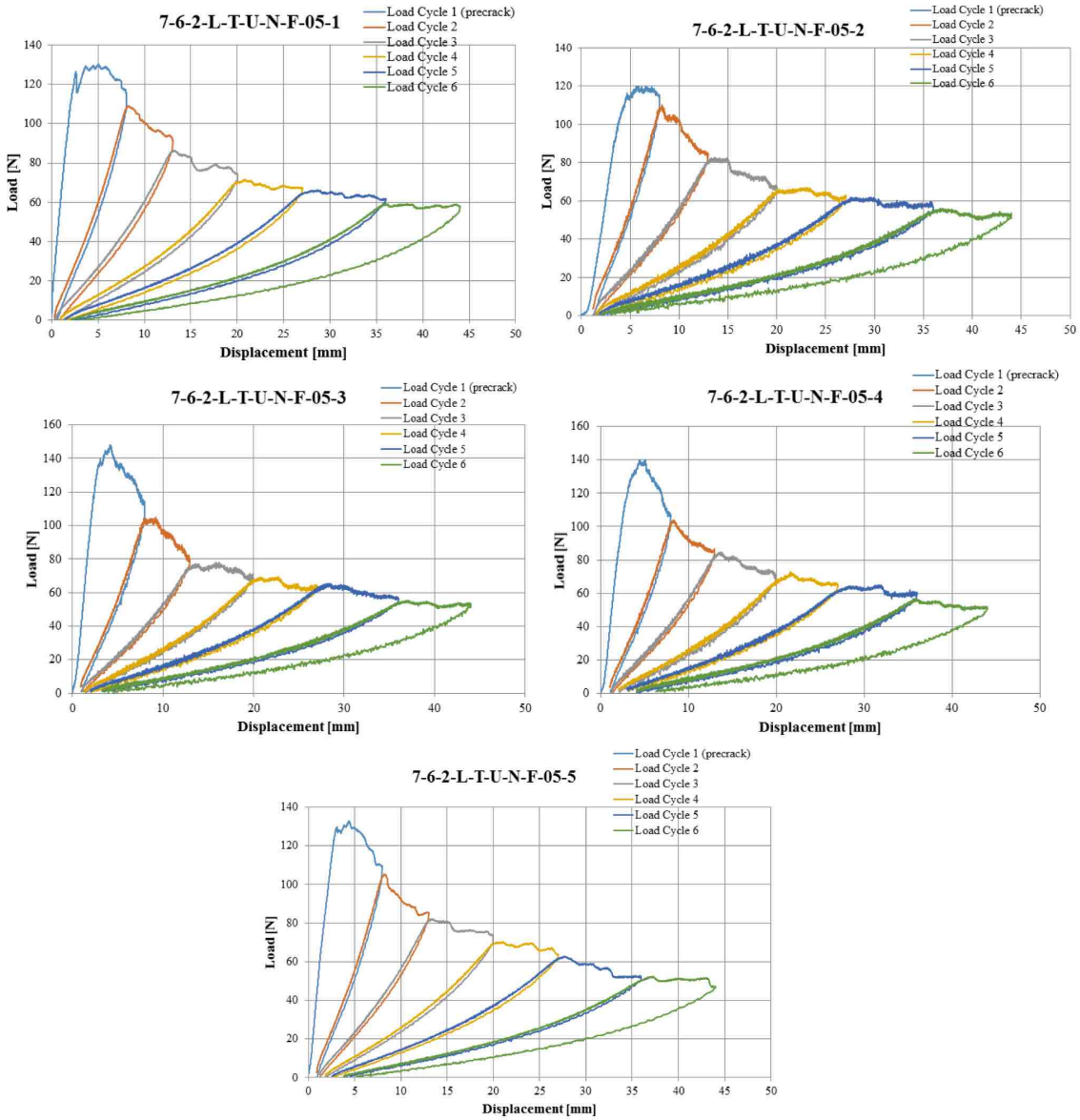

(a). *Load/displacement plots with six loading and unloading cycles for five specimens.*

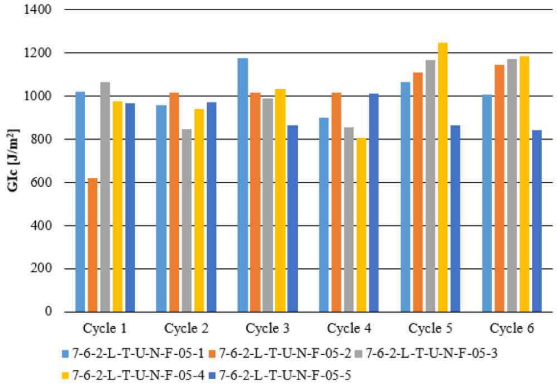

(b). *Fracture toughness values obtained from area method for all five specimens tested.*

Figure D7. Results obtained from baseline configurations tested at DTU.

APPENDIX E – RESULTS FROM SPECIMENS WITH DISBOND PROPAGATION IN W-DIRECTION

E.1 Lab 3: DuPont International Operations, Geneva, Switzerland

Results from tests performed at DuPont using specimens where the disbond propagated in the W-direction (specimens 5-9-1-W-T-U-N-F-20-06, 5-9-1-W-T-U-N-F-20-07, 5-9-1-W-T-U-N-F-20-08 and 5-9-1-W-T-U-N-F-20-09) are shown in Figure E1. A power shut down occurred during one test (specimen 5-9-1-W-T-U-N-F-20-10) and invalidated the results. The load vs. displacement data obtained are plotted in Figure E1a. Fracture toughness results, obtained from the area method, are shown in Figures E1b.

E.2 Lab 5: Fraunhofer Institute for Microstructure of Materials and Systems IMWS, Halle, Germany

Results from tests with disbond propagation in the W-direction of the honeycomb core, performed at Fraunhofer IMWS, (specimens 5-9-1-W-T-U-N-F-20-01, 5-9-1-W-T-U-N-F-20-02, 5-9-1-W-T-U-N-F-20-03, 5-9-1-W-T-U-N-F-20-04, 5-9-1-W-T-U-N-F-20-05) are shown in Figure E2. The load vs. displacement data obtained are plotted in Figure E2a. Fracture toughness results, obtained from the area method, are shown in Figure E2b.

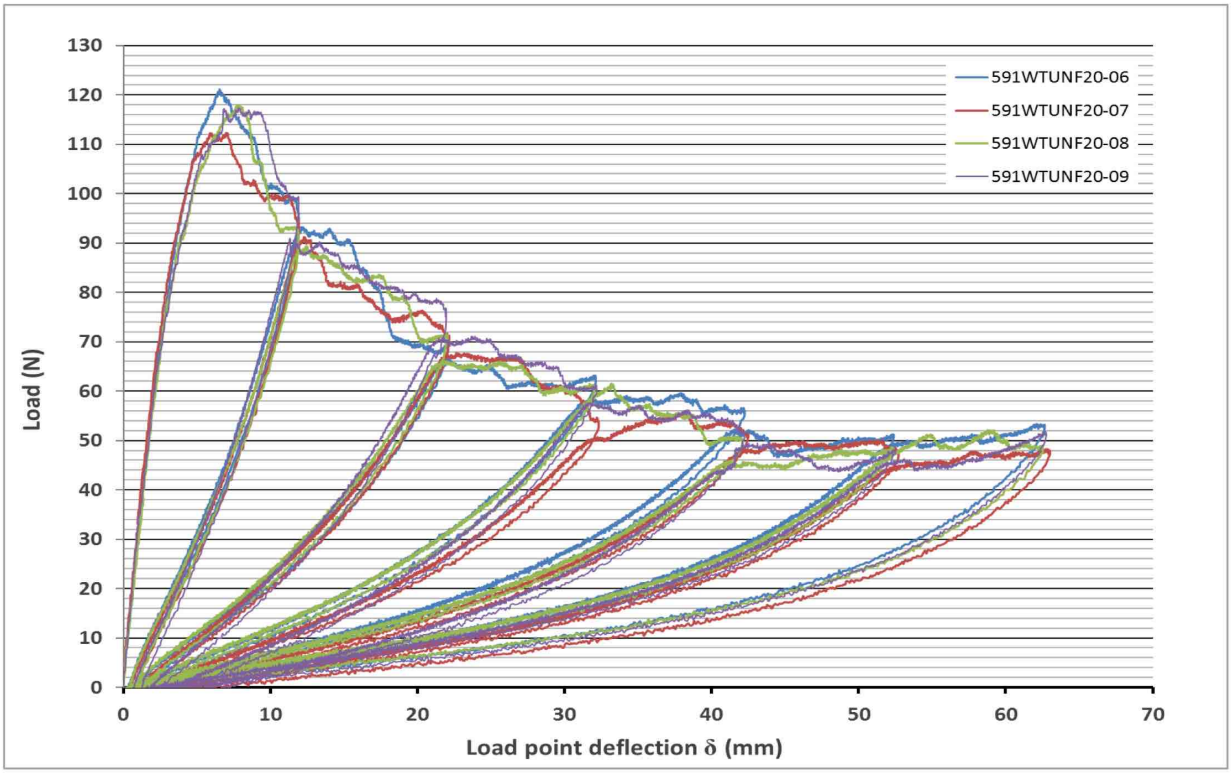

(a). *Load/displacement plots with six loading and unloading cycles for four specimens.*

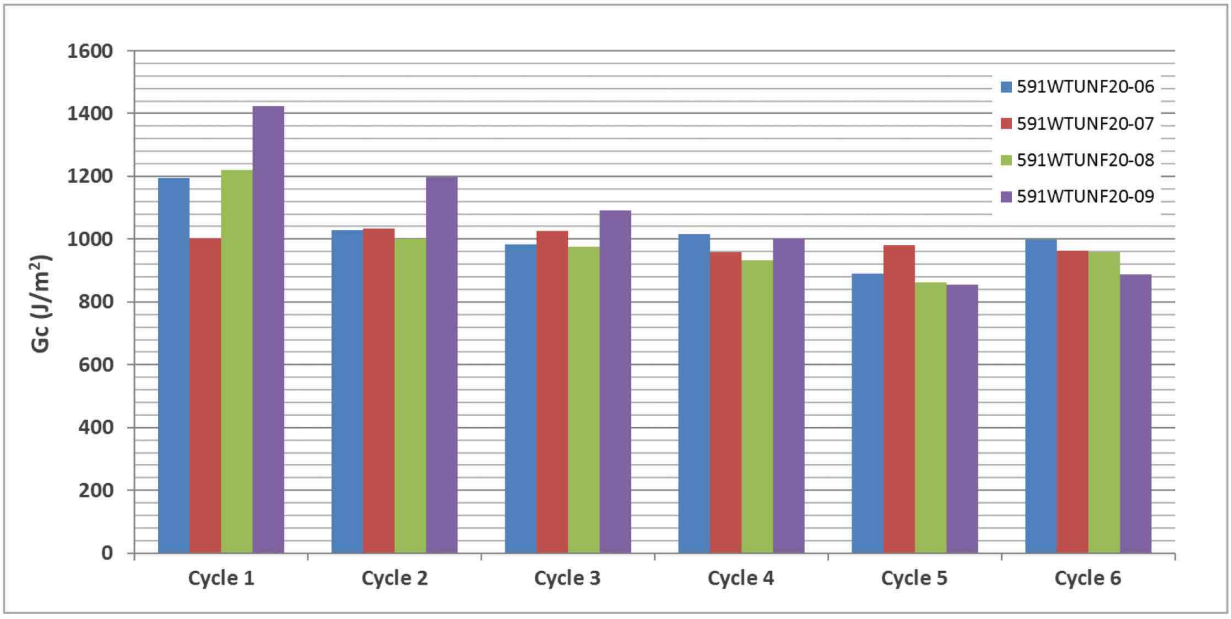

(b). *Fracture toughness values obtained from area method for five specimens tested.*

Figure E1: Results obtained from tests at DuPont where delamination propagated in the W-direction.

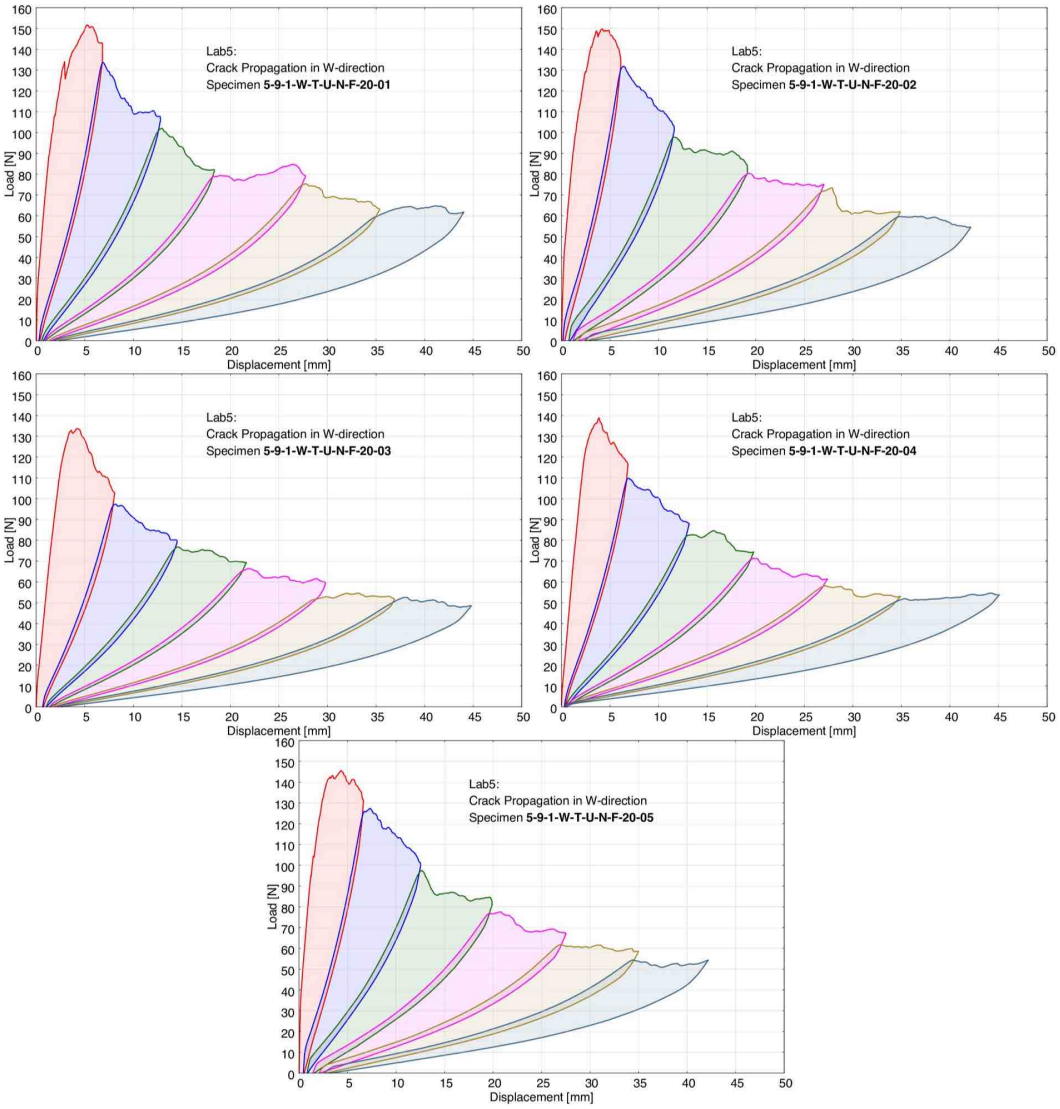

(a). *Load/displacement plots with six loading and unloading cycles for four specimens.*

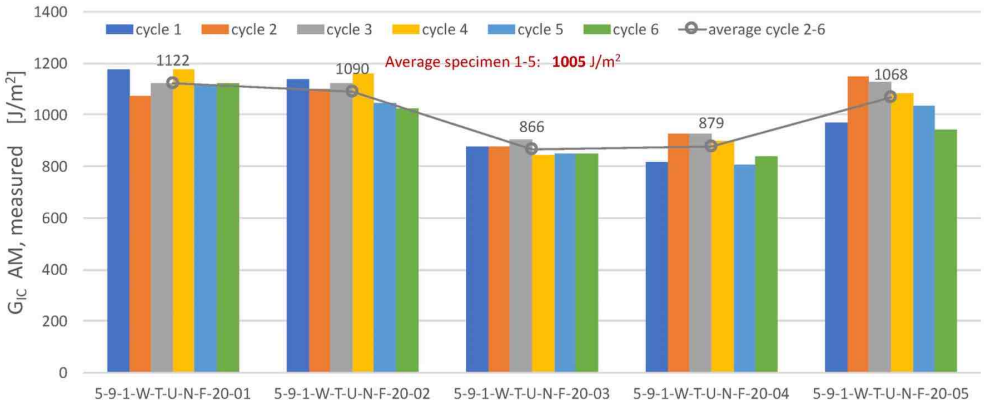

(b). *Fracture toughness values obtained from area method for five specimens tested.*

Figure E2: Results obtained from tests at Fraunhofer IMWS where delamination propagated in the W-direction.

APPENDIX F – RESULTS FROM SPECIMENS WITH STARTER SAW CUT

F.1 Lab 2: NIAR, Wichita State University, Wichita, KS, USA

Results from the tests performed at NIAR (specimens 8-3-2-W-S-X-N-F-XX-01, 8-3-2-W-S-X-N-F-XX-02, 8-3-2-W-S-X-N-F-XX-03, 8-3-2-W-S-X-N-F-XX-05, and 8-3-2-W-S-X-N-F-XX-08) are shown in Figure F1. The load vs. displacement data obtained are plotted in Figure F1a. Fracture toughness results are shown in Figure F1b.

F.2 Lab 6: Airbus Operations GmbH, Bremen

Results obtained at Airbus Operations GmbH, Bremen (specimens 6-4-1-L-S-x-D-F-05-01, 6-4-1-L-S-x-D-F-05-02, 6-4-1-L-S-x-D-F-05-03, 6-4-1-L-S-x-D-F-05-04, 6-4-1-L-S-x-D-F-05-05) are shown in Figure F2. The load vs. displacement data obtained are plotted in Figure F2a. Fracture toughness results, obtained from the area method, are shown in Figure F2b. Average results from different data reduction techniques are shown in Figure F2c.

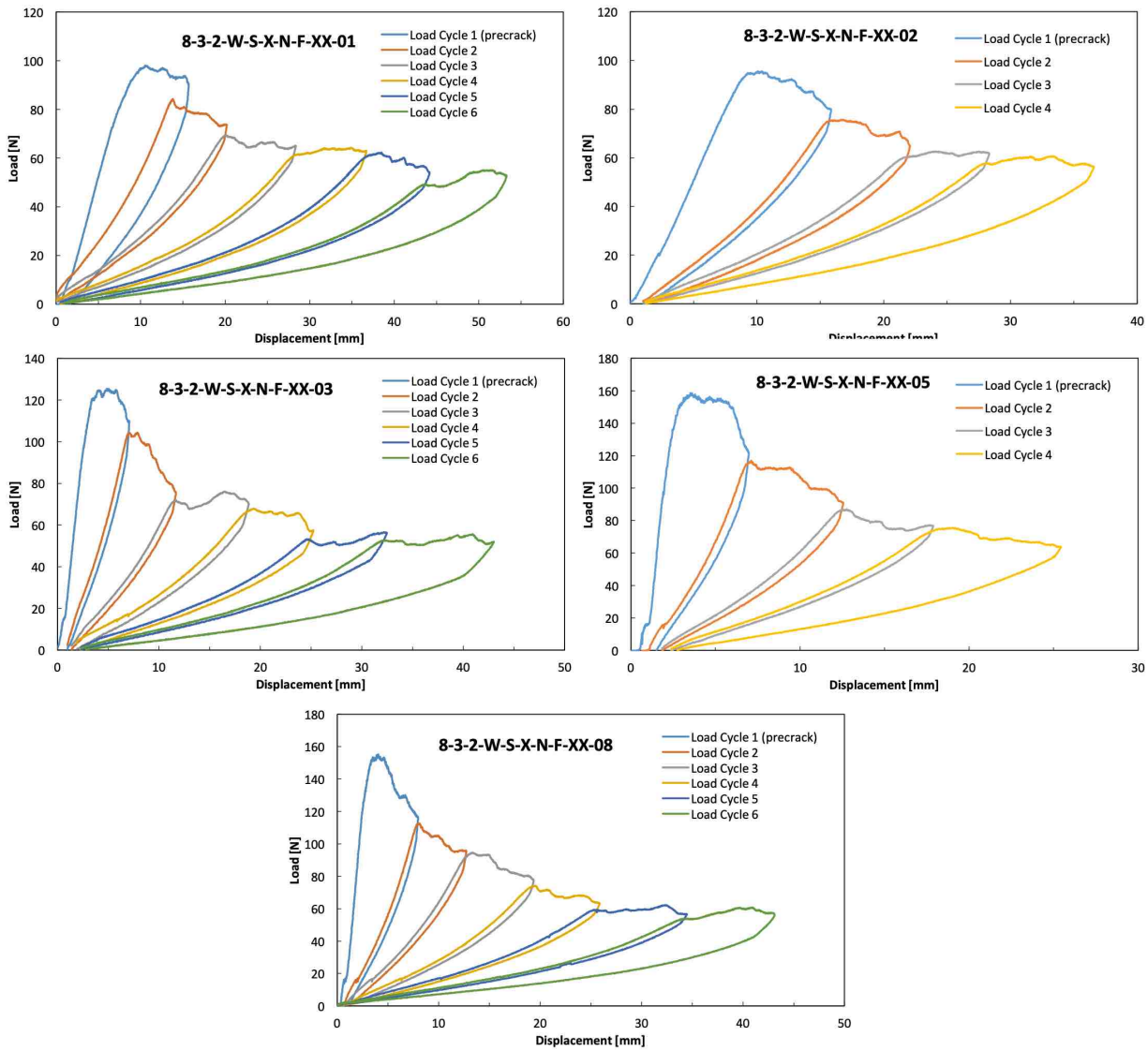

(a). *Load/displacement plots with six loading and unloading cycles for five specimens.*

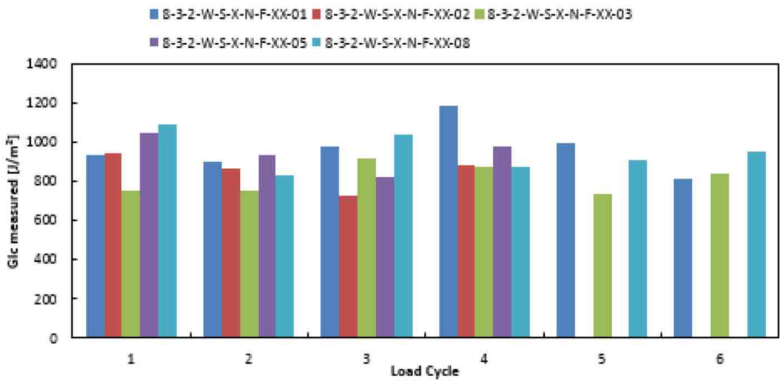

(b). *Fracture toughness values obtained from area method for all five specimens tested.*

Figure F1. Results obtained from specimens with starter saw cut tested at NIAR.

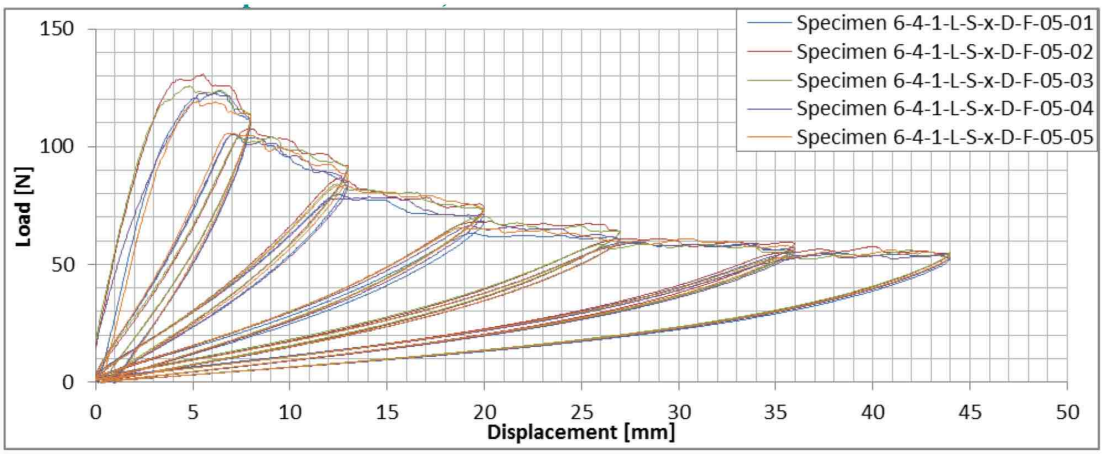

(a). *Load/displacement plots with six loading and unloading cycles for five specimens.*

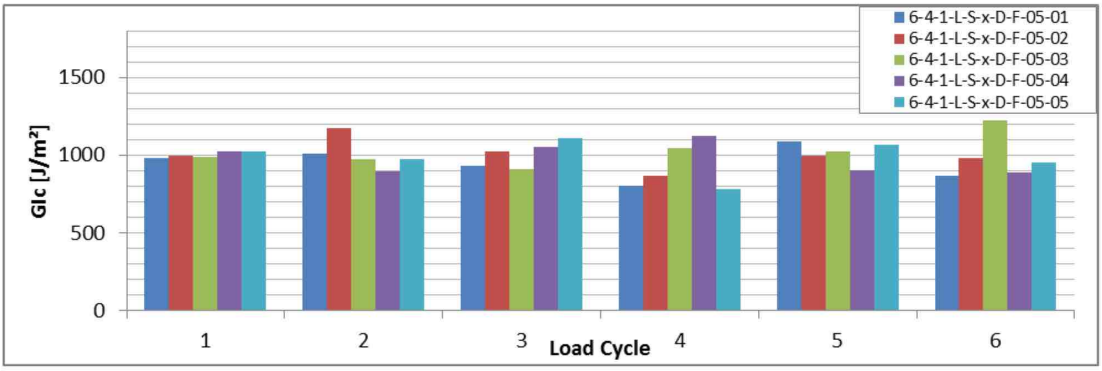

(b). *Fracture toughness values obtained from area method for all five specimens tested.*

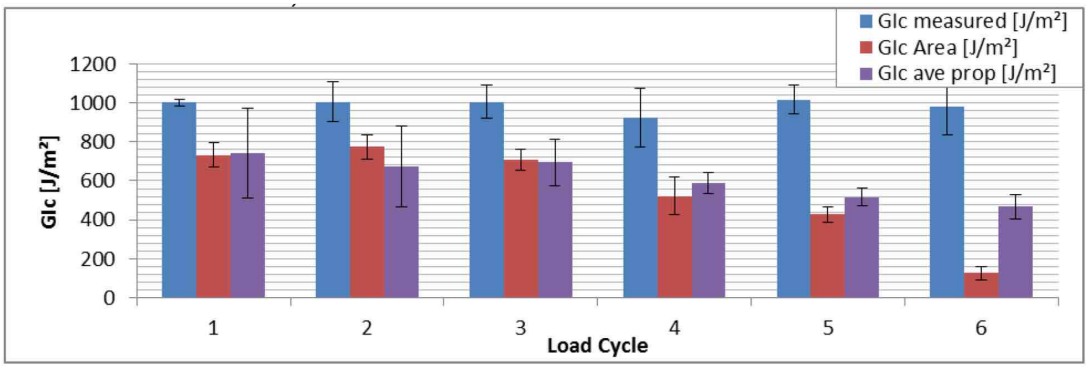

(c). *Average fracture toughness values obtained from different data reduction methods.*

Figure F2. Results obtained from specimens with starter saw cut tested at Airbus Bremen.

APPENDIX G – RESULTS FROM SPECIMENS WITH DOUBLERS

G.1 Lab 4: NASA Langley Research Center, Hampton, VA, USA

Results obtained from specimens with doublers tested at NASA Langley Research Center (specimens 4-2-2-L-T-U-D-F-05-07, 4-2-2-L-T-U-D-F-05-08, 4-2-2-L-T-U-D-F-05-09 and 4-2-2-L-T-U-D-F-05-10,) are shown in Figure G1. The load vs. displacement data obtained are plotted in Figure G1a. Fracture toughness results, obtained from the area method and MBT, are shown in Figures G1b and G1c, respectively.

G.2 Lab 6: Airbus Operations GmbH, Bremen

Results obtained from specimens with doublers tested at Airbus Operations GmbH, Bremen (specimens 6-4-1-L-S-x-D-F-05-06, 6-4-1-L-S-x-D-F-05-07, 6-4-1-L-S-x-D-F-05-08, 6-4-1-L-S-x-D-F-05-09, 6-4-1-L-S-x-D-F-05-10) are shown in Figure G2. The load vs. displacement data obtained are plotted in Figure G2a. Fracture toughness results, obtained from the area method, are shown in Figure G2b. Average results from different data reduction techniques are shown in Figure G2c.

G.3 Lab 7: Technical University of Denmark, Kgs. Lyngby, Denmark

Results obtained from specimens with doublers tested at the Technical University of Denmark (specimens 7-2-2-L-T-U-D-F-05-01, 7-2-2-L-T-U-D-F-05-02, 7-2-2-L-T-U-D-F-05-03 and 7-2-2-L-T-U-D-F-05-05) are shown in Figure G3. The load vs. displacement data for all the specimens are provided in Figure G3a. Fracture toughness results, obtained using the area method, are presented in Figure G3b.

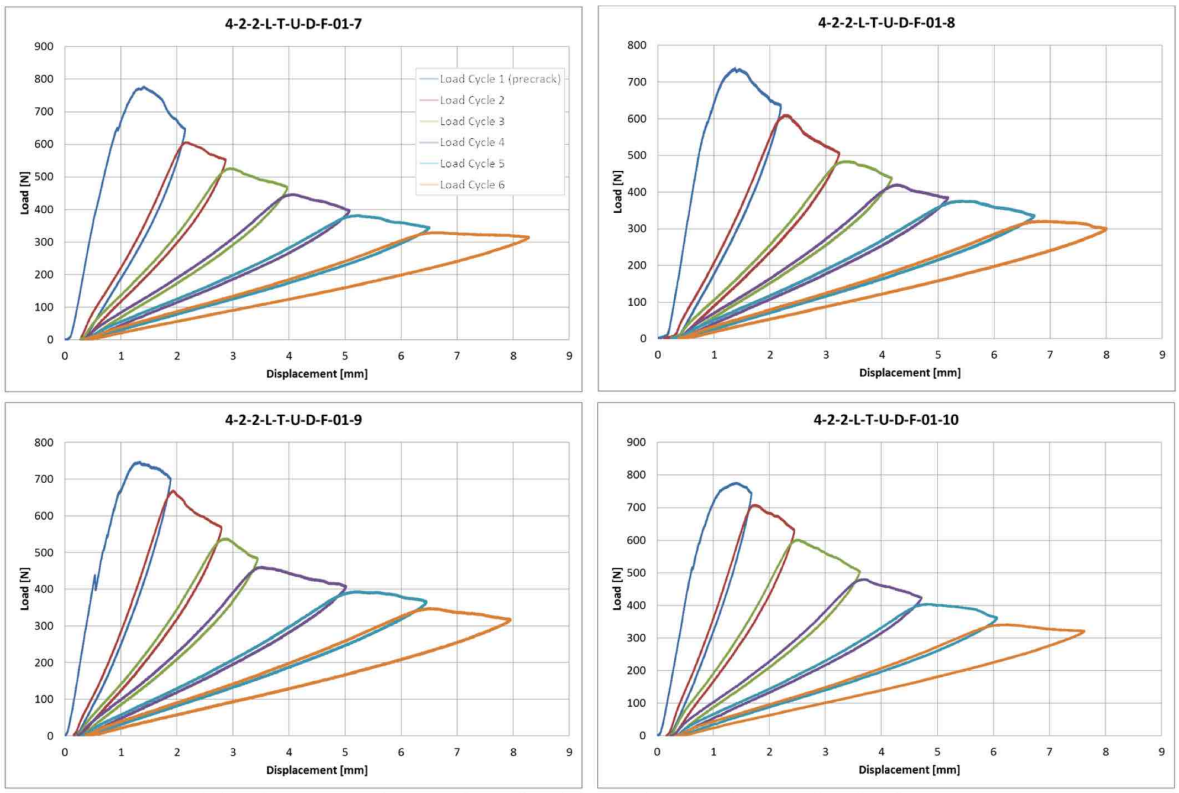

(a). *Load/displacement plots with six loading and unloading cycles for four specimens.*

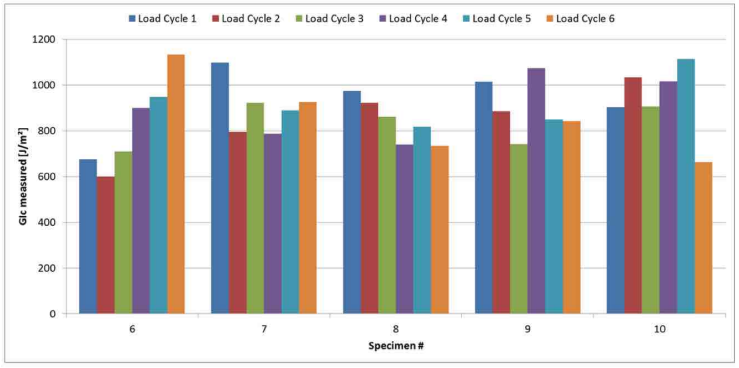

(b). *Fracture toughness values obtained from area method for all five specimens tested.*

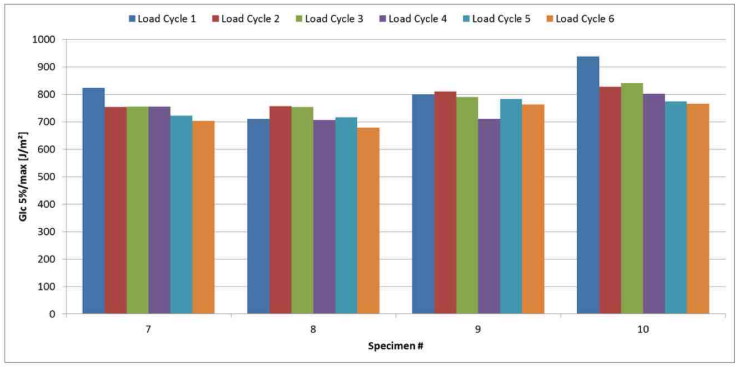

(c). *Fracture toughness values obtained from modified beam theory for all five specimens tested.*

Figure G1. Results obtained from specimens with doublers tested at NASA LaRC.

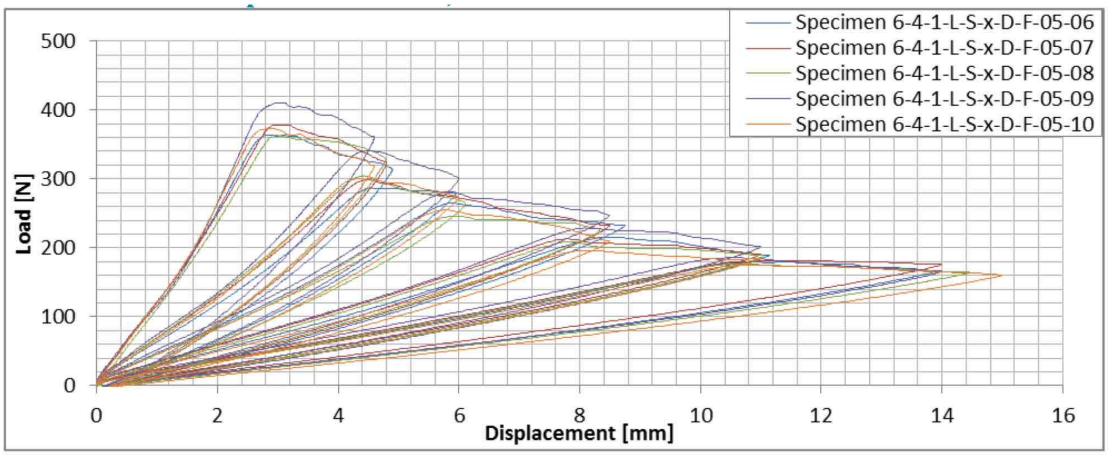

(a). *Load/displacement plots with five loading and unloading cycles for five specimens.*

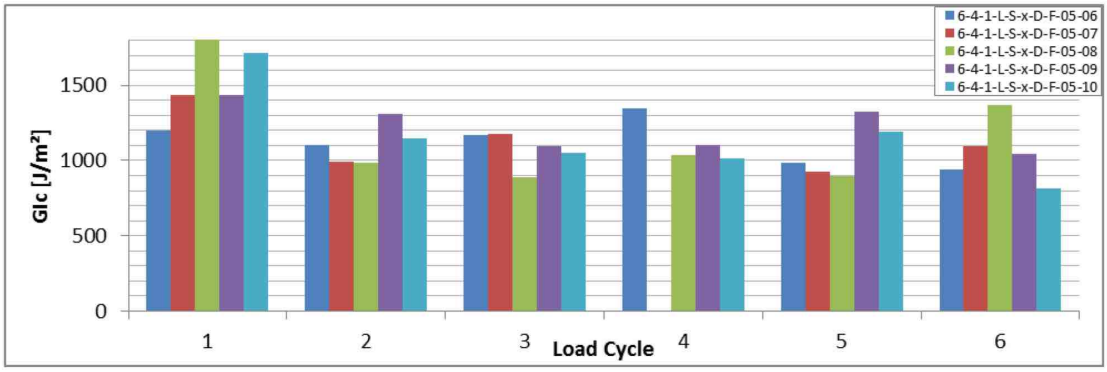

(b). *Fracture toughness values obtained from area method for all five specimens tested.*

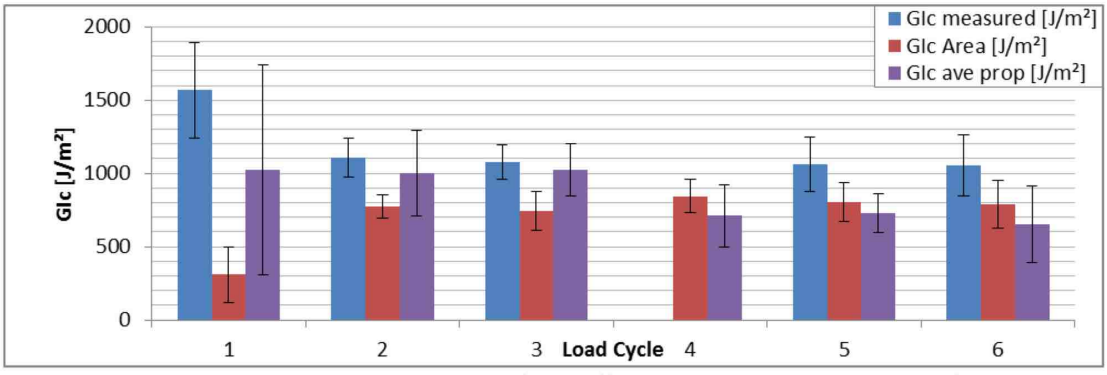

(c). *Average fracture toughness values obtained from different data reduction methods.*

Figure G2. Results obtained from specimens with doublers tested at Airbus Bremen.

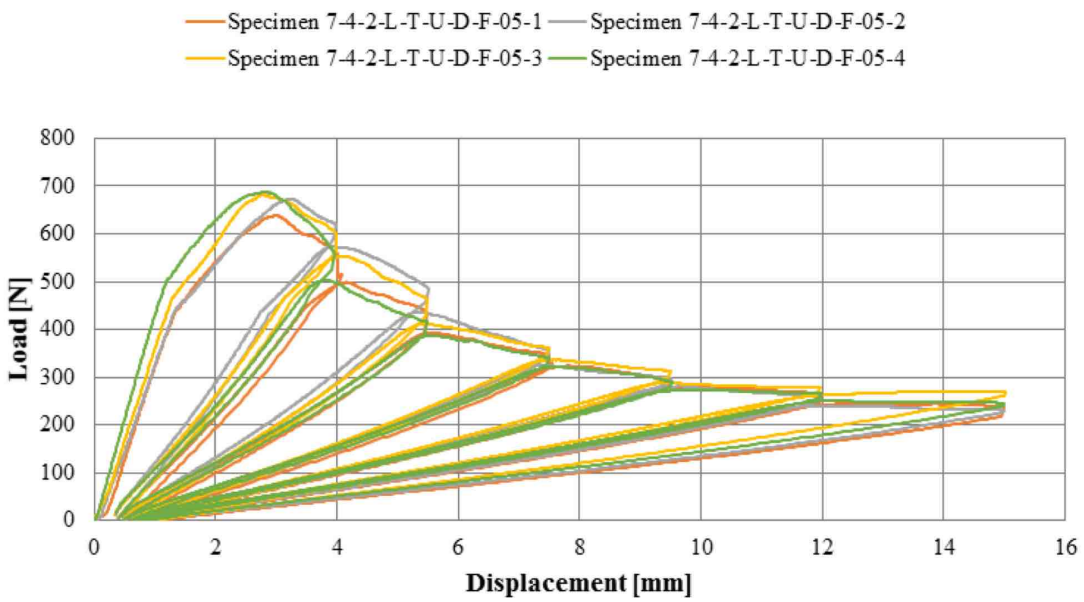

(a). *Load/displacement plots with six loading and unloading cycles for four specimens with doublers.*

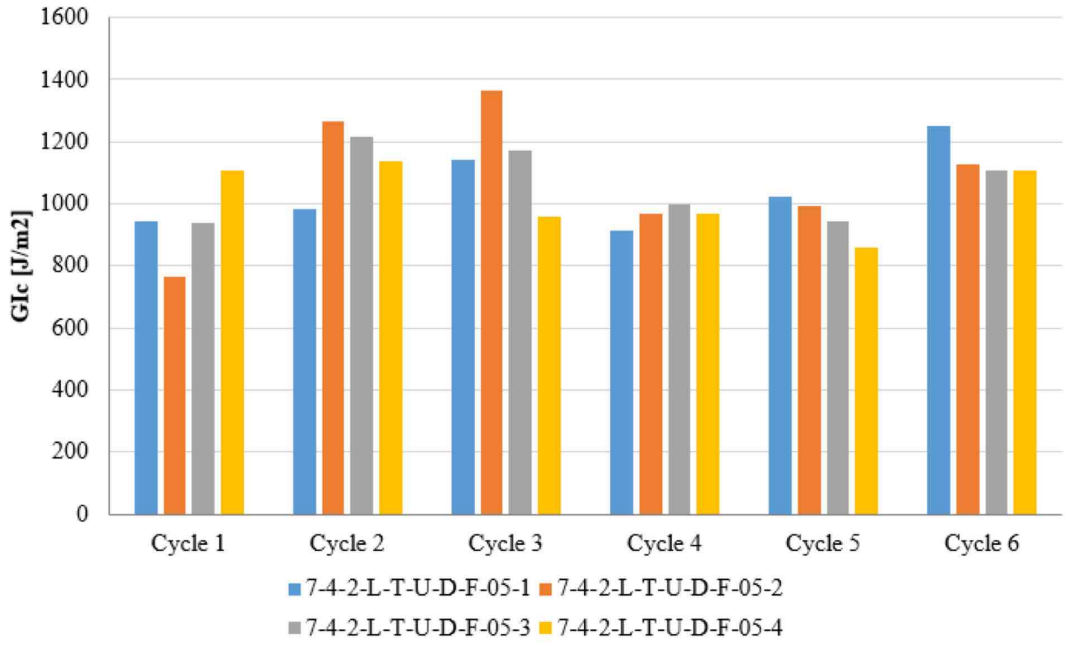

(b). *Fracture toughness values obtained from area method for four specimens with doublers.*

Figure G3. Results obtained from specimens with doublers tested at DTU.

APPENDIX H – RESULTS FROM TESTS USING A SLIDING CARRIAGE

H.1 Lab 2: NIAR, Wichita State University, Wichita, KS, USA

Results from the tests where a sliding carriage was used at NIAR (specimens 8-3-2-W-S-X-N-F-XX-04, 8-3-2-W-S-X-N-F-XX-06, 8-3-2-W-S-X-N-F-XX-07, 8-3-2-W-S-X-N-F-XX-09, and 8-3-2-W-S-X-N-F-XX-10) are shown in Figure H1. The load vs. displacement data obtained are plotted in Figure H1a. Fracture toughness results are shown in Figures H1b.

H.2 Lab 7: Technical University of Denmark, Kgs. Lyngby, Denmark

Results obtained from specimens tested using a sliding carriage at the Technical University of Denmark (specimens 7-4-2-L-T-U-D-S-05-01, 7-4-2-L-T-U-D-S-05-02, 7-4-2-L-T-U-D-S-05-03, 7-4-2-L-T-U-D-S-05-04 and 7-4-2-L-T-U-D-S-05-05) are shown in Figure H2. The load vs. displacement data obtained are plotted in Figure H2a. Fracture toughness results, obtained from the area method, are presented in Figure H2b.

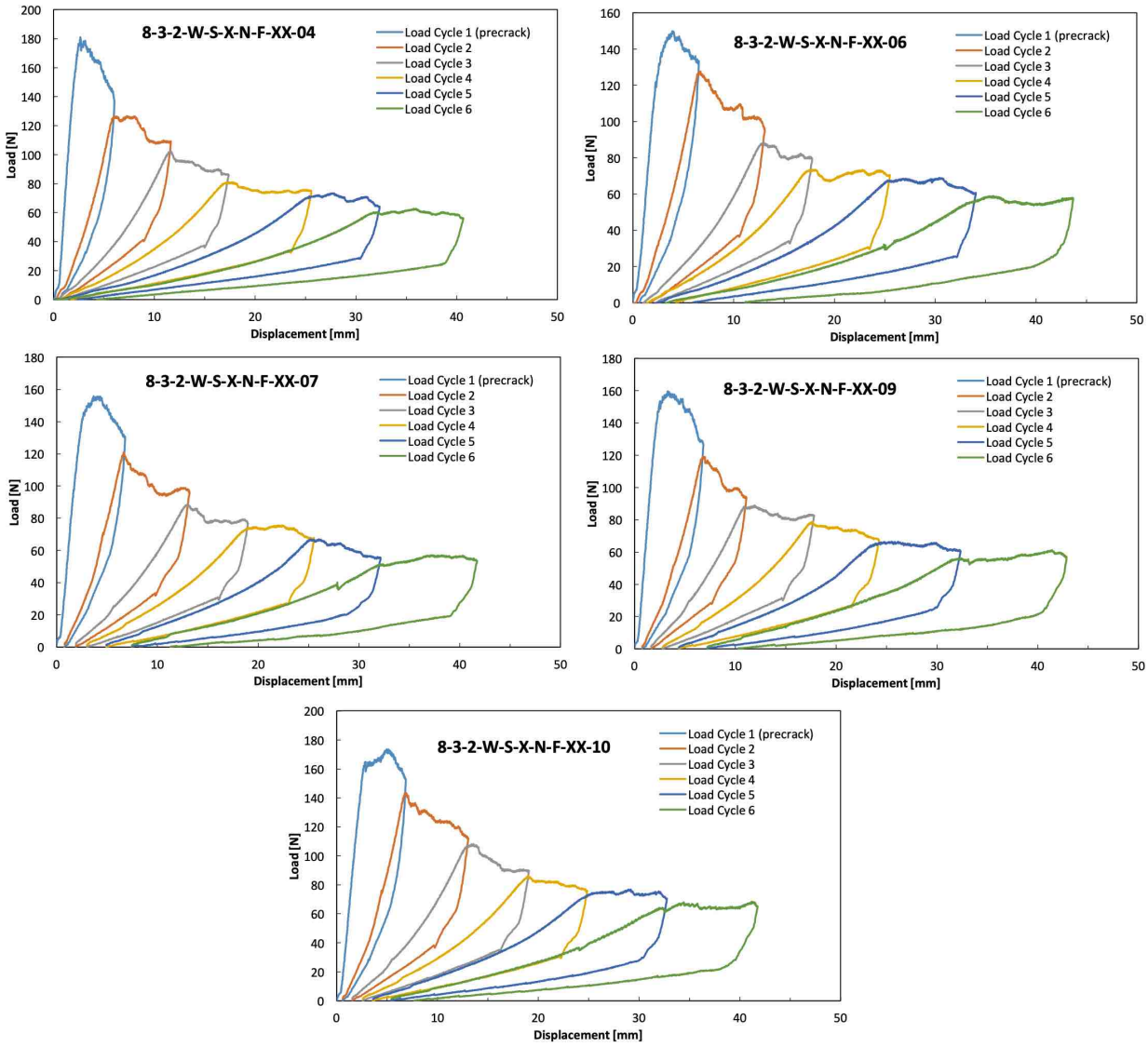

(a). *Load/displacement plots with six loading and unloading cycles for five specimens.*

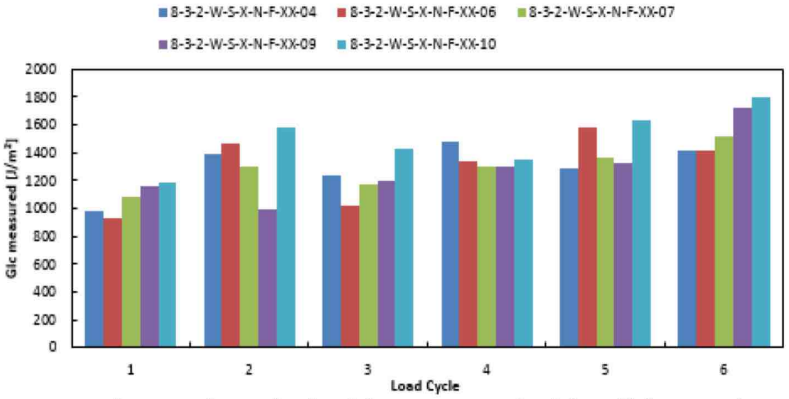

(b). *Fracture toughness values obtained from area method for all five specimens tested.*

Figure H1. Results obtained from tests using a sliding carriage performed at NIAR.

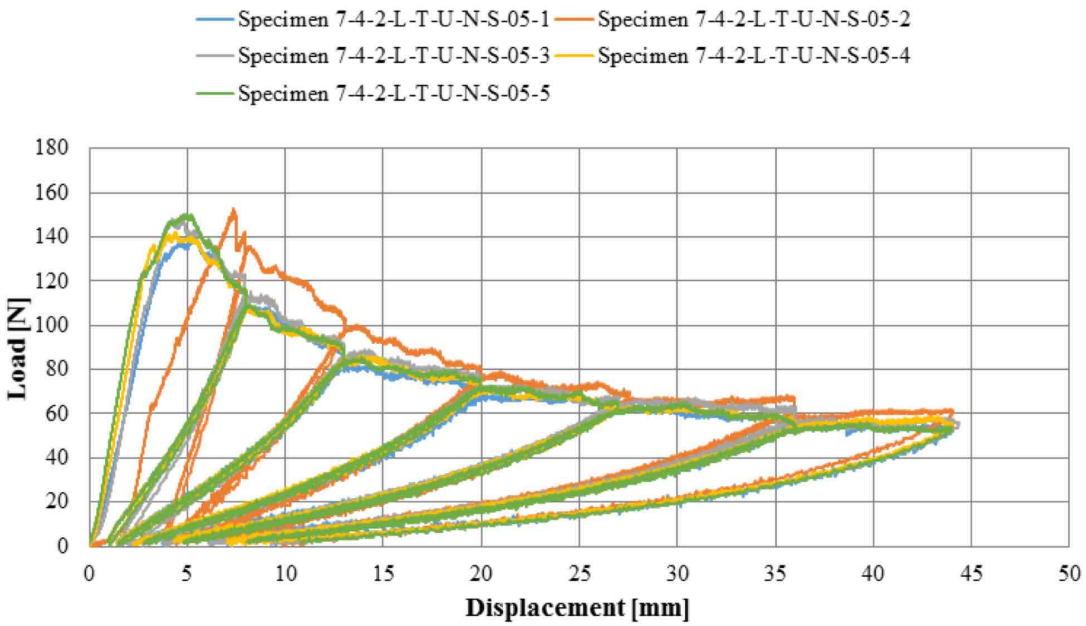

(a). *Load/displacement plots with six loading and unloading cycles for five specimens.*

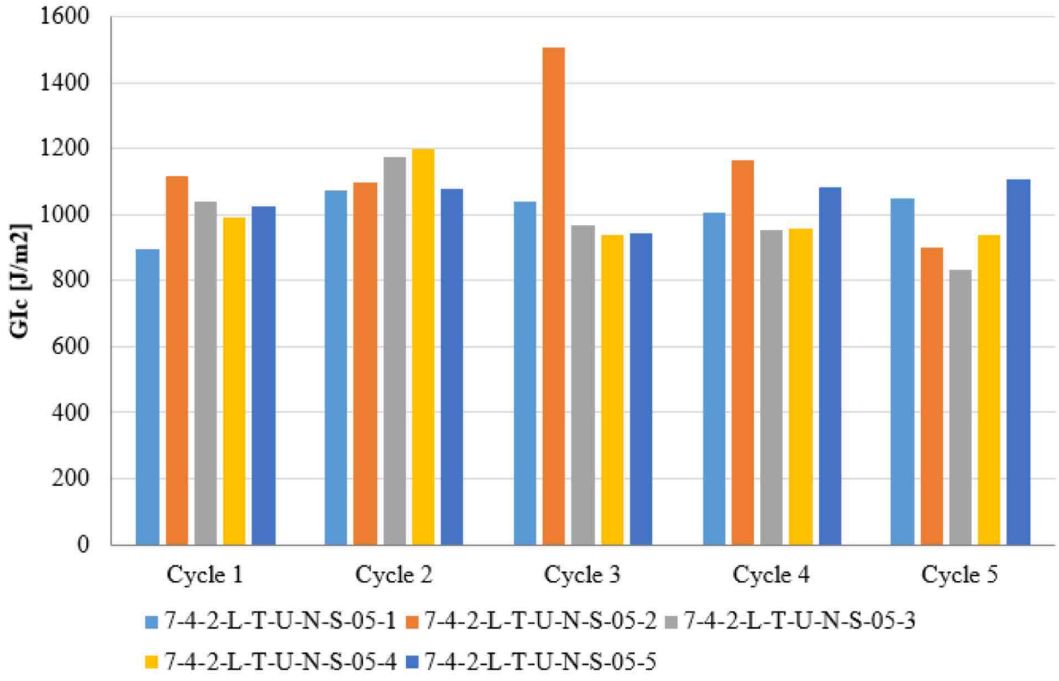

(b). *Fracture toughness values obtained from area method for five specimens.*

Figure H2. Results obtained from tests using a sliding carriage performed at DTU.

APPENDIX I – RESULTS FROM TESTS WITH UNLOADING TO ZERO DISPLACEMENT

I.1 Lab 1: University of Utah, Salt Lake City, UT, USA

Results obtained from The University of Utah tests with an unloading cycle to zero displacement ($\delta = 0$ mm) (specimens 1-5-1-L-T-U-N-F-05-1, 1-5-1-L-T-U-N-F-05-2, 1-5-1-L-T-U-N-F-05-3, 1-5-1-L-T-U-N-F-05-4 and 1-5-1-L-T-U-N-F-05-5) are shown in Figure I1.

I.2 Lab 4: NASA Langley Research Center, Hampton, VA, USA

Results obtained at NASA Langley Research Center from tests with an unloading cycle to zero displacement ($\delta = 0$ mm) (specimens 4-2-2-L-T-U-N-F-05-02, 4-2-2-L-T-U-N-F-05-03, 4-2-2-L-T-U-N-F-05-04 and 4-2-2-L-T-U-N-F-05-05,) are shown in Figure I2. The load vs. displacement data obtained are plotted in Figure I2a. Fracture toughness results, obtained from the area method and MBT, are shown in Figures I2b and I2c, respectively.

I.3 Lab 5: Fraunhofer Institute for Microstructure of Materials and Systems IMWS, Halle, Germany

Results obtained at Fraunhofer IMWS from tests with an unloading cycle to zero displacement ($\delta = 0$ mm) and accelerated speed (load at 20 mm/min, unload at 30 mm/min) (specimens 3-2-1-L-T-U-N-S-20-06, 3-2-1-L-T-U-N-S-20-07, 3-2-1-L-T-U-N-S-20-08, 3-2-1-L-T-U-N-S-20-09 and 3-2-1-L-T-U-N-S-20-10) are shown in Figure I3. The load vs. displacement data obtained are plotted in Figure I3a. Fracture toughness results, obtained from the area method, are shown in Figures I3b.

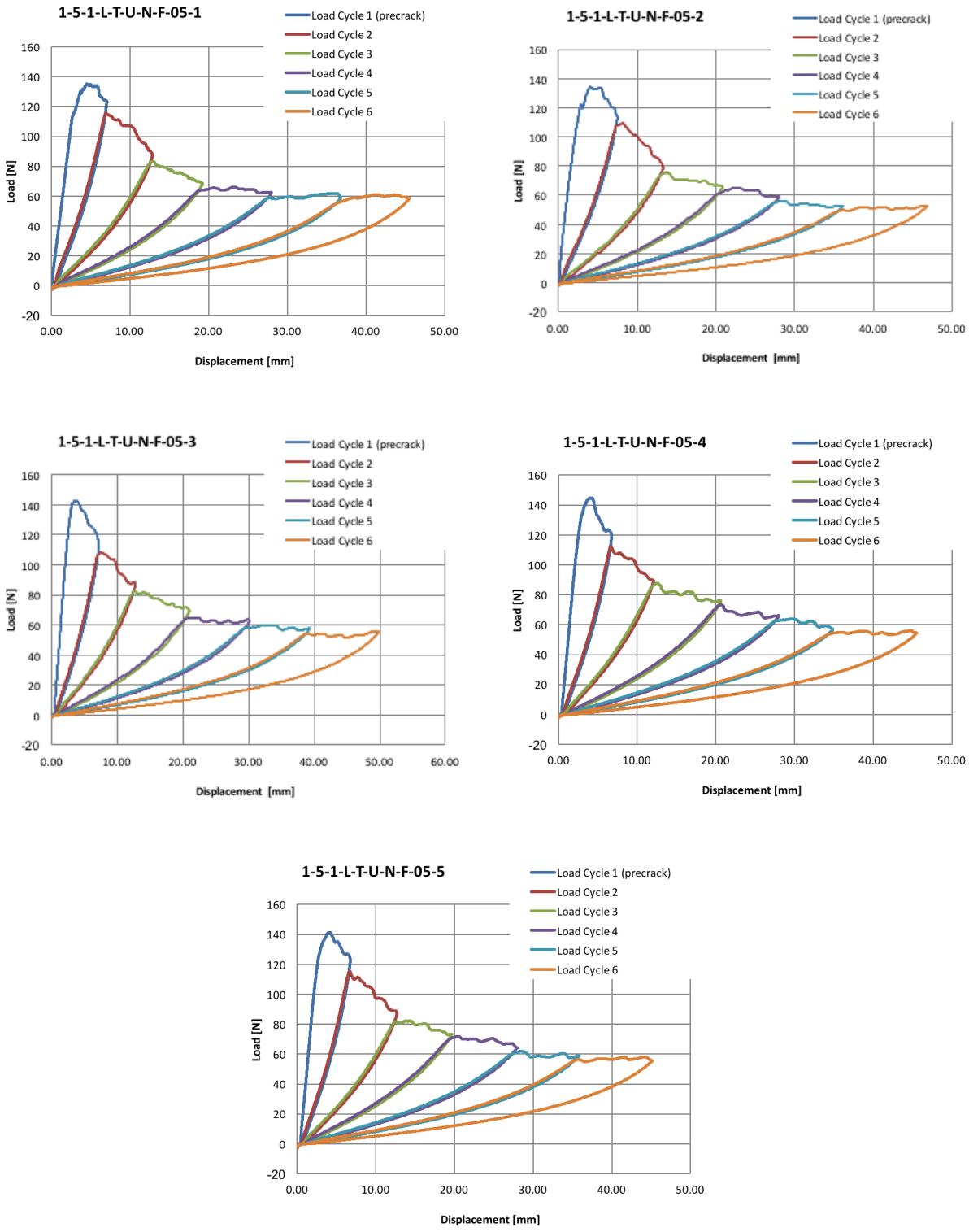

Figure I1. Results obtained at The University of Utah for tests performed with an unloading cycle to zero displacement.

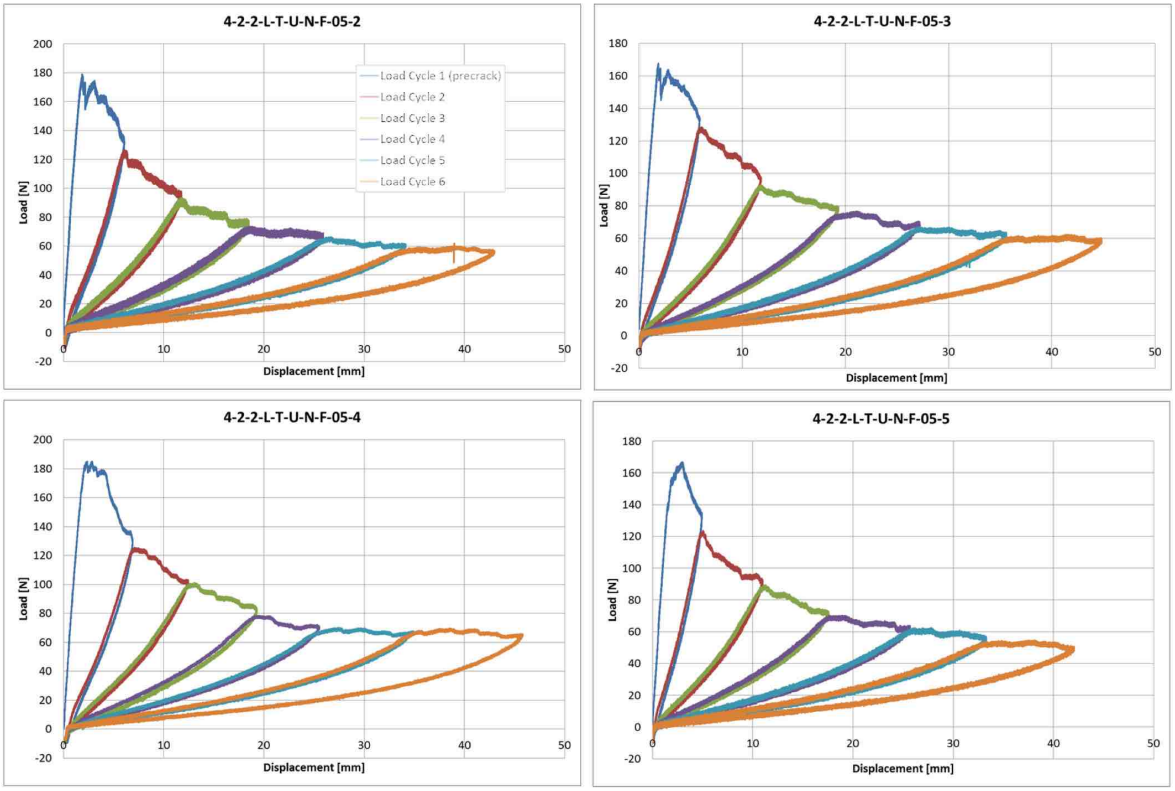

(a). *Load/displacement plots with six loading and unloading cycles for four specimens.*

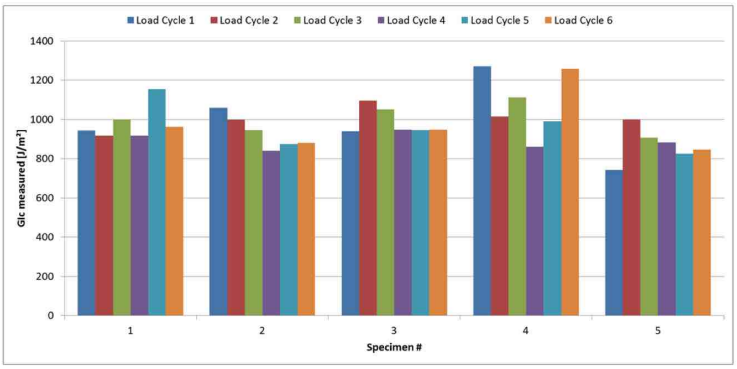

(b). *Fracture toughness values obtained from area method for all five specimens tested.*

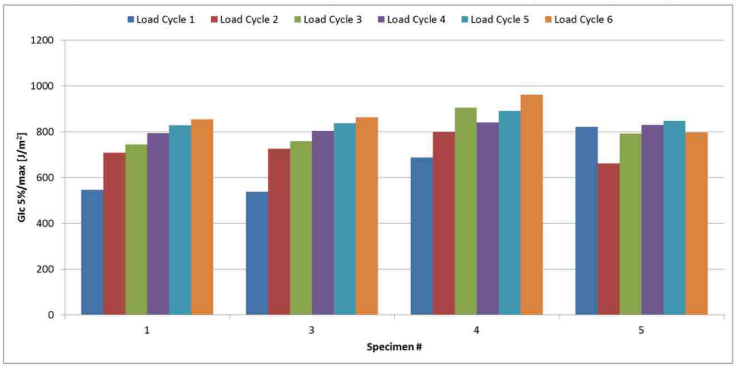

(c). *Fracture toughness values obtained from modified beam theory for all five specimens tested.*

Figure I2. Results obtained at NASA LaRC for tests performed with an unloading cycle to zero displacement.

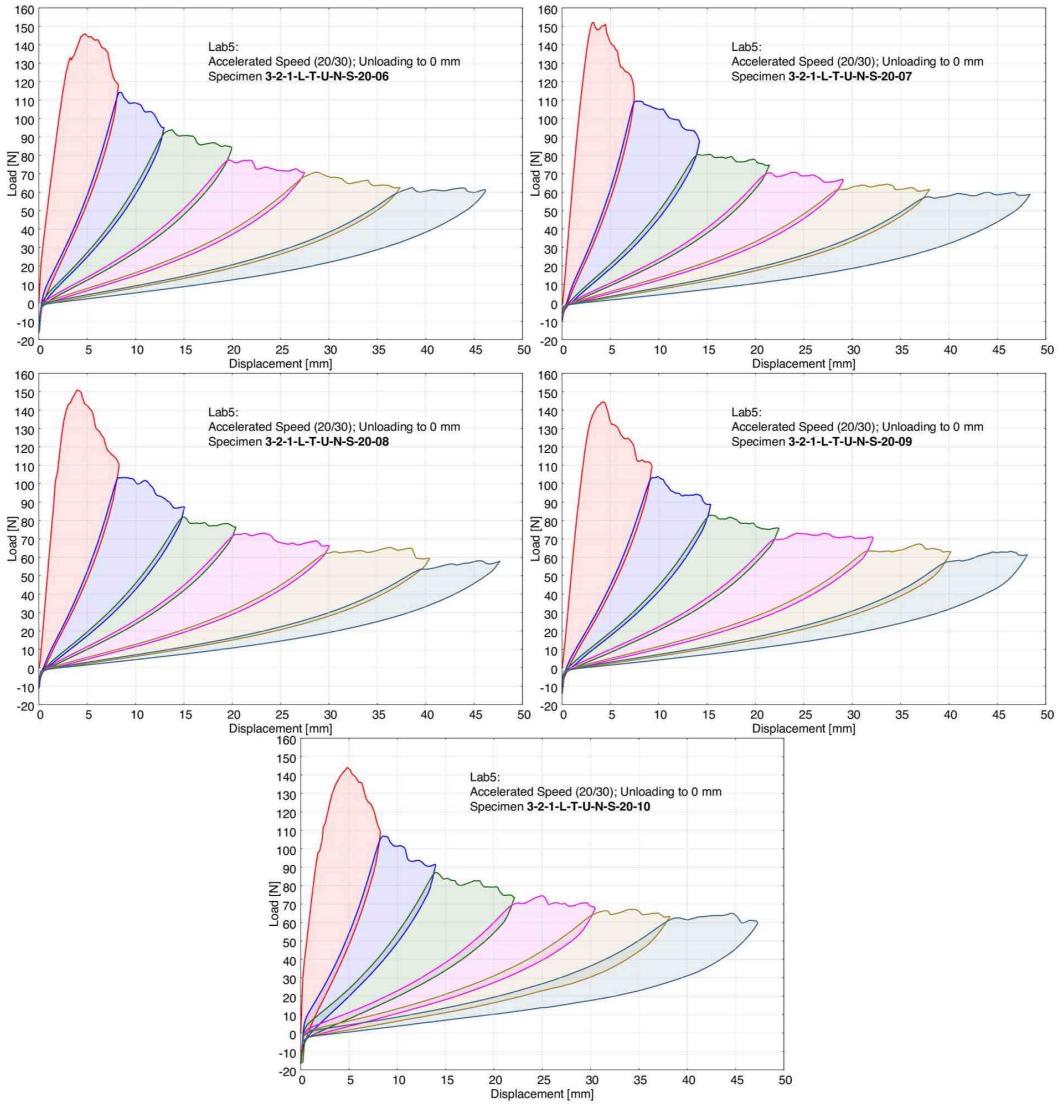

(a). *Load/displacement plots with six loading and unloading cycles for five specimens.*

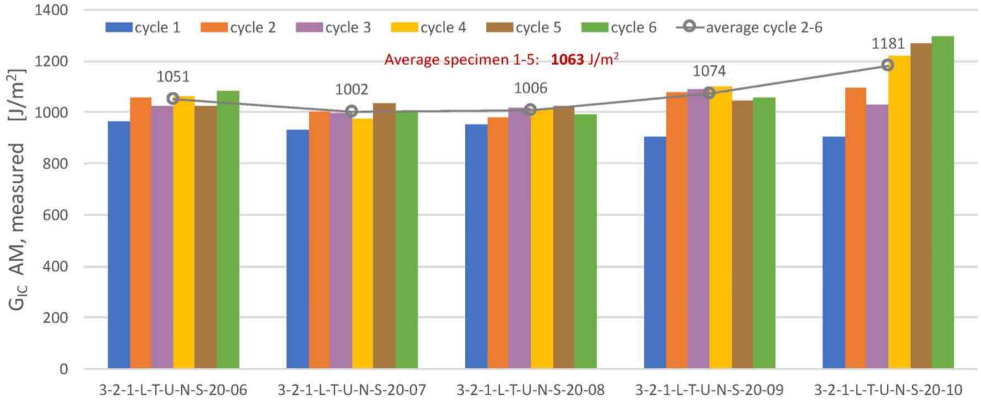

(b). *Fracture toughness values obtained from area method for all five specimens tested.*

Figure I3. Results obtained at Fraunhofer IMWS for tests performed with an unloading cycle to zero displacement and an accelerated loading rate of 20 mm/min.

APPENDIX J – RESULTS FROM ACCELERATED TESTING

J.1 Lab 1: University of Utah, Salt Lake City, UT, USA

Results from accelerated tests performed at The University of Utah (specimens 1-1-1-L-S-X-N-F-30-01, 1-1-1-L-S-X-N-F-30-02, 1-1-1-L-S-X-N-F-30-03, 1-1-1-L-S-X-N-F-30-04 and 1-1-1-L-S-X-N-F-30-05) are shown in Figure J1. The load vs. displacement data obtained are plotted in Figure J1a. Fracture toughness results are shown in Figure J1b.

J.2 Lab 3: DuPont International Operations, Geneva, Switzerland

Results from accelerated tests performed at DuPont at speeds of 100 mm/min during loading and unloading (specimens 3-2-1-L-T-U-N-S-20-01, 3-2-1-L-T-U-N-S-20-02, 3-2-1-L-T-U-N-S-20-03, 3-2-1-L-T-U-N-S-20-04 and 3-2-1-L-T-U-N-S-20-04) are shown in Figure J2. The load vs. displacement data obtained are plotted in Figure J2a. Fracture toughness results, obtained from the area method, are shown in Figure J2b.

J.3 Lab 5: Fraunhofer Institute for Microstructure of Materials and Systems IMWS, Halle, Germany

Results obtained at Fraunhofer IMWS from tests with accelerated speed (load at 20 mm/min, unload at 30 mm/min) and an unloading cycle to zero displacement ($\delta = 0$ mm) (specimens 3-2-1-L-T-U-N-S-20-06, 3-2-1-L-T-U-N-S-20-07, 3-2-1-L-T-U-N-S-20-08, 3-2-1-L-T-U-N-S-20-09 and 3-2-1-L-T-U-N-S-20-10) are shown in Figure J3. The load vs. displacement data obtained are plotted in Figure J3a. Fracture toughness results, obtained from the area method, are shown in Figure J3b. These results are identical to those discussed in paragraph I3 and shown in Figure I3.

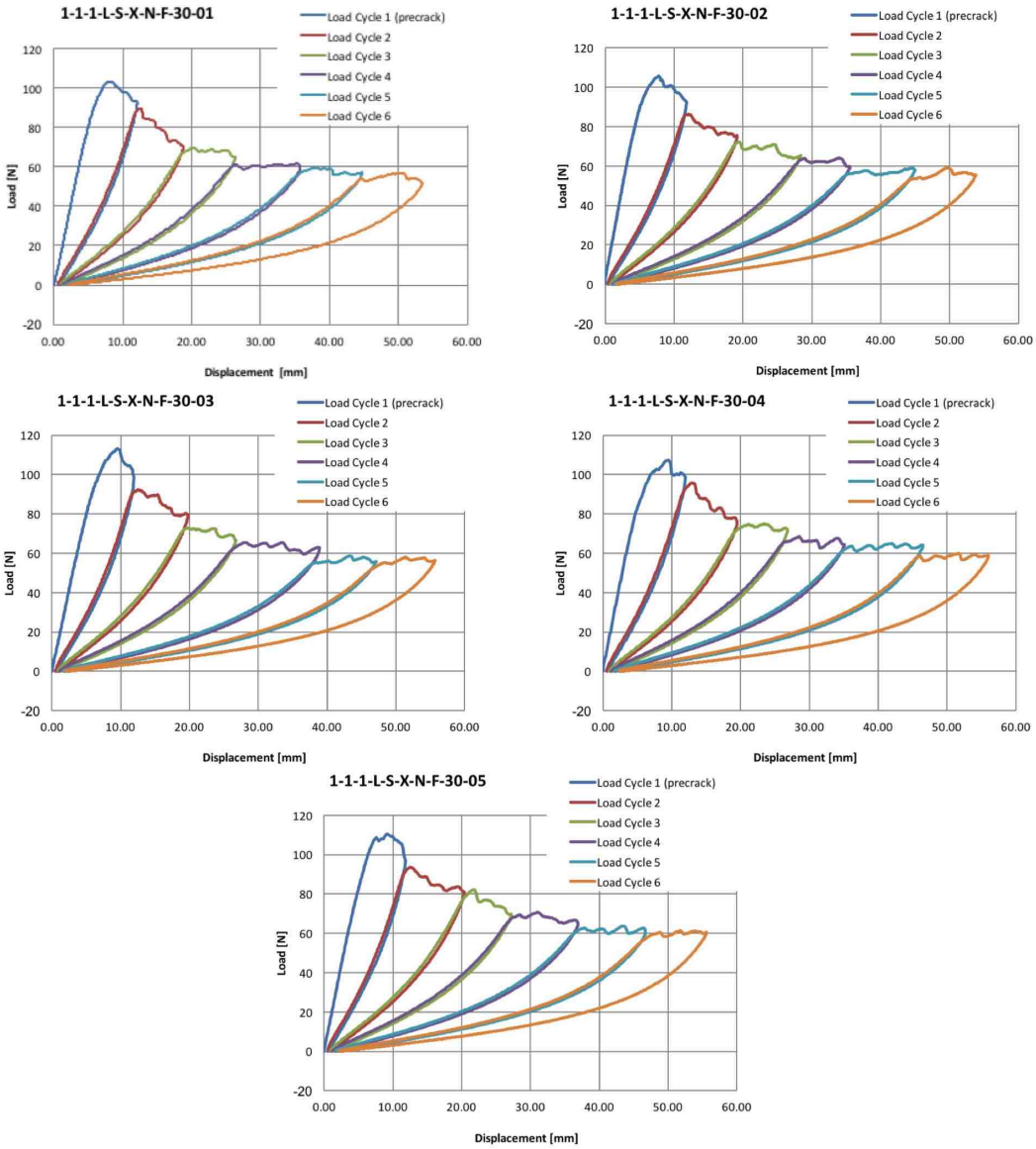

(a). *Load/displacement plots with six loading and unloading cycles for five specimens.*

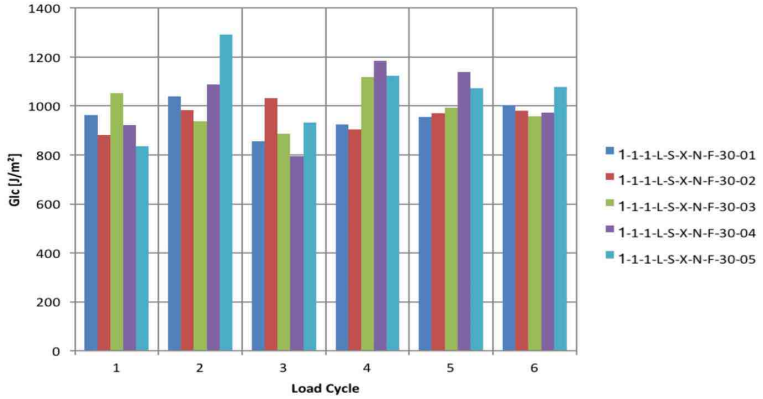

(b). *Measured G_c for individual load rate effect test specimens.*

Figure J1. Results obtained at The University of Utah for tests performed with an accelerated loading rate.

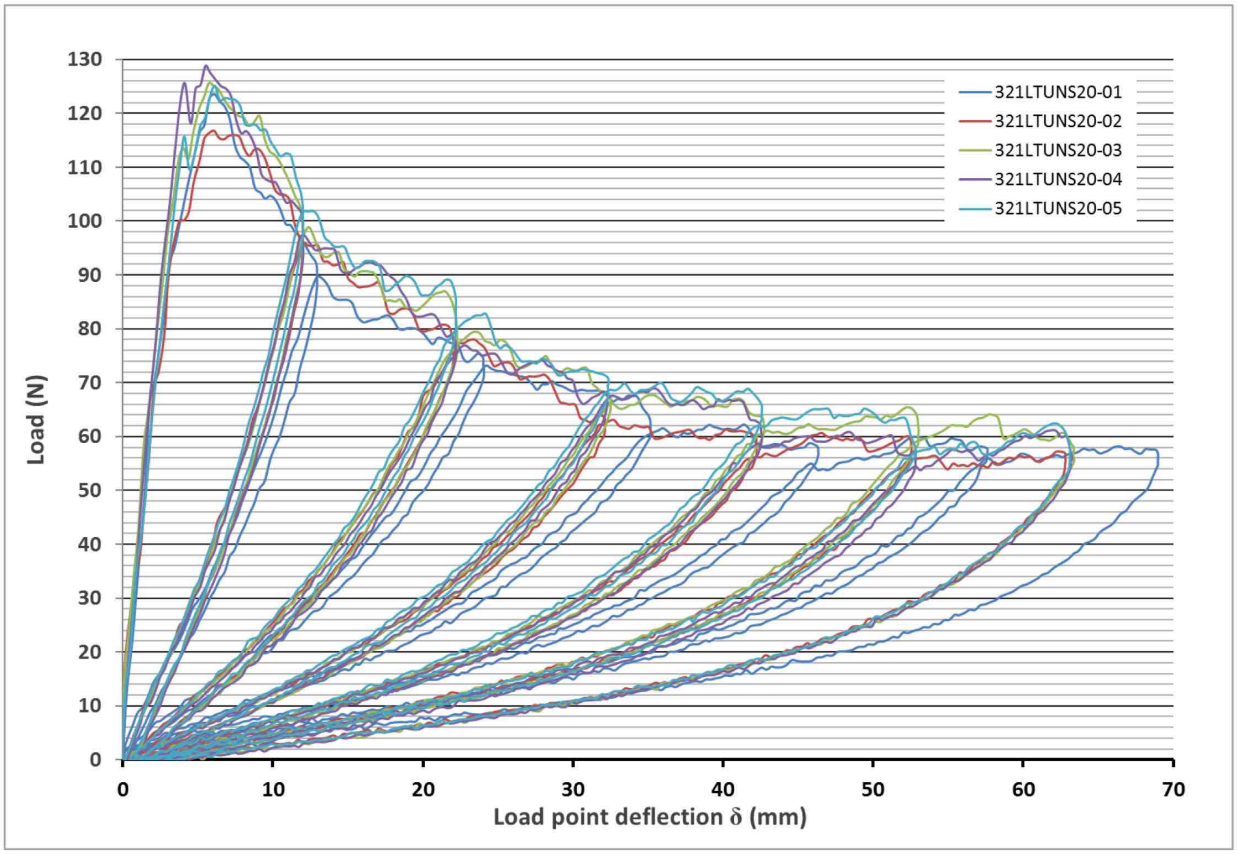

(a). *Load/displacement plots with six loading and unloading cycles for five specimens.*

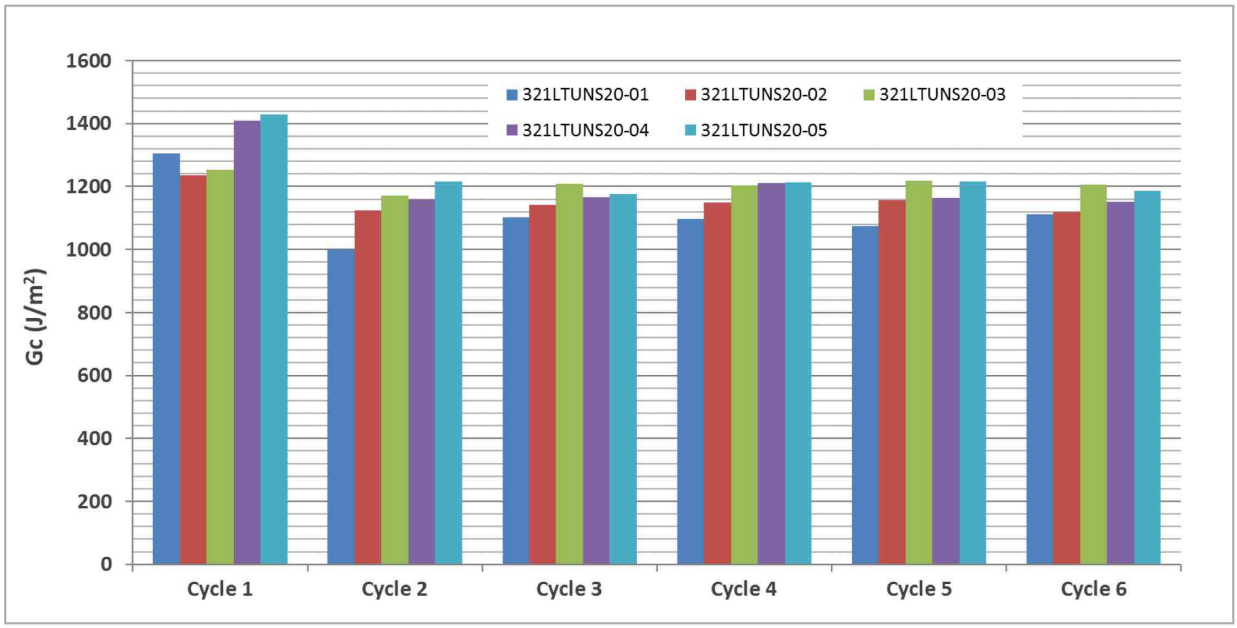

(b). *Fracture toughness values obtained from area method for five specimens tested.*

Figure J2. Results obtained at DuPont for accelerated testing at 100 mm/min during loading and unloading.

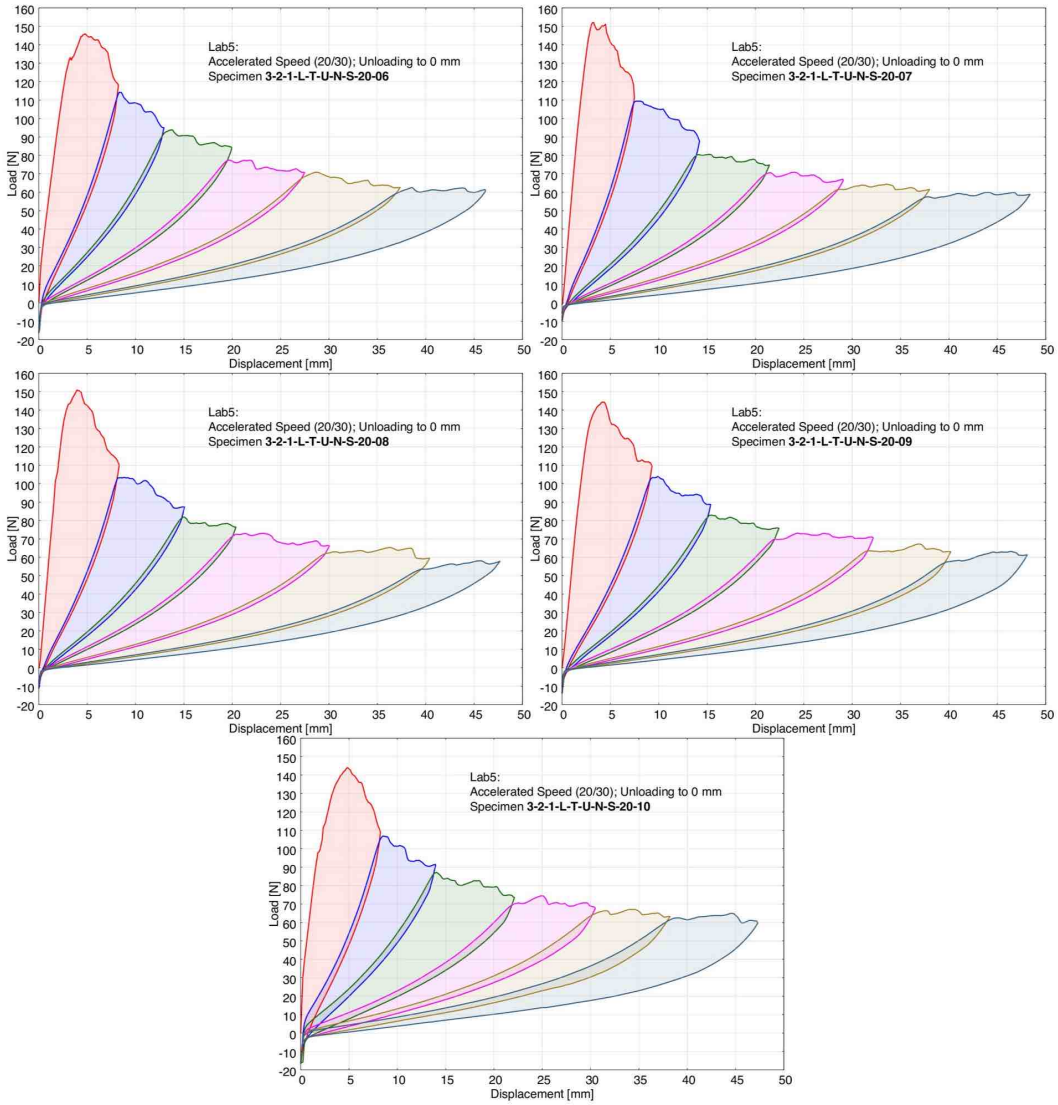

(a). *Load/displacement plots with six loading and unloading cycles for five specimens.*

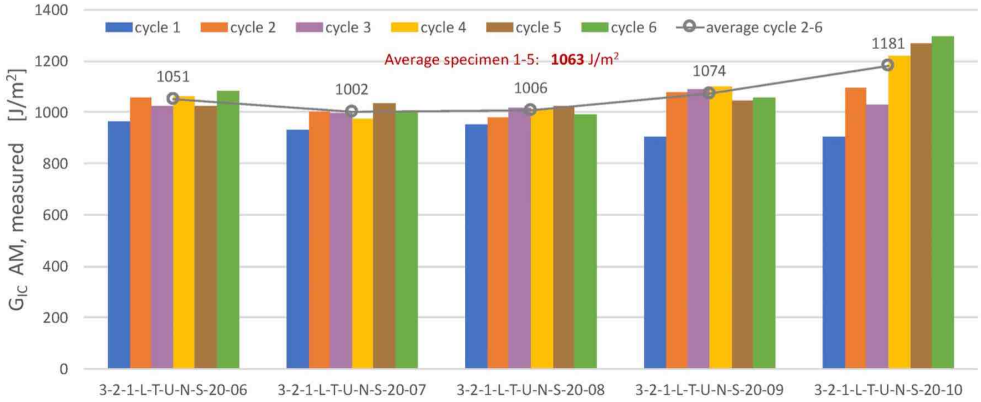

(b). *Fracture toughness values obtained from area method for all five specimens tested.*

Figure J3. Results obtained at Fraunhofer IMWS for tests performed with an accelerated loading rate of 20 mm/min and an unloading cycle to zero displacement.

APPENDIX K – RESULTS FROM DCB-UBM TESTS

Technical University of Denmark, Kgs. Lyngby, Denmark

Results obtained from specimens tested using the DCB-UBM test methodology at the Technical University of Denmark (specimens 8-7-1-L-T-U-N-F-05-01, 8-7-1-L-T-U-N-F-05-02, 8-7-1-L-T-U-N-F-05-03 and 8-7-1-L-T-U-N-F-05-04) are shown in Figure K. The moment vs. rotation data obtained are shown in Figure Ka. Energy release rate results, obtained using the closed-form expression in Equation 6 , are presented in Figure Kb. Disbond opening for a typical DCB-UBM specimen prior to unloading is shown in Figure Kc.

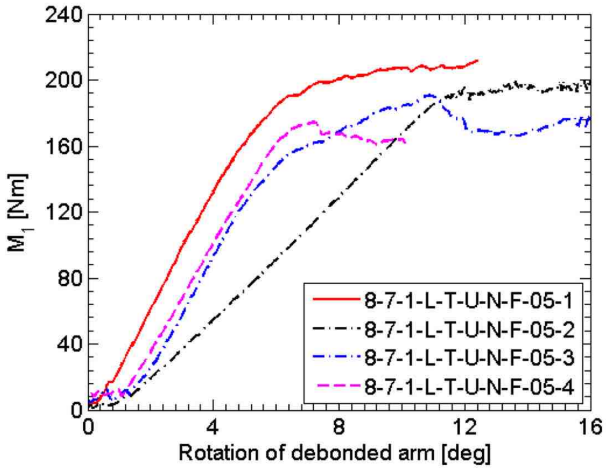

(a). *Moment vs. rotation plot of DCB-UBM specimens 8-7-1-L-T-U-N-F-05-1 to 8-7-1-L-T-U-N-F-05-4.*

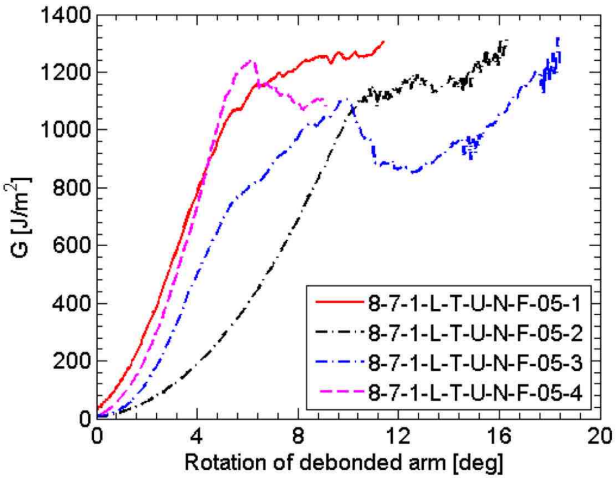

(b). *Energy-release rate vs. rotation plot of specimens 8-7-1-L-T-U-N-F-05-1 to 8-7-1-L-T-U-N-F-05-4.*

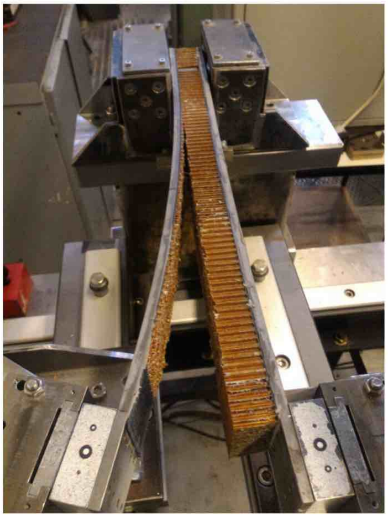

(c). *Typical crack opening for a DCB-UBM specimen. Id: 8-7-1-L-T-U-N-F-05-02.*

Figure K. Results obtained from specimens tested using the DCB-UBM test method carried out at DTU.